

# Contribution of Western Arabian Sea Tropical cyclones to rainfall in the Horn of Africa

Pierre Camberlin<sup>1</sup>, Omar Assowe<sup>2</sup>, Benjamin Pohl<sup>3</sup>, Moussa Mohamed Waberi<sup>2</sup>, Karl Hoarau<sup>4</sup>, and Olivier Planchon<sup>3</sup>

<sup>1</sup>CRC / Biogéosciences, Université de Bourgogne

<sup>2</sup>Observatoire Régional de Recherche sur l'Environnement et le Climat (ORREC)

<sup>3</sup>CRC / Biogéosciences

<sup>4</sup>University of Cergy-Pontoise

March 11, 2024

## Abstract

The occurrence of tropical cyclones (TC) in the Horn of Africa and nearby areas is for the first time examined to document their contribution to local rainfall and their trends over the period 1990-2020. An average 1.5 TC (of any intensity) per year was observed over the Western Arabian Sea, with two asymmetrical seasons, namely May-June (30% of cyclonic days) and September-December (70%). Case studies reveal that in many instances, TC-related rainfall extends beyond 500 km from the TC center, and that substantial rains occur one to two days after the lifecycle of the TC. Despite their rarity, in the otherwise arid to semi-arid context characteristic of the region, TCs contribute in both seasons to a very high percentage of total rainfall (up to 30 to 60%) over the northwestern Arabian Sea, the Gulf of Aden and their coastlines. Over inland northern Somalia, contributions are much lower. TCs disproportionately contribute to some of the most intense daily falls, which are often higher than the mean annual rainfall. A strong increase in the number of TCs is found from 1990 to 2020, hence their enhanced contribution to local rainfall. This increase is associated with a warmer eastern / southern Arabian Sea, a decrease in vertical wind shear, and a strong increase in tropospheric moisture content.

1 Contribution of Western Arabian Sea Tropical cyclones to rainfall in the Horn of Africa.

2

3

4 P. Camberlin <sup>1</sup>, O. Assowe <sup>2</sup>, B. Pohl <sup>1</sup>, M. Mohamed Waberi <sup>1,2</sup>, K. Hoarau <sup>3</sup>, O. Planchon <sup>1</sup>

5

6

7 <sup>1</sup> Centre de Recherches de Climatologie, UMR 6282 Biogéosciences, CNRS/Université de  
8 Bourgogne, Dijon, France.

9 <sup>2</sup> Observatoire Régional de Recherche sur l'Environnement et le Climat (ORREC), Centre  
10 d'Etudes et de Recherche de Djibouti (CERD), Djibouti-ville, République de Djibouti.

11 <sup>3</sup> PLACES, CY Cergy Paris Université, France

12

13

14

15

16

17

18

19

20

21

22 Submitted to Journal of Geophysical Research : Atmospheres

23

28 February 2024

24

25 Abstract

26 The occurrence of tropical cyclones (TC) in the Horn of Africa and nearby areas is for the first time  
27 examined to document their contribution to local rainfall and their trends over the period 1990-2020.  
28 An average 1.5 TC (of any intensity) per year was observed over the Western Arabian Sea, with two  
29 asymmetrical seasons, namely May-June (30% of cyclonic days) and September-December (70%). Case  
30 studies reveal that in many instances, TC-related rainfall extends beyond 500 km from the TC center,  
31 and that substantial rains occur one to two days after the lifecycle of the TC. Despite their rarity, in the  
32 otherwise arid to semi-arid context characteristic of the region, TCs contribute in both seasons to a  
33 very high percentage of total rainfall (up to 30 to 60%) over the northwestern Arabian Sea, the Gulf of  
34 Aden and their coastlines. Over inland northern Somalia, contributions are much lower. TCs  
35 disproportionately contribute to some of the most intense daily falls, which are often higher than the  
36 mean annual rainfall. A strong increase in the number of TCs is found from 1990 to 2020, hence their  
37 enhanced contribution to local rainfall. This increase is associated with a warmer eastern / southern  
38 Arabian Sea, a decrease in vertical wind shear, and a strong increase in tropospheric moisture content.

39

40 1. Introduction

41 Tropical cyclones (TCs) develop over sufficiently warm off-equatorial oceanic regions, which are  
42 generally wet areas receiving well over 1000 mm of precipitation per year. Although the Arabian Sea  
43 is not among the most active cyclonic basins, accounting, together with the Bay of Bengal, for only 4-  
44 6% of the world's TCs (Ramsay, 2017; Neumann, 2017 ; Singh and Roxy, 2022), it stands out by its low  
45 mean annual rainfall, which does not exceed 500 mm in its northwestern half. Very few other arid  
46 regions, like northwestern Mexico (Fors, 1977; Breña-Naranjo et al., 2015) and Western Australia (Ng  
47 et al., 2014), similarly experience TCs. Although considered a very rare occurrence along the coasts of  
48 northern Somalia, Yemen, and to some extent Oman (Pedgley, 1969; Al-Manji, 2021), the recent past  
49 provided evidence of several high intensity systems, e.g. the "very severe cyclonic storms" Gonu in  
50 2007, Chapala and Megh in 2015, Mekunu and Luban in 2018. Their landfall in arid environments  
51 provides unusually high rainfall amounts in a short period of time, which have major short-term  
52 consequences (e.g., flash floods destroying infrastructure, settlements, claiming lives and killing  
53 livestock) as well as longer-term impacts, for instance on groundwater recharge (Abdalla and Al-Abri,  
54 2011) and the dynamics of endangered tree species (Lvonicik et al., 2020). In the late 2010s, the  
55 succession of several unusually wet seasons, in which TCs played a dominant role, induced the worst  
56 locust outbreak of the last decades in Southern Arabia and the Horn of Africa (Salih et al., 2020 ; Owuor  
57 and David-McRae, 2022). In the Republic of Djibouti alone, the desert locust infestation in 2019-2020  
58 caused a loss of 5 million USD over crops and pastures. Even moderately strong tropical systems have  
59 large impacts because of the associated heavy rains. For instance, cyclonic storm Sagar brought 181  
60 mm of rainfall in Djibouti-city on two days in May 2018, extensively flooding huge urban  
61 neighbourhoods and schools, and destroying transportation and sanitation infrastructures (Cherel et  
62 al., 2020). The low income populations of the Horn of Africa, usually confronted to harsh climatic  
63 conditions related to recurrent droughts, are particularly vulnerable to such high intensity rainfall  
64 events, yet to the best of our knowledge there has never been any systematic study of how frequently  
65 TCs affect this part of the continent.

66 Over the Western Arabian Sea (WAS hereafter) and neighbouring coastal areas (Yemen, Somalia,  
67 Djibouti), more generally, the average contribution of TCs to local rainfall is little known. Pedgley (1969)  
68 found that at Salalah (southern Oman), a quarter of the total rainfall from 1943 to 1967 was associated  
69 with cyclones. Jiang and Zipser (2010) and Prat and Nelson (2013) quantified the contribution of  
70 tropical storms to global precipitation from TRMM data. Over the period 1998-2006, it varied from 3  
71 to 11% depending on the basins (Jiang and Zipser, 2010), and 5% for the North Indian Ocean basin  
72 which includes both the Bay of Bengal and the Arabian Sea. Comparable values were obtained by Prat  
73 and Nelson (2013) using 12 years of data from 1998 to 2009. Much higher contributions were found  
74 over localised areas such as the coasts of Baja California in Mexico (Breña-Naranjo et al., 2015) and

75 northwest Australia (Ng et al., 2014), but they decrease significantly within the first 150 km from the  
76 coast (Prat and Nelson, 2013). Khouakhi et al. (2017) examined the contribution of TCs to rain-gauge  
77 precipitation amounts and found that they account for a large portion (35-50%) of mean annual rainfall  
78 in a few regions including northwestern Australia, southeastern China, the northern Philippines, and  
79 northwestern Mexico. However, their study did not document the Arabian Sea area. Prat and Nelson  
80 (2013) published a map covering the North Indian Ocean basin, but due to the small number of years,  
81 the TC-related rainfall contribution is relatively noisy over the WAS. Kabir et al. (2022) studied TC  
82 exposure in the North Indian Ocean. TC-associated rainfall is much higher around the Bay of Bengal  
83 sub-basin than over the Arabian Sea, partly due to the larger number of TCs making landfall around  
84 the Bay of Bengal (155 between 1989 and 2018, as compared to 30 around the Arabian Sea).  
85 Nevertheless, the latter have a high contribution to TRMM total rainfall along the southeastern coasts  
86 of Arabia, reaching 50% in parts of Oman (Kabir et al. 2022).

87 The objectives of the present study are to quantify the mean rainfall amount resulting from TCs in the  
88 WAS, Gulf of Aden and riverine countries (Somalia, Djibouti, Yemen), and their contribution to the total  
89 rainfall amounts, which have never been comprehensively analysed before, since all previous studies  
90 on TC-induced precipitation were actually carried out at a much broader scale. Daily rainfall extremes  
91 associated with TCs will also be examined and compared to local absolute 24-hr maxima. Some case  
92 studies of TCs making landfall over the coasts of Somalia and Djibouti will also be presented in order  
93 to better apprehend the spatial distribution of rainfall during such events and its relationship to the  
94 storms size and track. A better knowledge of TCs in the region and their contribution to the local  
95 climatology is an important issue, because several studies point to a recent (Wang et al. 2012 ;  
96 Murakami et al. 2017 ; Baburaj et al. 2020 ; Deshpande et al. 2021 ; Priya et al., 2022 ; Tiwari et al.  
97 2022) and forthcoming increase (Murakami et al. 2013 ; Knutson et al. 2015 ; Bell et al. 2020) in the  
98 frequency of Arabian Sea TCs. While Murakami et al. (2013) attributed the recent increase to  
99 anthropogenic climate change, more ambiguous results were obtained by Wang et al. (2023). Evan et  
100 al. (2011) found that a recent increase in storm intensity could have been driven by enhanced  
101 anthropogenic black carbon and sulphate emissions, resulting in a reduction of vertical wind shear, but  
102 this was challenged by Wang et al. (2012).

103 Besides documenting the patterns of TC-related rainfall over the north-eastern tip of Africa and  
104 adjacent regions, the present study analyses trends of TC-related and total rainfall over the last 20-30  
105 years. Given the major changes found in TC occurrence in the last decades, a comparison is also made  
106 of the regional oceanic and atmospheric conditions which may have triggered these changes. Section  
107 2 presents the cyclone and precipitation data used in the study. The TC and precipitation climatologies  
108 are depicted in section 3.1, followed by the selected TC case studies (3.2). The statistical analysis of

109 mean rainfall amounts associated with TCs is then presented (3.3), before an appraisal of TC-related  
110 rainfall trends since 1990 (3.4) and the associated oceanic and atmospheric conditions (3.5).

## 111 2. Data and methods

### 112 2.1 Cyclone tracks

113 Data on 3-hourly North Indian Ocean TC locations were extracted from the IBTrACS (International Best  
114 Track Archive for Climate Stewardship, Knapp et al., 2010 & 2018) dataset. All observations west of  
115 75°E were retained. This is slightly further east than the WAS target area (33-65°, 0-22°N) because it is  
116 necessary to extract TC-related rainfall over a wide radius from the TC center. Given that some of the  
117 rainfall data are at daily timescale, the successive locations of each cyclone are averaged over each 24-  
118 hr period. As discussed below, the wide radius which will be retained around the TC center  
119 accommodates the TC propagation within each day.

120 All TC categories were retained in the study, i.e. including weak systems like tropical depressions (wind  
121 speeds between 17 and 34 knots). Substantial rains are sometimes associated with tropical  
122 depressions, which justifies the inclusion of these weaker systems. For instance, Arabian Sea tropical  
123 depression 02A, with weak maximum sustained winds (25 knots), which in 2008 made landfall in  
124 Yemen, caused widespread flooding, 180 deaths and 22 000 displaced people (Evan and Camargo,  
125 2011). Some analyses will be separately carried out on the Very Severe Cyclonic Storms (VSCS  
126 hereafter), the third highest category used by the India Meteorological Department to classify North  
127 Indian Ocean tropical cyclones, and which is equivalent to the Hurricane category (winds of at least 64  
128 knots). Hereafter, TC refers to all categories of disturbances, not just VSCS.

129 The study is restricted to the period from 1990 (2000 for some analyses) to 2020. Data for the pre-  
130 satellite era over the North Indian Ocean are not fully reliable due to a possible undercount of TCs  
131 (Evan and Camargo, 2011 ; Singh et al. 2020 ; Deshpande et al. 2021 ; Wahiduzzaman et al. 2022).  
132 Additionally, Kabir et al. (2022) and Tiwari et al. (2022) warned that TC records over the North Indian  
133 Ocean may not be fully complete prior to 1990 due to missing intensity records. Hoarau et al. (2012)  
134 re-analysed TC data over the Northern Indian Ocean using the Dvorak (1984) method. They warned of  
135 a probable undercount of intense TCs during 1980-1989. From 1990 onwards, the agreement between  
136 North Indian Ocean TC track-data from the Indian Meteorological Department (IMD) and the Joint  
137 Typhoon Warning Center (JTWC) greatly improved (Evan and Camargo, 2011 ; Schreck et al. 2014),  
138 suggesting that working on this period is less uncertain.

139

## 140 2.2 Precipitation data

141 Two daily gridded precipitation datasets based on satellite information calibrated with some ground  
142 data were used and complemented by rain-gauge data for northern Somalia and Djibouti. The gridded  
143 datasets were selected to document both land and oceanic areas, at a relatively high spatial resolution.

144 PERSIANN-CDR (Precipitation Estimation from Remotely Sensed Information using Artificial Neural  
145 Networks–Climate Data Record – Ashouri et al., 2015) uses infrared satellite data as the main input,  
146 from which a neural network model is developed whose parameters are based on radar data. The  
147 resulting rainfall estimates are next calibrated using the monthly Global Precipitation Climatology  
148 Project (GPCP) data. The product is available from 1 January 1983 to the present, at 0.25° spatial  
149 resolution.

150 IMERG (Integrated Multi-satellitE Retrievals for the Global Precipitation Measurement, Huffman et al.  
151 2015) is a gridded rainfall product with global coverage, based on NASA's precipitation algorithm,  
152 applied to data from the TRMM (Tropical Rainfall Measurement Mission) and the GPM (Global  
153 Precipitation Measurement) satellite missions. It covers the period from 2000 to the present day, at a  
154 high spatial (0.1 degree) and temporal (30 minute) resolution. The input data include passive  
155 microwave (PMW) precipitation estimates, considered as more direct retrievals, calibrated to the  
156 combined radar-radiometer product from TRMM and GPM. An interpolation of the PMW estimates is  
157 performed by propagating them forward and backward in time using motion vectors. The resulting  
158 estimates are further combined to infrared (IR) precipitation estimates, and a final bias adjustment to  
159 rain-gauge observations is made over land areas.

160 For both data sets, the region 3°S-22°N, 35-65°E, i.e. the Greater Horn of Africa (GHA) and nearby  
161 regions, was extracted. The period retained is 1990-2020 (2000-2020 for IMERG) to take into account  
162 TC data reliability as exposed above. Note that, unless otherwise stated, the results obtained for  
163 PERSIANN and IMERG are qualitatively similar, hence will not be systematically duplicated. Below,  
164 IMERG is generally preferred to PERSIANN, because it slightly better agrees with rain-gauge data.

165 Daily rain-gauge data for 25 stations in Northern Somalia (mainly Somaliland and Puntland areas) were  
166 obtained from SWALIM (Somalia Water and Land Information Management), a project managed by  
167 FAO. The period covered is 2005-2020, with data availability varying from 10 to 16 years. For the  
168 Republic of Djibouti, data from Djibouti-Airport station, with complete daily rainfall records between  
169 2000 and 2020, were obtained from the National Meteorological Agency of Djibouti.

## 170 2.3 Methods for quantifying TC-associated precipitation

171 Quantifying the contribution of TCs to rainfall requires defining to what distance of the TC center  
172 rainfall is considered as being related to the TC. Most studies consider a 500 km radius (e.g., Jiang and

173 Zipster, 2010 ; Prat and Nelson, 2013; Lavender and McBride, 2021). This threshold is meant to be  
174 within the range of the outer edge of the TC cloud shield (550–600 km) (Englehart et al. 2001, Kabir et  
175 al. 2022). Rather than blindly adopting the same threshold, mean daily rainfall was plotted as a function  
176 of distance to the TC center, for all TCs reported in the period 2000-2020 in the WAS area. Boxplots  
177 were constructed to derive the median rainfall and its variability for 40 km bins (section 3.3). From  
178 these plots an adapted threshold was defined, and all rainfall which fell within this distance from the  
179 TC center was considered as TC-related. Rainfall in the days immediately following the demise of each  
180 TC was also examined in order to find out whether part of it can be ascribed to remnants of the  
181 disturbance. This procedure was used to quantify TC-related rainfall for each disturbance, and to  
182 compute statistics for the period 2000-2020 based on the gridded PERSIANN and IMERG rainfall  
183 estimates, and the stations available in the years 2005-2020 in Northern Somalia and Djibouti.

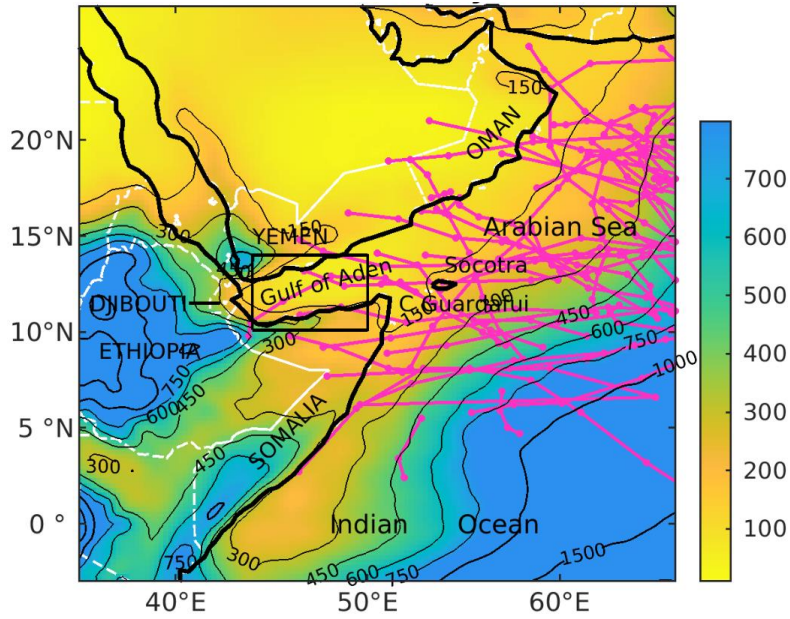
184 The contribution of TC-related rainfall to total rainfall was computed. To document the part played by  
185 TCs on intense rainfall, days recording above 30 mm were extracted and the proportion which are TC-  
186 induced was computed. Maximum 24-hr rainfall at available rain-gauges was also examined to assess  
187 to which extent it relates to TC occurrence. These analyses were carried out separately on the two  
188 cyclonic seasons, i.e. the pre-monsoon (May-June) and the post-monsoon (September-December).

189 Rainfall trends over the period 2000-2020 (extended to 1990-2020 for PERSIANN) were mapped for  
190 total rainfall, TC-related rainfall, non-TC related rainfall and the contribution of TC-related rainfall to  
191 total rainfall amounts. Mann-Kendall Tau statistics were computed to assess the statistical significance  
192 of the trends.

### 193 3. Results

#### 194 3.1 Rainfall and TC climatologies

195 The region around the northeastern tip of Africa is mostly an arid to semi-arid area, with less than 500  
196 mm/yr (fig.1). Mean annual rainfall (MAR) increases to the southeast, in the Central Indian Ocean, in  
197 the west over highland areas (Ethiopia, Kenya, Yemen), and along a narrow subcostal belt stretching  
198 northward from Southern Kenya. The region covering most of South Arabia, the Gulf of Aden and  
199 neighbouring areas is particularly arid (less than 200 mm/yr), with no well-defined rainy season. Much  
200 of Somalia and its surroundings have two brief rainy seasons, in March-May and October-November.  
201 Due to the divergence of large-scale air flows, most of the region experiences dry boreal winters  
202 (December-February) and summers (June-September), the main exception being the Ethiopian  
203 highlands.



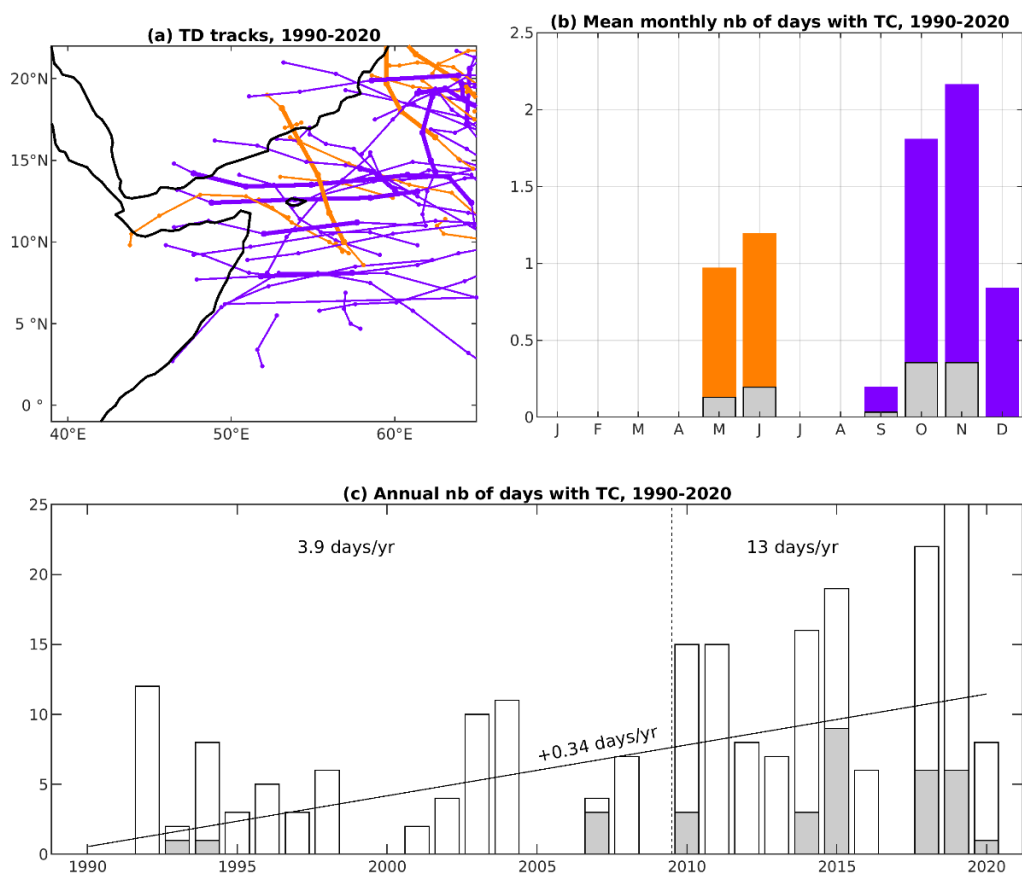
204

205 Figure 1 : Location map, with shadings representing mean annual rainfall (PERSIANN data, 1990-  
 206 2020, in mm) and pink lines TC tracks (same period). The box shows the area over which the Gulf of  
 207 Aden rainfall index is computed (section 3.4).

208 From 1990 to 2020, a total of 47 TCs crossed the WAS, with a mean life-time (within the region) of 4.6  
 209 days. The number of TCs gradually decreases from east to west (fig.2), with tracks generally showing  
 210 E-W or SE-NW directions. A minority of the TCs display more meridional tracks, with southerly  
 211 propagations on rare occasions (e.g. TC Kyarr in 2019). Only about a third of these TCs made landfall  
 212 over the continent, either on the coasts of Southern Arabia or on those of Somalia, with a few  
 213 additional TCs which approached close to the coasts or crossed Socotra island. A small proportion of  
 214 these disturbances belong to the VSCS category. On average, only 1.1 days.year<sup>-1</sup> record a VSCS, as  
 215 compared to 7.1 days.year<sup>-1</sup> for all TC categories.

216 TCs reaching or developing over the WAS are found in two distinct seasons (fig.2), which correspond  
 217 to the pre-monsoon season (May-June) and post-monsoon season (September-December, clearly  
 218 peaking in October-November). During the monsoon season (boreal summer), the strong wind shear  
 219 between the low-level westerlies and the upper-tropospheric Tropical Easterly Jet, as well as lower SST  
 220 over parts of the WAS, disable the development of TCs (Gray, 1968 ; Evan and Camargo, 2011 ; Baburaj  
 221 et al. 2020). TCs are much less frequent in May-June (MJ) than in September-December (SOND). The  
 222 latter season makes up about two thirds of the number of TCs, and 70% of the cyclonic days. This is  
 223 specific to the WAS: for the Arabian Sea as a whole the number of TCs is approximately the same in  
 224 the two seasons (Evan and Camargo, 2011), with some decadal variations (Al-Manji et al. 2021). The  
 225 smaller number of pre-monsoon TCs in the western part of the Arabian Sea compared to post-  
 226 monsoon has rarely been highlighted (Ray-Choudhuri et al. 1959), though it is obvious in Singh and

227 Roxy (2022, their figure 3). There is no current explanation for this difference, but it is not related to  
 228 SST, which are higher in the pre- than in the post-monsoon seasons. Dynamical conditions could be  
 229 more conducive to a westward motion of the TCs initiated over the eastern Arabian Sea. The  
 230 predominantly east-west tracks of many of the post-monsoon TCs is shown on figure 2a. May-June  
 231 tracks are slightly more uneven, and few of them make landfall over northeastern Africa or southern  
 232 Arabia.



233  
 234 Figure 2 : TC tracks and TC statistics for the Western Arabian Sea, 1990-2020. Orange colours refer to  
 235 the May-June season, purple colours to the September-December season. Grey bars in panels (b) and  
 236 (c) stand for VSCS, which are identified by bold lines in panel (a). In panel (c), white bars show the  
 237 yearly total of TC days (TC center located west of 65°E), with the linear trend computed as Sen's  
 238 slope. The vertical dashed line is the breaking point according to Pettitt's test ( $p < 0.01$ ), with the  
 239 mean number of TC days for the two sub-periods in the top part of the panel.

240 Large interannual variations are found in the number of TC days (fig. 2c). In some years, no TCs are  
 241 recorded in the WAS. There has been a clear and strong positive trend in the number of TC days in the  
 242 period 1990-2020 (+0.34 per year, significant at  $p < 0.01$ ), corroborating Deshpande et al. (2021).  
 243 Pettitt's test for change-point detection indicate a significant upward increase ( $p < 0.01$ ) after 2009. In  
 244 the first sub-period (1990-2009), there was an average of 3.9 TC days/year in the WAS, rising to 13

245 days/year between 2010 and 2020. Statistics for WSCS are less robust, given the rare occurrence of  
246 disturbances in this category. While these storms were exceptional between 1990-2009, they became  
247 much more common from 2010, with each of the last three years (2018, 2019 and 2020) recording  
248 VSCS.

### 249 3.2 Case-studies

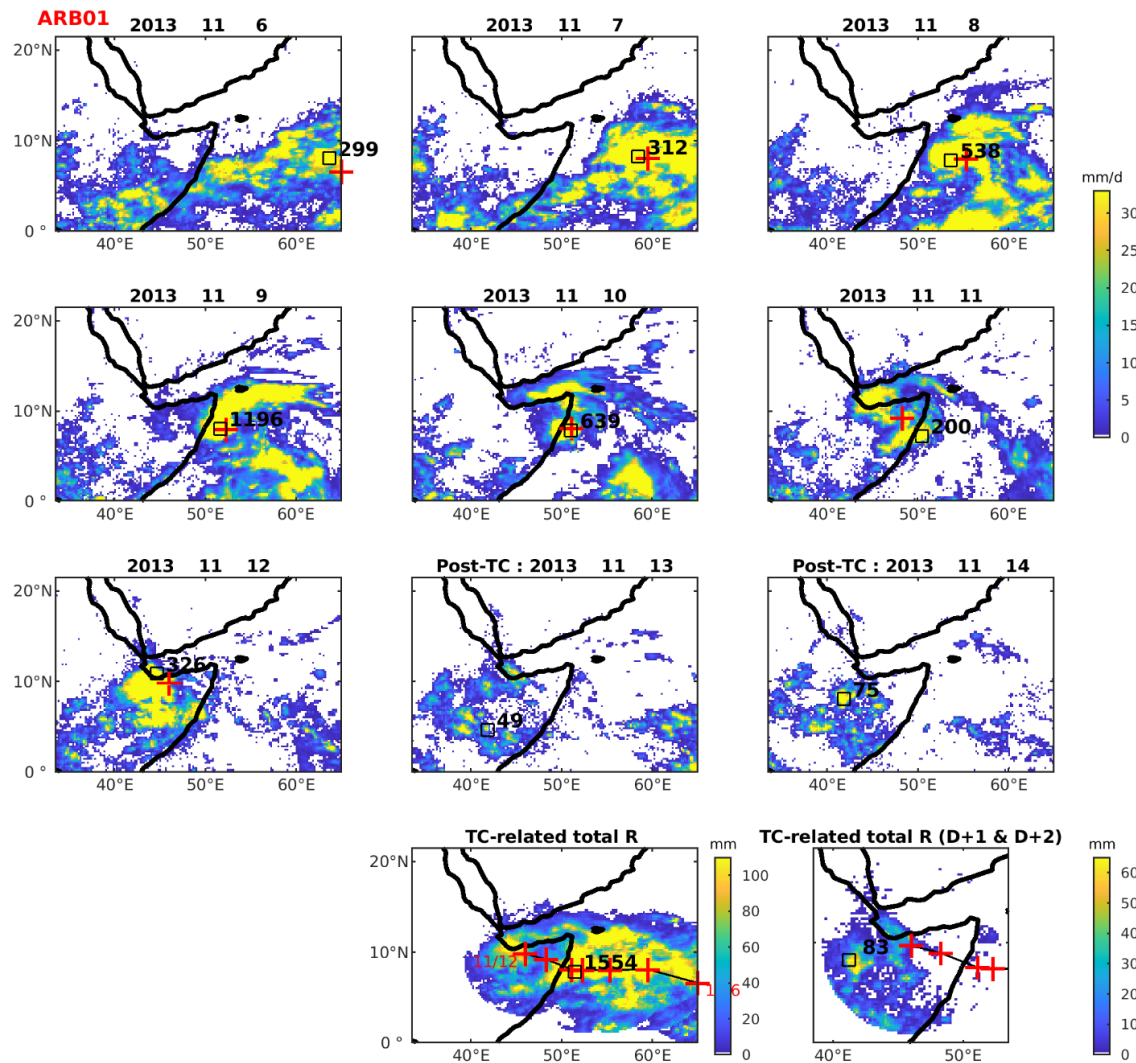
250 Four case studies of TCs which made landfall over the northeastern tip of Africa have been selected,  
251 to document the relationship between the tracks of these systems and the rainfall distribution. They  
252 are ordered here by increasing intensity.

#### 253 - Deep depression ARB01/2013 (November 2013) :

254 This disturbance was first identified as a low pressure centre on 6 November 2013 near 6°N, 65°E  
255 (fig.3), then classified by the IMD as a tropical depression on 8 November 2013, while located 680 km  
256 east of Ras Binnah on the northeastern Somalian coast, moving westward. It slightly intensified on 9  
257 November, with 3-mn sustained winds of 55 km/h, developed an eye feature, and was classified as a  
258 deep depression. It made landfall on 10 November at 8°30'N, north of Eyl in Puntland, northern  
259 Somalia. A large area of active convection was associated with the TC. Very high daily point rainfall  
260 estimates were obtained by IMERG along the track, from 199 mm to an unreliable 1196 mm on 9  
261 November near the coast (fig.3, bottom), in conjunction with very low cloud top temperatures (-70 to  
262 -75°C, not shown). As the TC made landfall, very high rainfall estimates were still shown on 11 and 12  
263 November over a large area covering northern Somalia. On 13-14 November, while the TC is no longer  
264 singularized, scattered but significant convective rains occurred from Djibouti to Central Somalia.

265 Rain-gauge data (fig.4) show that coastal rains associated with the disturbance started on 8 November,  
266 but the bulk of the rains fell on 11 November in arid Puntland (20 to 100 mm, and a peak of 139 mm  
267 at Eyl). The rains shifted westward on 12 November, with substantial rains (40-50 mm) still found on  
268 13 November in western Somaliland. The accumulated rainfall during the TC lifetime (within 750 km  
269 of the TC center, fig.4) generally exceeds 100 mm in the east, and is more contrasted further west.  
270 However, if one adds the precipitation recorded in the following two days (fig.4, bottom right panel),  
271 rainfall amounts ranging from 49 to 144 mm are found in the inland part of western Somaliland. The  
272 coastal town of Berbera (55-yr MAR : 50 mm) even recorded 195 mm during this period. In Somalia,  
273 TC ARB01/2013 caused the death of 162 people, about 100,000 livestock losses and the destruction of  
274 over 1,000 houses according to official statistics (IFRC, 2013).

275



276

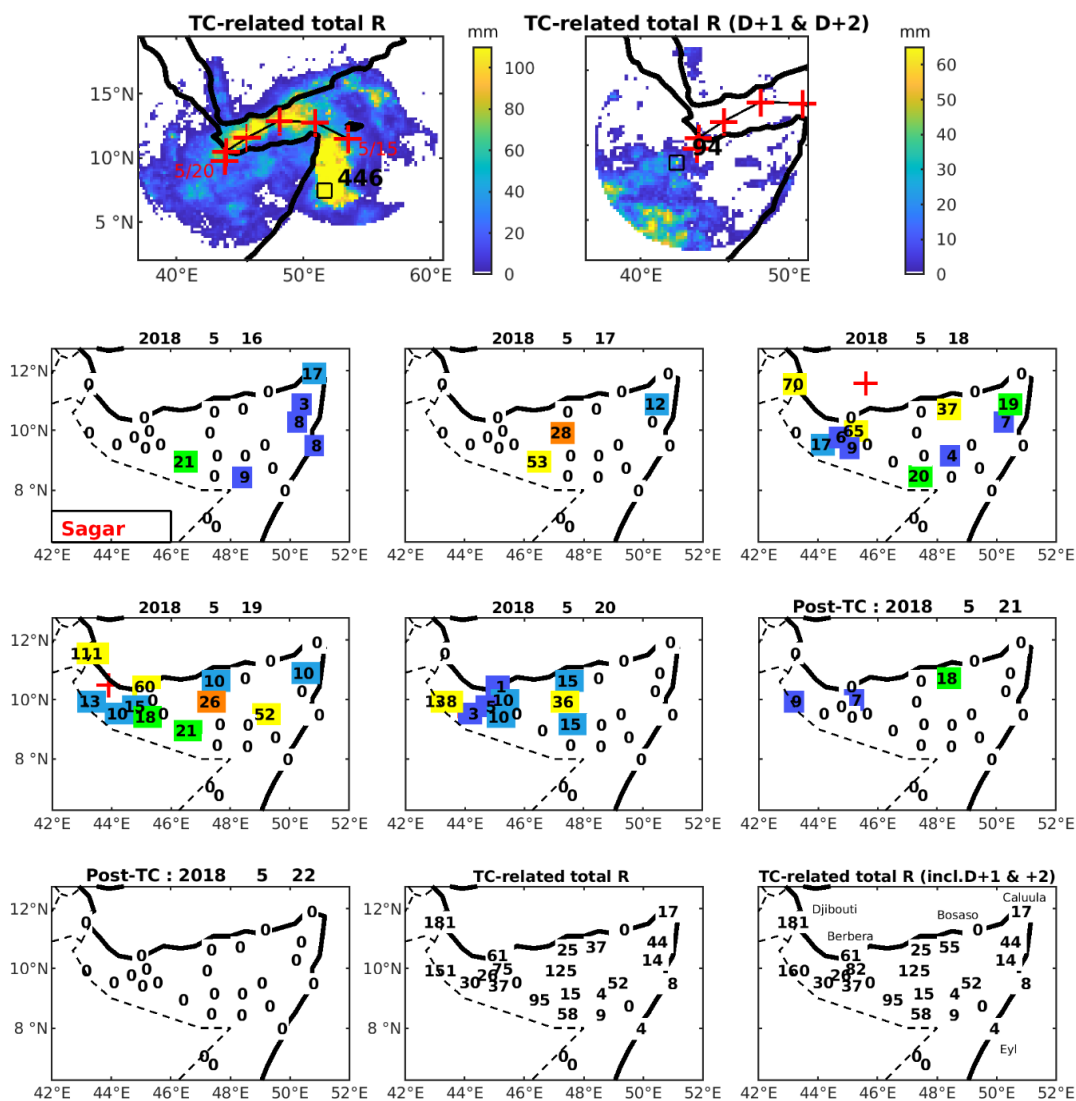
277 Figure 3 : IMERG daily rainfall during the lifetime of deep depression ARB01/2013 and in the two  
 278 following days (“post-TC”). Bottom panels : accumulated rainfall amount associated with the TC  
 279 (within 750 km of its center) during its lifetime (left) and in the two following days (right panel). Red  
 280 crosses show the location of the TC center. Black figures : maximum rainfall amount within 750 km.



296 Djibouti from 18 to 20 May (fig.5, bottom panels). Substantial rains were also found on the following  
 297 two days in eastern Ethiopia, associated with the overall atmospheric instability and Sagar remnants,  
 298 causing landslides and flash floods destroying villages in the Sitti area.

299 Wadi Ambouli, which crosses Djibouti-city, overflowed and caused heavy damages, particularly on  
 300 the right bank in the Boulaos neighbourhood. Around 20,000 people were affected in the Republic of  
 301 Djibouti. Damage to transport infrastructure amounted to approximately 1.9 billion Djiboutian francs  
 302 (US\$10 million), with a similar figure for the sanitation system (Cherel et al. 2020). At least 53 victims  
 303 were numbered in northern Somalia, particularly in western Somaliland, herds were swept away, and  
 304 many boats were destroyed in the ports of Puntland.

305



306

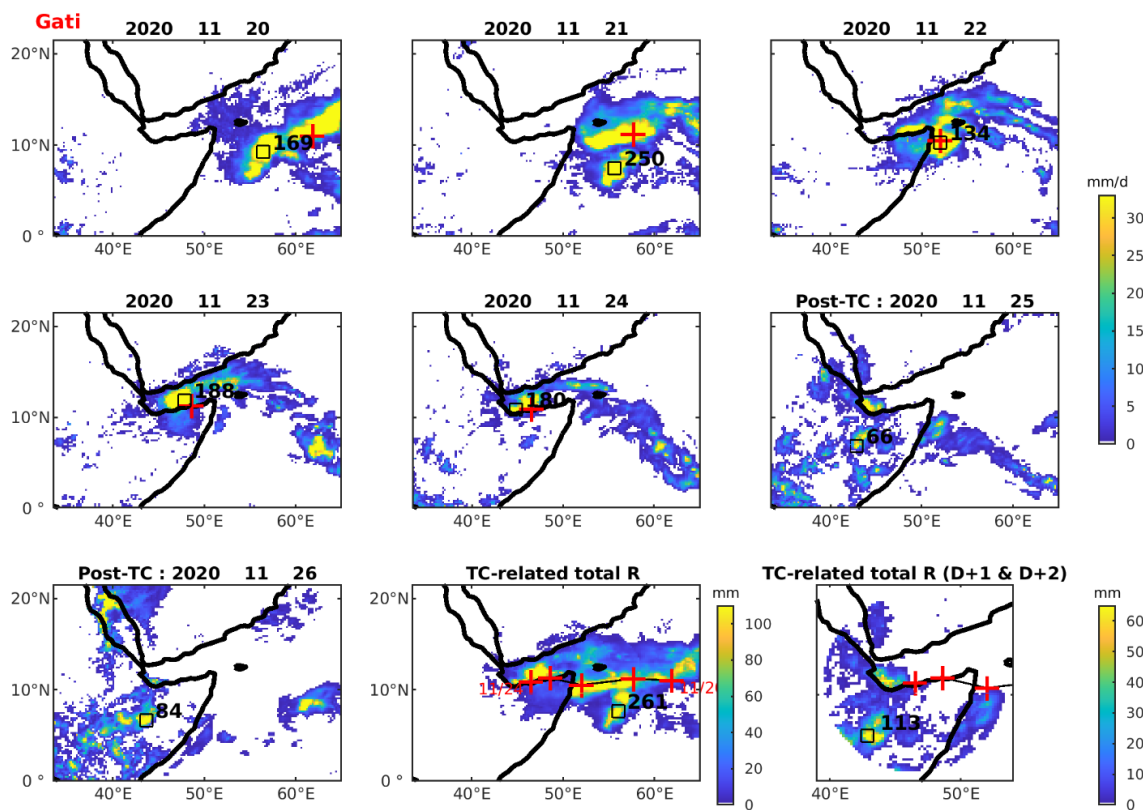
307 Figure 5 : Rainfall associated with TC Sagar. Top panels : accumulated IMERG rainfall during Sagar  
 308 lifetime (15-20 May, top left) and in the two following days (21-22 May, top right). Red crosses show  
 309 the location of the TC center, with indication of the first and last dates of its lifetime. Black squares

310 indicate the maximum accumulated rainfall amount (mm) within the 750 kms of the center. Bottom  
311 panels : daily rainfall over Northern Somalia and Djibouti and in the two following days (“post-TC”).

312 - VSCS Gati (November 2020)

313 Gati is a recent example of a VSCS which showed an explosive intensification from a low pressure area  
314 located in the central Arabian Sea on 20 November 2020. Moving westwards (fig.6), it made landfall  
315 near Hafun in northeastern Somalia on 22 November as a VSCS. Gati quickly weakened as it crossed  
316 land, with a last warning issued on 23 November over the gulf of Aden. It resulted in maximum daily  
317 rainfall exceeding 100-200 mm every day from 20 to 23 November over the WAS, and in northeastern  
318 Somalia (fig.7) several stations recorded daily rains over 70 mm on 22 and 23 November (e.g., at the  
319 hyper-arid station of Bosaso, 128 mm on 23 November, i.e. 780% of the 51-yr MAR). Rainfall was lower  
320 further west, though an IMERG estimate of 180 mm is still noted in the Gulf of Aden on 24 November,  
321 and 65 mm recorded at Berbera on 25 November. Weaker rains were observed in Djibouti, but  
322 remnants of the storm brought heavy local rains on 25-26 November in eastern Ethiopia. 42,000  
323 people were displaced in Bari region, Puntland, Northeastern Somalia, with extensive damages due to  
324 flash floods, coastal submersion and winds (OCHA, 2020).

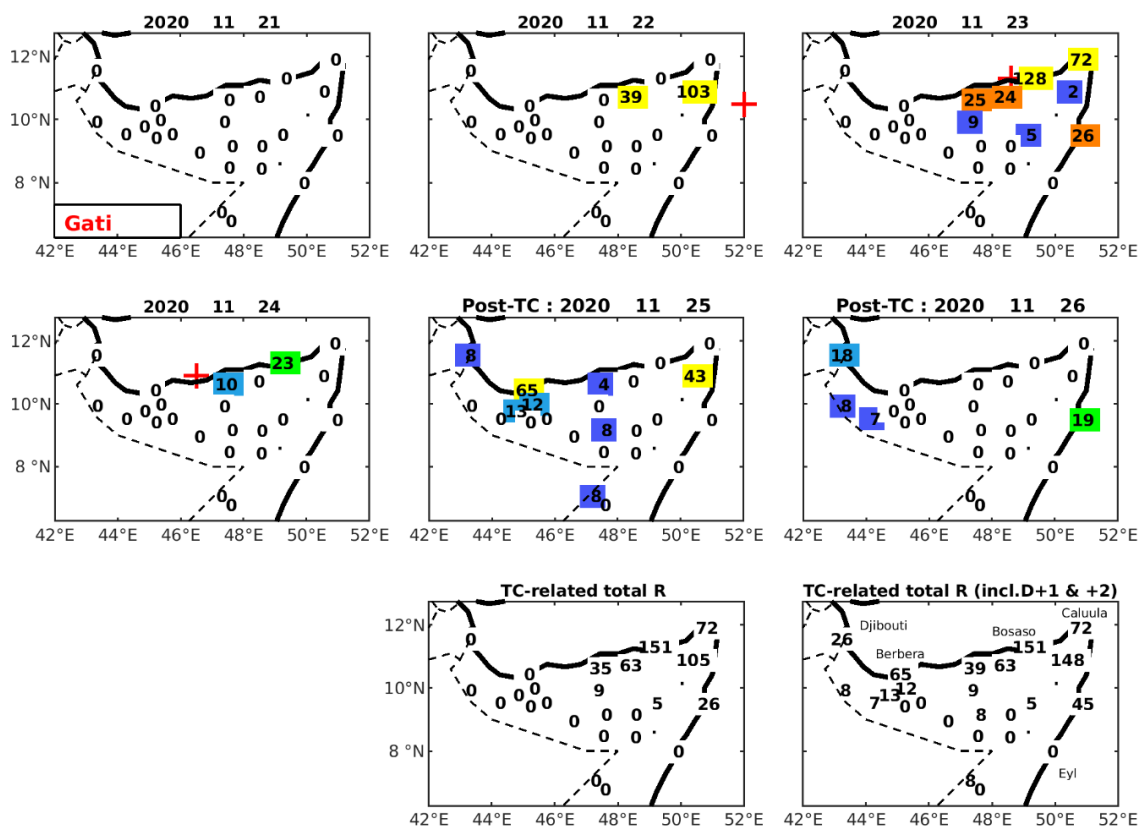
325 Although Gati had a trajectory roughly similar to that of Sagar, the heavy rains were felt more in the  
326 eastern than in the western part of its track. A detailed meteorological analysis is again out of scope,  
327 but the early landfall of Gati explained its fast weakening, hence the weaker rains in Western  
328 Somaliland and Djibouti. The more curvilinear path of Sagar, over the very warm Gulf of Aden (XBT  
329 soundings indicated that water temperature exceeded 27°C up to a depth of at least 29m, not shown),  
330 provided a considerable heat flux which was sufficient to feed Sagar, despite its relatively slow motion.



331

332

Figure 6 : same as figure 3 but for VSCS Gati



333

334

Figure 7 : same as figure 4 but for VSCS Gati.

335

336 - VSCS 12A (October 1972) :

337 Although rainfall maps are not available for this disturbance, since it predates the satellite era, it is an  
338 interesting case typical of the probable underreporting of some TC-related rainfall in the region, in this  
339 case due to incomplete TC tracks before 1982. Storm 12A originated from the southern Arabian Sea,  
340 moving northwestward to cross Socotra Island. It was classified as a VSCS (64-82 knots) just before its  
341 landfall over Socotra, then continued westwards while weakening. According to IBTrACS, this storm  
342 was last located at 12.2°N, 50.8°E, i.e. 20 km north of Caluula, near Cape Guardafui, on 25 October  
343 12:00 (with perfect agreement between the three IBTrACS sources). Yet the October 1972 monthly  
344 weather report in Djibouti (Résumé Mensuel du Temps, 1972) indicated that the storm, after entering  
345 the Gulf of Aden on 25 October at a speed of 5-6 knots, further penetrated westward with increased  
346 velocity (25-30 knots) and reached Djibouti in the morning of 27 October. Wind gusts of 36 knots were  
347 reported at Djibouti-Airport, 45 knots at Arta 40 km westwards. The track of this TC, along the Gulf of  
348 Aden, is therefore closer to Sagar in 2018 than Gati or ARB01. The relatively small size of the tropical  
349 systems which enter the Gulf of Aden, like storm 12A, may, before the satellite era, have resulted in  
350 their underreporting.

351 Exceptionally high rains fell in the Djibouti area (201 mm at Djibouti-Airport on 27 October, 118% of  
352 the MAR), over the Gouda mountains (at Randa, 133 mm on the same day, 94 mm on 28 October) and  
353 at the usually very dry northern coastal station of Obock (105 mm on 27-28 October, compared to a  
354 MAR of only 73 mm). Rainfall quickly decreased further west, with only 2 mm at Dikhil and no rain at  
355 all at As Eyla. There is no daily data available from the northern coast of Somalia, while heavy rains fell  
356 further south in Central Somalia, but unlikely to be directly TC-related. Stations located over the  
357 Northern Somalia Highlands, though close to the Gulf of Aden, reported only little rainfall (Hargeysa 6  
358 mm on 28-29 October 1972), suggesting that the storm was of moderate size at this stage. There is  
359 only scanty information to assess the human losses and damages resulting from the storm. In Djibouti  
360 60 people were reported dead and 5000 homeless. In Somalia, a third of the coastal palm groves in  
361 northeastern Somalia were destroyed by the storm, with long-lasting effects on spring discharges due  
362 to landslides (Chazée, 2017).

363 Overall, several inferences can be made from these four case studies. First, although defining the exact  
364 zone of TC-related rainfall is uneasy, it is clear (e.g., fig.3) that on several days this area extends beyond  
365 500 km from the TC center. Second, in the two days following the reported termination date of the  
366 system, substantial rainfall, especially over land where the disturbance does not meet all the criteria  
367 to qualify as a tropical storm, is associated with remnants of the TC. Land rainfall related to the TC  
368 matches reasonably well between IMERG and rain-gauge data, though a detailed comparison is out of

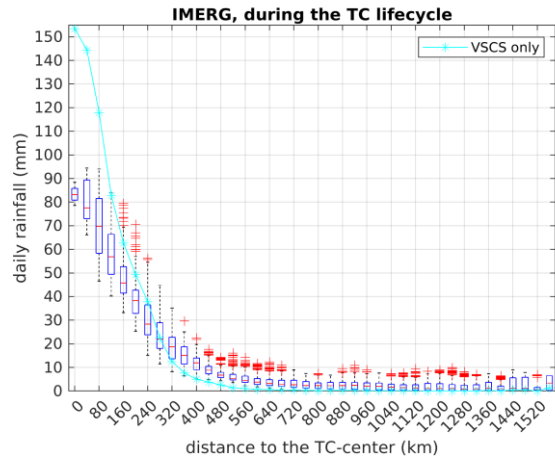
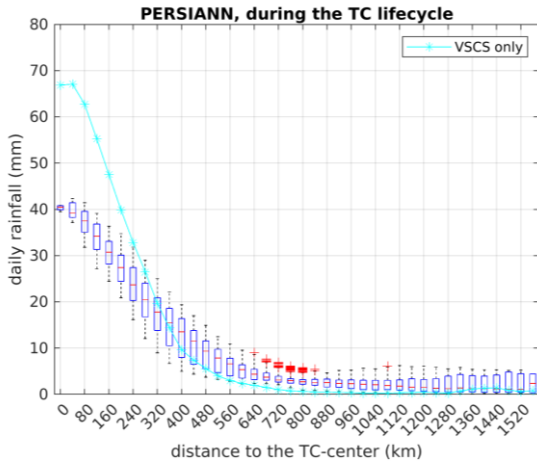
369 scope. Lastly, intense rainfall, with little relationship to the storm category, can be observed at arid  
370 locations. For instance, in northeastern Somalia, rainfall from deep depression ARB01/2013 (35 to 198  
371 mm) often equals or exceeds MAR, which is as little as 15 to 200 mm. Over the ocean, even higher  
372 rainfall amounts are found in IMERG, but they are highly localized.

### 373 3.3 Statistics of rainfall associated with TC occurrence

374 This section aims to produce a statistical analysis of TC-related rainfall, over the period 2000-2020 for  
375 which cyclone data are very reliable and different sources of rainfall data are available. Rainfall on TC-  
376 days is plotted as a function of the distance to the TC center, for PERSIANN and IMERG (figure 8). Both  
377 plots clearly show an exponential decay from the center. However, close to the center, rainfall is more  
378 intense in IMERG (83 mm at 0-20 km) than in PERSIANN (41 mm). This is partly due to the higher spatial  
379 resolution of IMERG, which better resolves very intense but highly localised downpours, and to the  
380 algorithm and input data used to estimating rainfall, which include microwave and radar data in  
381 IMERG. When screening for VSCS only (turquoise lines on fig.9), even higher rainfall is noted close to  
382 the TC center. Gaona et al. (2018) showed the added value of IMERG in depicting rainfall intensities  
383 close to the TC center.

384 After a strong decrease of rainfall amounts with increasing distance, the slope markedly reduces  
385 beyond 400 to 500 km, before gradually flattening out. The distance from which rainfall decreases  
386 becomes negligible and a mere straight line is around 600 km for IMERG and 700 km for PERSIANN.  
387 Given that the boxplot height is smallest around 750 km in PERSIANN, we retain this distance as a  
388 conservative threshold below which rainfall is considered as TC-related (and referred to as such  
389 hereafter). This distance is greater than in most previous studies (500 km), but it is justified by the fact  
390 the daily time-scale used in this study involves some propagation of the TC in a 24-hr period.  
391 Additionally, a cursory look at individual cyclones confirmed that a 500 km radius would exclude, in  
392 some cases, areas of convective activity which are clearly part of the disturbance. Note that for VSCS  
393 only, the drop to very low rainfall occurs at a slightly shorter distance, despite the much higher core  
394 intensities, suggesting more compact disturbances.

395

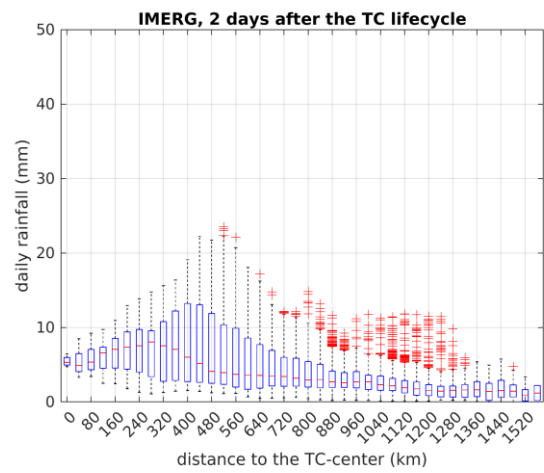
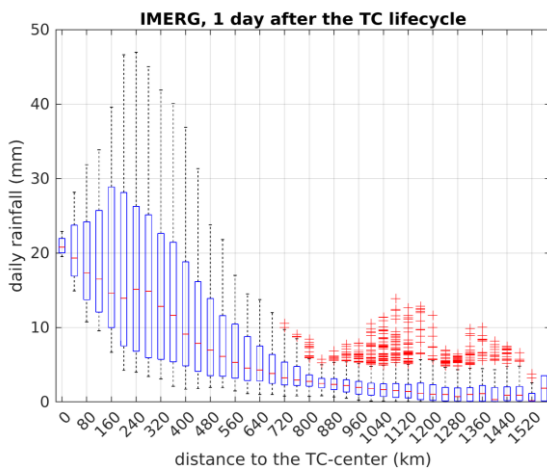


396

397

(a)

(b)



398

399

(c)

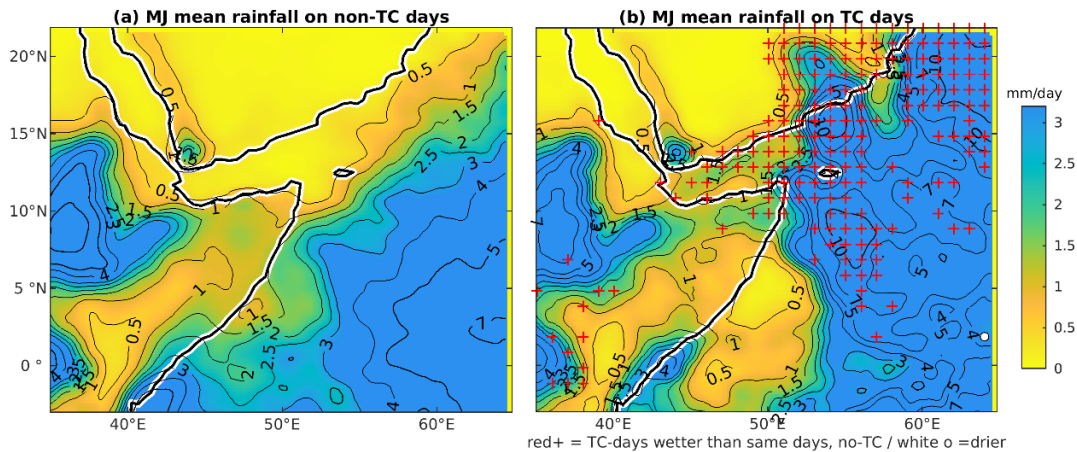
(d)

400 Figure 8 : Boxplots of mean daily rainfall observed on TC-days over the WAS, as a function of the  
 401 distance to the TC center, using PERSIANN (a) and IMERG (b) data for 2000-2020. Bottom row : mean  
 402 IMERG daily rainfall a day (c) and two days (d) after the end of the TC lifecycle (the TC center refers  
 403 to its last known location). The spread of the boxplots refers to spatial variations (i.e., in the mean  
 404 rainfall among the pixels located in each distance bin). On panels (a) and (b), turquoise lines and stars  
 405 show the median rainfall observed on VSCS only. Note the different vertical scales.

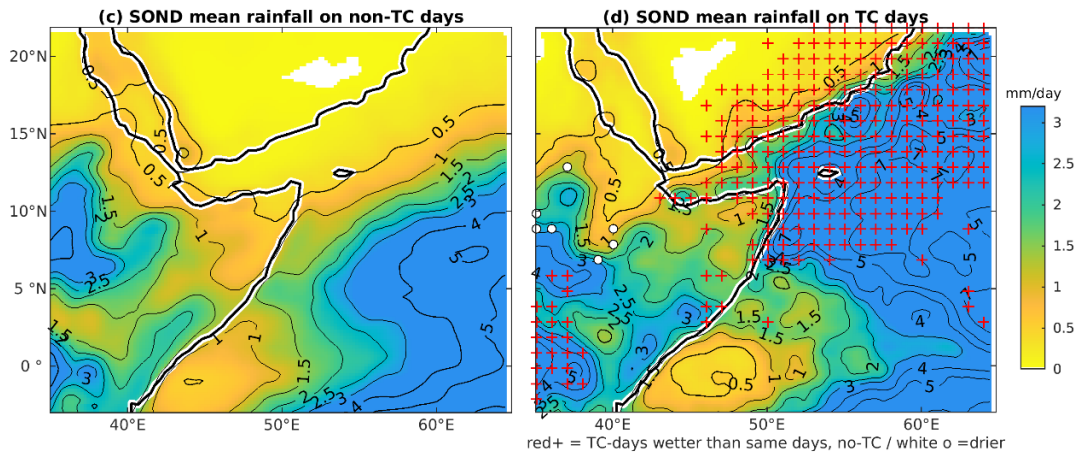
406 As suggested by the above case-studies, TC-related rainfall does not necessarily stop as soon as the TC  
 407 is no longer defined. Figure 8 shows rainfall one (panel c) and two days (panel d) after the TC lifecycle.  
 408 On day+1, heavy rains (median of 21 mm/day) are still found within 20 km of the last known TC  
 409 location. Between 40 and 400 km, although the elongated boxplots denote a diversity of patterns,  
 410 substantial rains (medians from 9 to 19 mm/day) reflect active remnants of the storm. On day+2,  
 411 rainfall markedly decreases, but rains above 5 mm/day (again with a high dispersion) are found up to  
 412 400 km, with a median peaking at 8 mm at 280 km because of the shift of the storm remnants. This

413 suggests that post-TC rainfall cannot be neglected. Hence, in the following, TC-related rainfall will be  
414 considered as the accumulated rainfall during the entire TC lifetime plus the following two days.

415 Mean rainfall on TC days and non-TC days is plotted for MJ and SOND (figure 9). TCs bring substantial  
416 rains in the northwestern Arabian Sea, an otherwise relatively dry area in both seasons. Over the sea  
417 around Socotra and further to the north-east, intensities between 4 and 10 mm/day are recorded on  
418 TC days, while mean rainfall on other days of the same seasons is generally below 1.5 mm/day. The  
419 patterns are quite similar for the two seasons, although more noisy for AMJ because TCs are less  
420 frequent. Near and along the coasts of northern Somalia, southern Yemen, southern Oman and in the  
421 Gulf of Aden, TC-related intensities are lower but in a context of even more arid conditions (<0.5  
422 mm/day on non-TC days). This mostly reflects the smaller number of TCs reaching these areas. Over a  
423 broad area covering the northwestern Arabian Sea and nearby regions, the mean rainfall intensity is  
424 statistically higher (t-test,  $p < 0.05$ ) on TC-days than during the same calendar days for years with no  
425 TCs (i.e., same day climatology: Fig. 9b & d). Interestingly, some significant rainfall anomalies are also  
426 found remotely from the WAS. Over central Ethiopia, localised drier than normal conditions (white  
427 circles) are found in SOND when a TC occurs in the WAS. By contrast, more rains than normal occur  
428 over Western Kenya (36-38°E, 2°S-5°N) in both seasons. This points to the distant effect of TCs, which  
429 will not be addressed here, but was already discussed for Southern Hemisphere cyclones (Shanko and  
430 Camberlin, 1998 ; Finney et al., 2020 ; Kebacho, 2022).



431

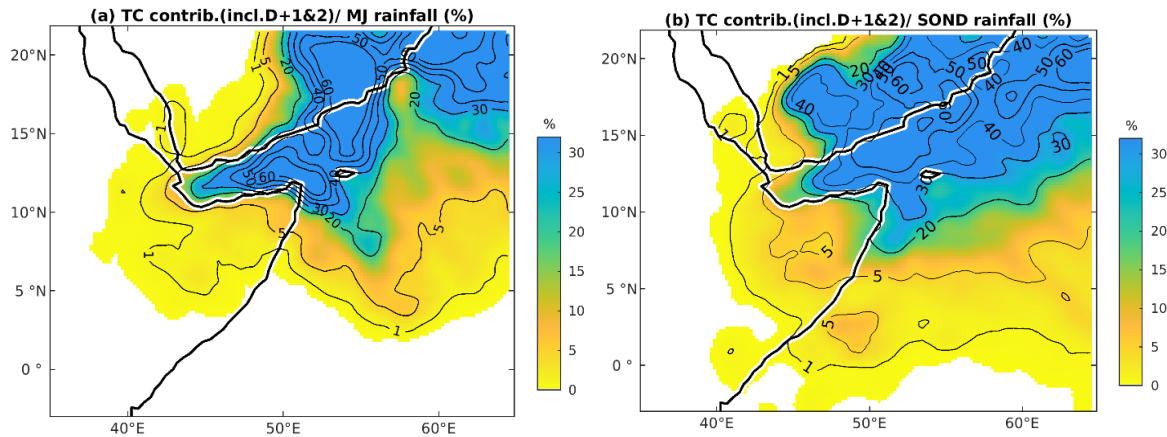


432

433 Figure 9: Rainfall (mm/day) on non-TC days (left panels) and TC days (right panels) for May-June (a,b)  
 434 and September-December (c, d), based on IMERG data (2000-2020). Red plus signs (white circles)  
 435 indicate grid-points where rainfall on TC-days is significantly higher (lower) ( $p < 0.05$ ) than that  
 436 recorded on the same calendar days but with no-TC.

437 TC-related rainfall makes a very high contribution to seasonal rainfall over the Arabian Sea northeast  
 438 of Cape Guardafui (fig.10). Over the northwestern Arabian Sea and Gulf of Aden, contributions reach  
 439 30 to 50% along a belt running from the Gulf of Aden to Socotra island and the Yemen and Oman  
 440 coasts. Contributions are more variable in MJ than SOND due to the small number of disturbances and  
 441 their haphazard tracks. Values locally exceed 60% near the coasts, including inland southern Arabia  
 442 near the border between Oman and Yemen. High contributions are also found at the northeastern tip  
 443 of Somalia (30-50%), quickly decreasing inland. On an annual basis (not shown), contributions exceed  
 444 30%, and even more than 50% over some areas according to PERSIANN. These values are quite  
 445 remarkable given the relatively low occurrence of TCs in this basin. They are higher than those  
 446 published in Prat and Nelson (2013) for the Arabian Sea, for several reasons like the different data set  
 447 they used (TRMM), methodology, and their period of study (1998-2009) which does not include the  
 448 recent very active years. These are among the highest values in the world. Among the cyclonic regions  
 449 examined by Khouakhi et al. (2017), such high contributions are reached over only a few coastal areas

450 in the world, like Northwestern Australia, Baja California, the northern Philippines and Hainan island  
451 in China, although their study did not consider oceanic areas.



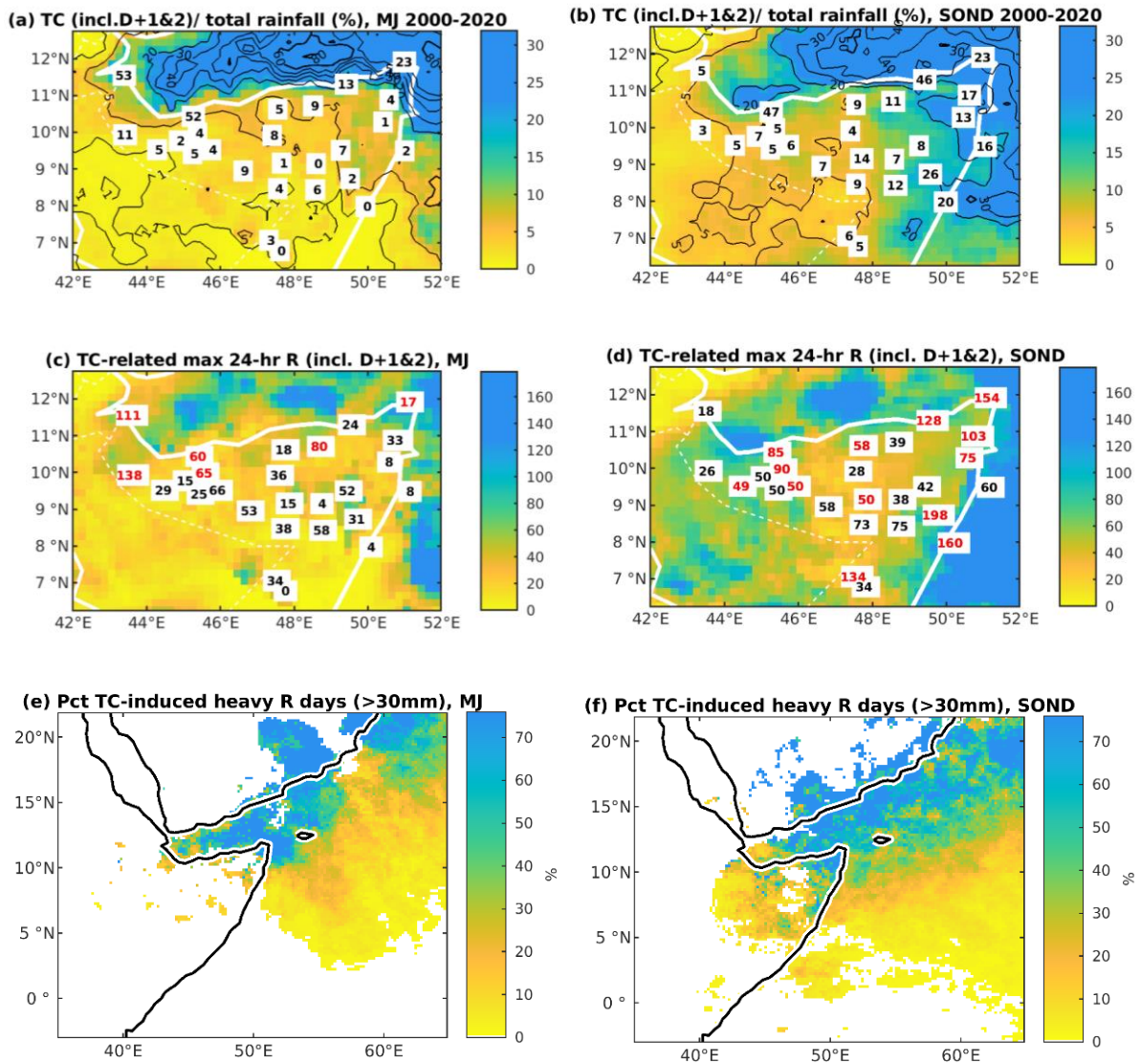
452

453 Figure 10: Percentage contribution of TC-related rainfall to mean seasonal rainfall (IMERG data,  
454 2000-2020), for MJ (a) and SOND (b). TC-related rainfall refers to rainfall within 750 km of the TC  
455 center, during its lifetime or in the next two days

456 Rain-gauge records confirm that over Northern Somalia the contribution of TC-related rainfall is often  
457 moderate, though it strongly increases along the coasts (fig.11). In MJ (fig.11a), it is below 10% inland,  
458 but much higher along the shores of the Gulf of Aden, in agreement with the higher contributions  
459 found over the sea in IMERG. In the western part of the Gulf, a high value (53%) is obtained at Djibouti,  
460 much higher than IMERG (10%). In agreement with IMERG, and with the exception of the Gulf of Aden,  
461 SOND contributions (fig.11b) are generally higher than in MJ, due to a larger number of TCs. A broad  
462 east to west decrease is noted, which highlights the dominant westward tracks (figure 2). However,  
463 arid stations along the Gulf of Aden get SOND contributions as high as 46% (Bosaso) and 47% (Berbera).  
464 Given the small number of TCs making landfall over the GHA, these are exceptionally high  
465 contributions.

466 The importance of TCs on rainfall is further underlined by focusing on intense rainfall events. Rain days  
467 recording more than 30 mm (IMERG data) are examined to find out how much TCs were contributing  
468 to these events. Over most of the Horn of Africa, the northern Arabian Sea, and moreover the southern  
469 Arabian Peninsula, the number of intense rainfall days is small (frequency <1%, i.e. less than 0.6  
470 day.year<sup>-1</sup> in MJ and 1.2 in SOND, not shown). Conspicuously, a large share of these days (>40%, fig.  
471 11e-f) is brought by TCs in the northwestern Arabian Sea and the Gulf of Aden, and in northeastern  
472 Somalia in SOND. This share even exceeds 60% over a belt extending from NE to SW along and offshore  
473 the Arabian Coast.

474



475

476

477 Fig. 11: Rainfall statistics associated with TCs over Northern Somalia, Djibouti and neighbouring  
 478 areas, based on rain-gauge data (figures) and IMERG (shadings), for MJ (left panels) and SOND (right  
 479 panels). Percentage contribution of TC-related rainfall to mean seasonal rainfall (a,b) ; maximum TC-  
 480 related 24-hr rainfall in mm (c,d) ; percent of days above 30 mm which are TC-induced (e,f), 2000-  
 481 2020. In panels c,d, a value in red indicates that it is the highest 24-hr amount recorded at a given  
 482 station in the respective season. TC-related rainfall refers to rainfall within 750 km of the TC center,  
 483 during its lifetime or in the two following days.

484 Rain-gauge data for northern Somalia and Djibouti confirm that in SOND at many stations the highest  
 485 24-hr rainfall is attributed to a TC (figure 11d). In general, the maximum TC-related 24-hr rainfall is  
 486 over 50 mm in this season, reaching values beyond 100 mm in most of the eastern stations. This is  
 487 broadly in line with IMERG values. In MJ (figure 11c), the highest TC-related 24-hr rainfall amounts are  
 488 lower over the continent, and clearly more patchy (over the sea as well) as a result of fewer TCs.

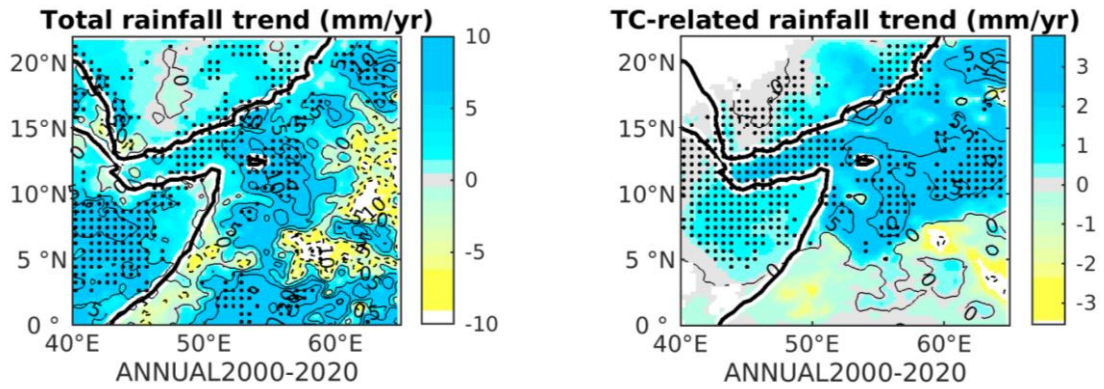
489 Interestingly, high values are nevertheless obtained in the north-west (60 mm at Berbera, 111 mm at  
490 Djibouti and 138 mm at Borama). Very intense rains are also associated with TC landfall over Oman (in  
491 Salalah for example, the absolute maximum rainfall measured during 1990-2020, 238.8 mm, was  
492 associated with the passage of cyclone Mekunu on May 25, 2018), but TC occurrence in this country is  
493 more thoroughly discussed in Pedgley (1969) and Al-Manji et al. (2021). Though IMERG also shows high  
494 values in the Gulf of Aden itself, near the coast satellite estimates are often lower than the observed  
495 contributions, because occasional very heavy precipitation along the coast are not always adequately  
496 resolved by the gridded products. Such an underestimation of coastal intense precipitation in gridded  
497 products is found in other parts of Africa (e.g., the Guinea Coast ; Kpanou et al. 2021).

498 On the whole, despite the high expected variability associated with extreme point rainfall, relatively  
499 consistent patterns emerge in the northeastern Horn of Africa, which confirm the strong role of TCs  
500 on intense rainfall along the northern and eastern coasts in SOND, around the gulf of Aden in MJ, as  
501 well as a substantial contribution inland but in SOND only.

#### 502 3.4 Trends in rainfall and TC-related rainfall

503 Annual rainfall trends are first analysed over the period 2000-2020 (fig.12a). For IMERG data, positive  
504 trends largely dominate, with the largest values (+5 to 10 mm/yr) over inland Somalia and much of the  
505 WAS and Western Indian Ocean, although pockets of negative trends are found further offshore,  
506 notably around 5°N-60°E. There is some uncertainty about these negative trends, as PERSIANN data,  
507 over the same period, display positive trends even far offshore (not shown). Weaker but statistically  
508 significant positive trends ( $p < 0.05$ ) are found over the Gulf of Aden. When focusing on TC-related  
509 rainfall only (fig.12b), there are widespread positive trends for both IMERG and PERSIANN data, though  
510 their magnitude is smaller, except over the Arabian Sea near 10-12°N where trends over +5mm/yr are  
511 noticed. The latter are statistically significant, as well as the (weaker) positive trends which are found  
512 over the Gulf of Aden and neighbouring areas (Djibouti, Yemen, northwestern Somalia). The  
513 contribution of TCs to total rainfall shows significant positive trends over the same regions, with a 21-  
514 yr increase ranging from 20 to 35 points over the areas where the change is the largest, i.e. part of the  
515 WAS, the coasts of Oman and Yemen, and the Gulf of Aden (fig. 12d). When removing TC-related  
516 rainfall from total amounts (fig.12c), trend patterns become close to zero or weakly positive in the  
517 northern part of the region, suggesting that much of the recent increased rainfall is due to the more  
518 frequent (and more intense) TCs. Over the African continent, apart from some coastal areas, there is  
519 little difference between the total and non-TC-related rainfall trends, despite the trend associated with  
520 TCs being significant, because TCs only contribute to a minor fraction of the rains.

521

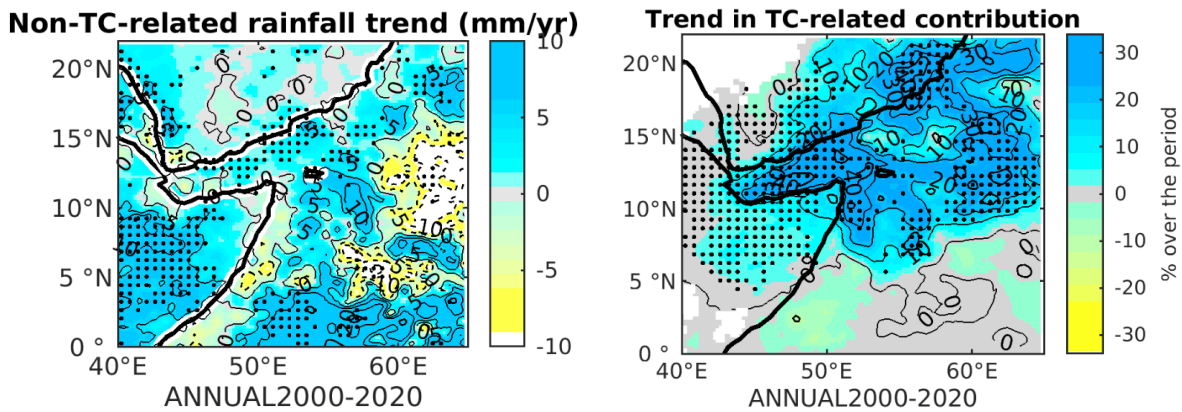


522

523

(a)

(b)



524

525

(c)

(d)

526 Figure 12 : Trends in annual rainfall, IMERG, 2000-2020. Total rainfall (a), TC-related rainfall (b), non-  
 527 TC related rainfall (c) and contribution of TC-related rainfall to the rainfall total (d). Dots indicate  
 528 significant trends ( $p < 0.05$ ) according to the Mann-Kendall test statistic.

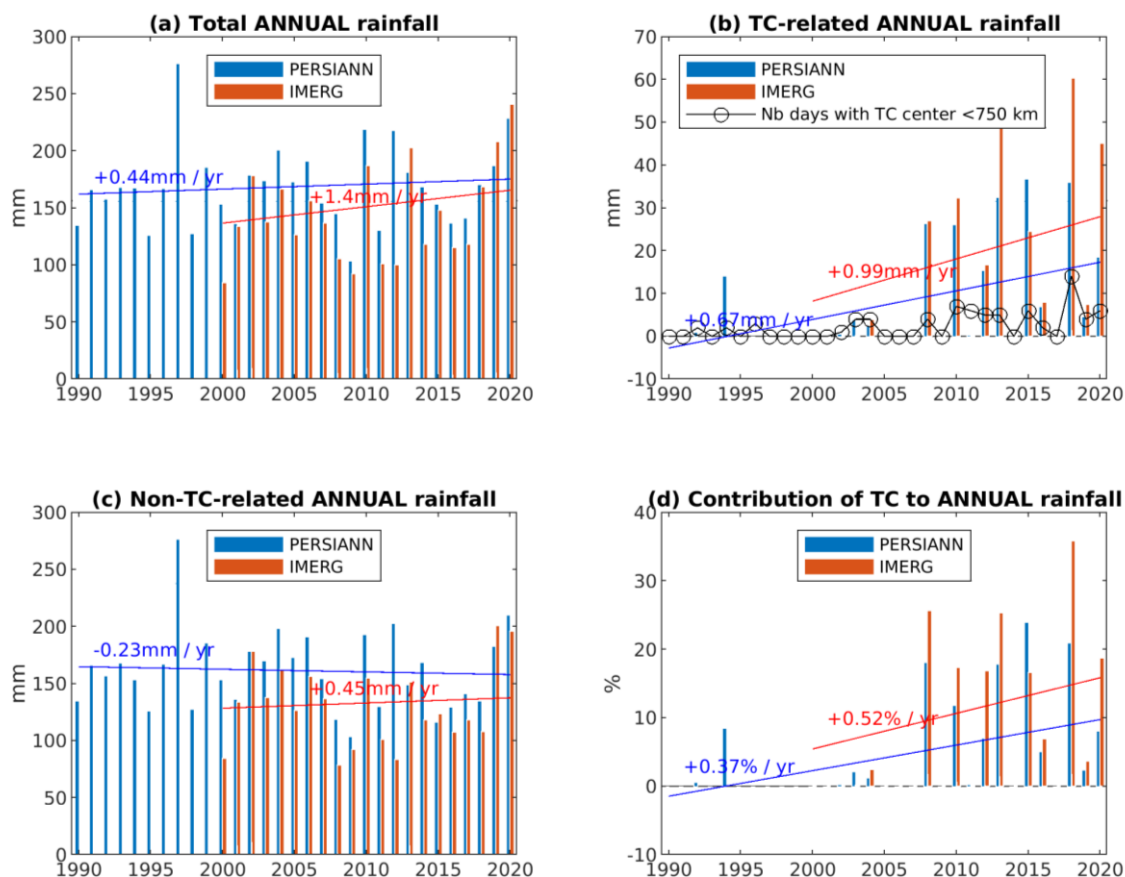
529

530 A seasonal analysis (not shown) indicates that these trends are found during both MJ and SON,   
 531 although they are stronger and spatially more consistent for SON. During this season, a very strong   
 532 and significant ( $p < 0.05$ ) increase in the TC contribution is noted between 10 and 17°N. In the 21-yr   
 533 period 2000-2020, the contribution of TCs to SON rainfall amounts increased by 30 to 50% in the Gulf   
 534 of Aden and the Arabian Sea east of Socotra island. A similar rise is found from the Gulf of Aden to   
 535 southern Oman in MJ, but it is more patchy and seldom significant, due to the rare occurrence of TCs   
 536 in the pre-monsoon season, resulting in many years (even in the more recent period) with nil TC-   
 537 related rainfall.

538 For a better appraisal of trends over the Gulf of Aden and its shores, a regional rainfall index (location   
 539 shown on figure 1) is extracted and plotted in figure 13. For PERSIANN, the time-series were extended

540 to include the full period from 1990 to 2020. Total rainfall shows a weak positive long-term trend  
 541 (+0.44 mm/yr from 1990 to 2020, i.e. +8% in 31 years). TCs strongly contribute to this trend, as shown  
 542 by the conspicuous increase in TC-related rainfall (+0.67 mm/yr fig.13b). If one deducts TC-related  
 543 rainfall from the annual rainfall, the trend becomes slightly negative (-0.23 mm/yr, i.e. about -4% in  
 544 31 years). The contrast between the almost absence of any TC in the sub-period 1990-2007 and the  
 545 relatively frequent TCs in the sub-period 2008-2020 is noteworthy. Besides the higher frequency of  
 546 TCs, rainfall associated with each TC tends to significantly increase between 1990 and 2020 (Mann-  
 547 Kendall tau,  $p < 0.01$ , not shown).

548 Over the period common to the two data sets, IMERG data show a relatively good agreement with  
 549 PERSIANN in the interannual variations of total and TC-related rainfall. Over this period (2000-2020),  
 550 the increase in TC-related rains is strong (+0.99 mm/yr in IMERG, fig.13b). This trend also strongly  
 551 contributes to the overall rainfall trend (+1.40 mm/yr), while the non-TC-related trend is weaker. As  
 552 described above, there is a marked increase in the contribution of TCs to total rainfall, which was close  
 553 to zero before 2007 and reached 9.3% in 2008-2020.



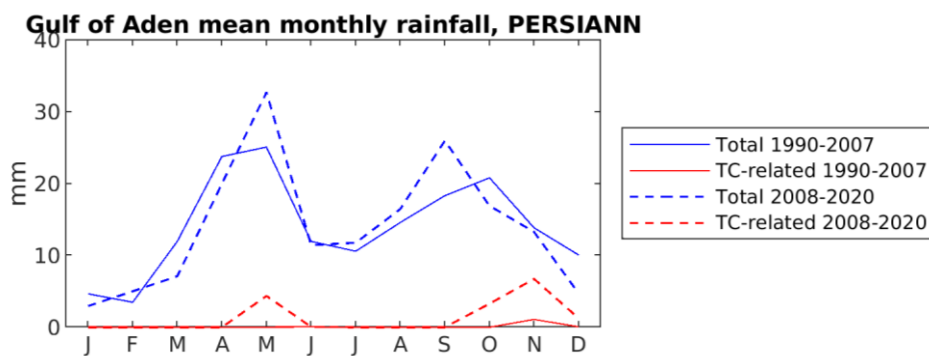
554

555 Figure 13 : Annual rainfall variations and trends over the Gulf of Aden and its shores (44-50°E, 10-  
 556 14°N): total rainfall (a), TC-related rainfall (b), non-TC-related rainfall (c), and contribution of TCs to  
 557 total rainfall (d).

558 The increase concerns both cyclonic seasons, although pre-monsoon TCs are still a rarity in the Gulf of  
 559 Aden (fig.14). The increase in TC-related rainfall boosts the May rainfall peak in the second sub-period,  
 560 and strongly contributes to alleviate the decrease which would have otherwise been found in October-  
 561 December. At that time, TCs have a strong effect on rainfall amounts in the arid environment of the  
 562 Gulf of Aden. In the sub-period 2008-2020, the increase in the frequency of TCs makes the contribution  
 563 of TCs to total October-December rainfall reach 32.4%, from 2.5% in 1990-2007. These statistics are  
 564 based on a sufficient number of events to be meaningful: during this season, from 2008 to 2020, 17  
 565 TCs hit the Gulf of Aden or approached it (within the 750 km radius), as against only 4 in the previous  
 566 sub-period.

567 The on-and-off TC activity in the Gulf of Aden (and the Arabian Sea in general) is a conspicuous feature  
 568 (fig.13). Roy Chowdhury et al. (2020) showed that the positive Indian Ocean Dipole (IOD) event that  
 569 occurred in 2015 stimulated the development of the dual TCs Chapala and Megh in the WAS in  
 570 October-November, through a warmer than normal western Indian Ocean and lower sea-level  
 571 pressure. Similar conclusions were reached by Akhila et al. (2022), who studied cyclones Kyarr and  
 572 Maha in 2019, a positive IOD year. However, Yuan and Cao (2013) and Sattar and Cheung (2019) got  
 573 more ambiguous results on the systematic role of the IOD on Arabian Sea cyclones.

574



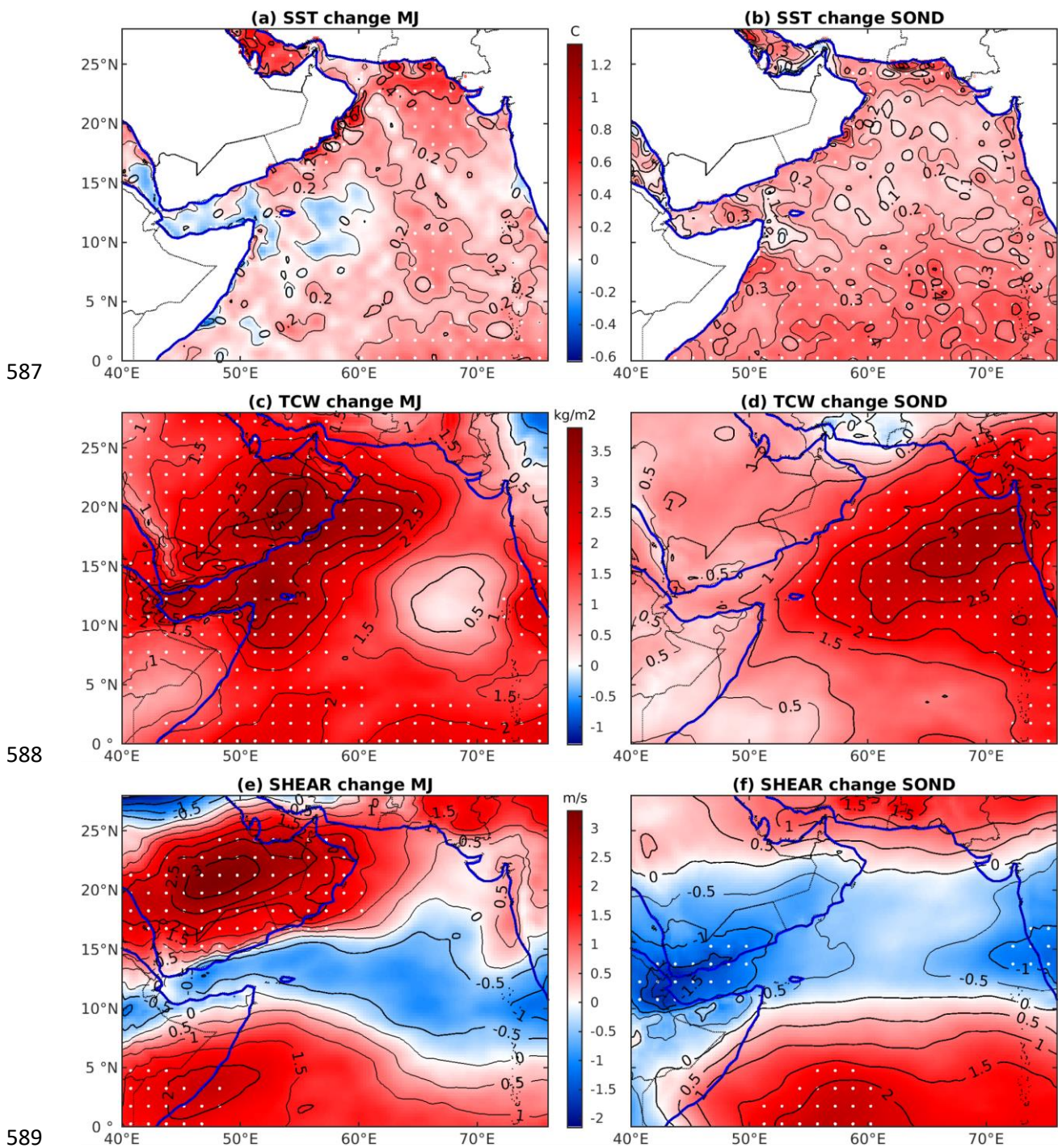
575

576 Figure 14: Mean monthly rainfall over the Gulf of Aden area (PERSIANN data ; IMERG data not shown  
 577 because of the small number of years available in the first sub-period), for 1990-2007 (solid lines) and  
 578 2008-2020 (dashed). Blue lines: total rainfall; red lines: TC-related rainfall.

### 579 3.5 Regional changes contributing to the TC increase

580 The changes in the oceanic and atmospheric conditions which may have accounted for the recent  
 581 increase in the number of TCs or severe storms in the Arabian Sea have been partly documented by  
 582 Deo et al. (2011), Deshpande et al. (2021) and Tiwari et al. (2022). This issue is further documented  
 583 here, separately for the two cyclonic seasons, and by taking into account the detection of a change-  
 584 point (in 2010) in the number of TC days in the WAS (figure 2). Differences between the sub-periods

585 1990-2009 and 2010-2020 are plotted in figure 15 using ERA5 reanalysis data (similar results are  
 586 obtained using the NCEP-NCAR reanalysis).



590 Figure 15: Changes in sea-surface temperature (a-b), total column water (c-d) and vertical wind shear  
 591 (e-f) from 1990-2009 to 2010-2020, for the MJ and SON seasons (ERA5 data). White dots indicate  
 592 statistically significant changes (t-test,  $p < 0.05$ ). The change in wind shear is computed as the  
 593 magnitude change between 200 and 850 hPa wind vectors (Pillay and Fitchett 2021).

594 The tripling of the number of days with TCs between 1990-2009 (4 days per year) and 2010-2020 (13  
 595 days per) in the WAS is found to be associated with three features favourable to TC activity :

596 (1) a decrease in vertical wind shear between 200 hPa and 850 hPa in a belt running from India to the  
597 Gulf of Aden, in both seasons (the decrease is significant in SOND only ; fig.15e-f)

598 (2) a sharp increase in relative humidity in the mid-troposphere (700 to 500 hPa) and of total column  
599 water (fig.15 c-d), mainly in the northwestern part of the region in MJ and in the eastern part in SOND

600 (3) an increase in sea surface temperature (SST, fig. 15a-b), which is more widespread in SOND than in  
601 MJ (for the latter, the Gulf of Aden and neighbouring areas do not show any clear warming)

602 The main source region of TCs, i.e. the southeastern Arabian Sea, displays the strongest sea surface  
603 warming, which may account for more favourable conditions for TC genesis, given that other factors  
604 in the same region (wind shear, atmospheric moisture) also tend to be more favourable. In the WAS,  
605 it is the strong increase in total column water vapour, in MJ, and the reduced wind shear, in SOND,  
606 which seem to constitute the key triggers, likely enabling existing systems to have a longer lifetime or  
607 to intensify. Part of these changes denote the effect of decadal-scale variability, since during the pre-  
608 monsoon vertical wind shear in the WAS for the decade 2000-09 was higher than in 1990-99. This  
609 impacted the lower cyclone activity during part of the first sub-period. Deshpande et al. (2021) also  
610 pointed to an increase of TC genesis at lower latitudes, which due to the dominant easterlies across  
611 the Somalia and Yemen shorelines, contribute to the increased number of WAS cyclones during the  
612 most recent period (examples of 03A in November 2013, Sagar in 2018, Gati in 2020). It is unclear  
613 whether these trends denote changes in TC activity due to anthropogenic climate change, but the  
614 Arabian Sea is one of the ocean basins where models most consistently project a forthcoming increase  
615 in intense TCs (Murakami et al. 2013; Knutson et al., 2015 ; Bell et al. 2020).

#### 616 4. Conclusions

617 The northwestern Arabian Sea and adjacent land areas are among the few regions of the world where  
618 tropical cyclones occur in an arid context. Their contribution to rainfall and associated trends was  
619 analysed using two combined satellite-rain-gauge precipitation products (PERSIANN and IMERG) and  
620 daily rain-gauge data for northern Somalia and Djibouti. Based on case studies and a statistical analysis  
621 of rainfall amounts with respect to the distance to the TC center, it was found that rainfall was  
622 influenced by TCs over a wide area (up to 750 km from the center), and that heavy rains still occurred  
623 one to two days after the TC lifecycle. Despite the rare occurrence of tropical systems (1.5 per year,  
624 whatever the category, with a third making landfall), they strongly contribute (30-50%) to mean annual  
625 rainfall over the northwestern Arabian Sea, Gulf of Aden and their respective coastlines. On a seasonal  
626 basis, this contribution is even higher (40-60 %) in southern Arabia and the adjacent oceanic areas, for  
627 both cyclonic seasons (May-June and September-December). High values were also found at the Gulf  
628 of Aden stations in Somalia in SOND. Over inland northern Somalia, contributions are lower in MJ

629 (generally <5%) and SONND (5 to 20%, increasing eastwards). In a belt running northeastward from the  
630 Gulf of Aden, a large proportion (30-70%) of heavy rain days (>40 mm) are associated with TCs. In  
631 northern Somalia, many 24-hr maximum rainfall amounts are TC-related.

632 From 1990 to 2020, the number of tropical systems showed a marked increase in the region, hence  
633 their enhanced contribution to rainfall totals. Part of the overall upward rainfall trend over the  
634 northwestern Arabian Sea, is actually the outcome of increasing cyclonic activity. Though over the Gulf  
635 of Aden and neighbouring regions of the Horn of Africa (northern Somalia, Djibouti), TCs are very  
636 infrequent, the trend in TC-related rainfall shows a consistent and significant increase, highlighted by  
637 the contrast between the subperiods 1990-2007 and 2008-2020. Both cyclonic seasons are involved in  
638 this increase. The increase in TC frequency is related to a SST increase in the eastern and southern  
639 Arabian Sea, a decrease in vertical wind shear, and a strong increase in tropospheric moisture content.

640 Some caution should be exerted on the interpretation of these trends, which may not necessarily  
641 reflect the effect of anthropogenic climate change. Murakami et al (2013) noted that, under increased  
642 greenhouse gases scenarios, a future westward shift of the mean locations of tropical storms is  
643 projected over the North Indian Ocean during the post-monsoon season (matching the recent increase  
644 in TC days in the WAS). Murakami et al. (2017) found that anthropogenic forcing has likely increased  
645 the probability of post-monsoon severe cyclonic storms over the Arabian Sea. Wang et al. (2023)  
646 likewise found a potentially dominant role of anthropogenic forcing on coastal TC frequency changes  
647 in many basins of the world, including the western coast of the Arabian Sea, but for the latter region  
648 their simulations failed to specifically attribute these changes to the effect of aerosol or greenhouse  
649 gases. Additionally, the low number of TCs in the early part of the period should also be considered in  
650 a broader context, since Rajeevan et al. (2013) showed a decrease in the frequency of intense TCs in  
651 the Arabian Sea from the period 1955-1973 to 1974–1992, suggesting large decadal-scale variability in  
652 the basin. Evan and Camargo (2011) questioned spurious increases in Arabian Sea TC intensity, which  
653 could explain part of the rise in cyclonic storm days they noted between 1979-1991 and 1992-2008  
654 over the Arabian Sea as a whole. Duplicating this study for future periods is now needed, although this  
655 discussion highlights that internal climate variability cannot be neglected to obtain robust projections  
656 of TC activity, and their impacts on rainfall. Large ensembles from the CMIP6 (Eyring et al. 2016) or  
657 MENA-CORDEX (Bucchignani et al. 2015) modelling exercises could be used for that purpose.

658

## 659 Acknowledgements

660 The authors thank the National Meteorological Agency (ANM) of Djibouti for the provision of daily  
661 rainfall data for the Republic of Djibouti and SWALIM for northern Somalia. SWALIM is a project

662 managed by FAO with funding from The European Union, The Swiss Agency for Development and  
663 Cooperation, The Italian Cooperation, DFID, USAID and the Government of France. Calculations were  
664 performed using HPC resources from DNUM CCUB (Centre de Calcul de l'Université de Bourgogne).

665

## 666 References

667 Abdalla, O., & Al-Abri, R. B. Y. (2011). Groundwater recharge in arid areas induced by tropical  
668 cyclones: lessons learned from Gonu 2007 in Sultanate of Oman. *Environmental Earth Sciences*, *63*,  
669 229-239.

670 Akhila, R.S., Kuttippurath, J., Rahul, R. *et al.* (2022). Genesis and simultaneous occurrences of the  
671 super cyclone Kyarr and extremely severe cyclone Maha in the Arabian Sea in October 2019. *Nat*  
672 *Hazards* *113*, 1133–1150. <https://doi.org/10.1007/s11069-022-05340-9>

673 Al-Manji, S., Mitchell, G., and Al Ruheili, A. (2021). Arabian Sea Tropical Cyclones: A Spatio-Temporal  
674 Analysis in Support of Natural Hazard Risk Appraisal in Oman. in R.S. Meena (ed.) : *Agrometeorology*.  
675 IntechOpen. doi:10.5772/intechopen.96961.

676 Ashouri, H., Hsu, K. L., Sorooshian, S., Braithwaite, D. K., Knapp, K. R., Cecil, L. D., ... & Prat, O. P.  
677 (2015). PERSIANN-CDR: Daily precipitation climate data record from multisatellite observations for  
678 hydrological and climate studies. *Bulletin of the American Meteorological Society*, *96(1)*, 69-83.

679 Baburaj, P.P., Abhilash, S., Mohankumar, K., Sahai, A.K. (2020). On the epochal variability in the  
680 frequency of cyclones during the pre-onset and onset phases of the monsoon over the North Indian  
681 Ocean. *Advances in Atmospheric Sciences*, *37*, 634-651.

682 Bell, S.S., Chand, S.S., Tory, K.J., Ye, H. and Turville, C. (2020) North Indian Ocean tropical cyclone  
683 activity in CMIP5 experiments: future projections using a model-independent detection and tracking  
684 scheme. *International Journal of Climatology*, *40(15)*, 6492–6505. <https://doi.org/10.1002/joc.6594>.

685 Breña-Naranjo, J.A., Pedroso-Acuña, A., Pozos-Estrada, O., Jiménez-López, S.A., López-López, M.R.  
686 (2015). The contribution of tropical cyclones to rainfall in Mexico. *Physics and Chemistry of the Earth*,  
687 *Parts A/B/C*, *83-84*, 111-122.

688 Bucchignani, E., Mercogliano, P., Rianna, G., Panitz, H.J. (2015). Analysis of ERA-Interim-driven  
689 COSMO-CLM simulations over Middle East – North Africa domain at different spatial resolutions –  
690 *International Journal Of Climatology* DOI: 10.1002/joc.4559

691 Chazée, L. (2017). *Patrimoine socio-économique et naturel de la région du Cap Gardafui*.  
692 L'Harmattan, Paris, 330 p.

693 Cherel, J. P., Omar Ali, B., Nour Ayeh, M., & Vinet, F. (2020). Activités cycloniques et nouveaux  
694 risques dans le golfe d'Aden. Exemple des impacts socio-économiques du cyclone Sagar sur Djibouti  
695 en mai 2018. *EchoGéo*, 51. <https://doi.org/10.4000/echogeo.18859>

696 Deo, A.A., Ganer, D.W. & Nair, G. (2011). Tropical cyclone activity in global warming scenario. *Nat*  
697 *Hazards* 59,771–786.

698 Deshpande, M., Singh, V. K., Ganadhi, M. K., Roxy, M. K., Emmanuel, R., & Kumar, U. (2021). Changing  
699 status of tropical cyclones over the north Indian Ocean. *Climate Dynamics*, 57, 3545-3567.

700 Englehart, P. J., & Douglas, A. V. (2001). The role of eastern North Pacific tropical storms in the  
701 rainfall climatology of western Mexico. *International Journal of Climatology*, 21(11), 1357-1370.

702 Evan, A. T., & Camargo, S.J. (2011). A Climatology of Arabian Sea Cyclonic Storms. *J. Climate*, 24, 140–  
703 158.

704 Evan, A. T., Kossin, J. P., Chung, C. E. & Ramanathan, V. (2021). Arabian Sea tropical cyclones  
705 intensified by emissions of black carbon and other aerosols. *Nature* 479, 94–97.

706 Eyring, V., Bony, S., Meehl, G. A., Senior, C. A., Stevens, B., Stouffer, R. J., and Taylor, K. E. (2016).  
707 Overview of the Coupled Model Intercomparison Project Phase 6 (CMIP6) experimental design and  
708 organization. *Geosci. Model Dev.*, 9, 1937–1958, <https://doi.org/10.5194/gmd-9-1937-2016>.

709 Finney, D. L., Marsham, J. H., Walker, D. P., Birch, C. E., Woodhams, B. J., Jackson, L. S., & Hardy, S.  
710 (2020). The effect of westerlies on East African rainfall and the associated role of tropical cyclones  
711 and the Madden–Julian Oscillation. *Quarterly Journal of the Royal Meteorological Society*, 146(727),  
712 647-664.

713 Fors, J.R. (1977). *Tropical cyclone Kathleen*. NOAA Technical Memorandum NWS WR-114, 29 p.

714 Gaona, M. F. R., Villarini, G., Zhang, W., & Vecchi, G. A. (2018). The added value of IMERG in  
715 characterizing rainfall in tropical cyclones. *Atmospheric Research*, 209, 95-102.

716 Gray, W. M. (1968). Global view of the origin of tropical disturbances and storms. *Mon. Wea. Rev.*,  
717 96, 669–700.

718 Hari, V., Pathak, A., & Koppa, A. (2021). Dual response of Arabian Sea cyclones and strength of Indian  
719 monsoon to Southern Atlantic Ocean. *Climate Dynamics*, 56, 2149-2161.

720 Hoarau, K., Bernard, J., & Chalonge, L. (2012). Intense tropical cyclone activities in the northern  
721 Indian Ocean. *International journal of climatology*, 32(13), 1935-1945.

722 Huffman, G. J., Bolvin, D. T., Nelkin, E. J., & Tan, J. (2015). Integrated Multi-satellitE Retrievals for  
723 GPM (IMERG) technical documentation. *Nasa/Gsfc Code*, 612(47), 2019.

724 IFRC (2013). International Federation of Red Cross and Red Crescent Disaster Relief Emergency Fund :  
725 Somalia Tropical Cyclone. [https://reliefweb.int/report/somalia/somalia-tropical-cyclone-dref-](https://reliefweb.int/report/somalia/somalia-tropical-cyclone-dref-operation-n-mdrso002-update-no-1)  
726 [operation-n-mdrso002-update-no-1](https://reliefweb.int/report/somalia/somalia-tropical-cyclone-dref-operation-n-mdrso002-update-no-1) Accessed 25 September 2023.

727 Jiang, H., & Zipser, E. J. (2010). Contribution of tropical cyclones to the global precipitation from eight  
728 seasons of TRMM data: Regional, seasonal, and interannual variations. *Journal of climate*, 23(6),  
729 1526-1543.

730 Kabir, R., Ritchie, E.A., Stark, C. (2022). Tropical Cyclone Exposure in the North Indian Ocean.  
731 *Atmosphere*, 13, 1421. <https://doi.org/10.3390/atmos13091421>

732 Kebacho, L. L. (2022). The role of tropical cyclones Idai and Kenneth in modulating rainfall  
733 performance of 2019 long rains over East Africa. *Pure and Applied Geophysics*, 179(4), 1387-1401.

734 Khouakhi, A., Villarini, G., Vecchi, G.A. (2017). Contribution of Tropical Cyclones to Rainfall at the  
735 Global Scale. *J. Climate*, 30, 359–372.

736 Knapp, K. R., Kruk, M. C. , Levinson, D. H. , Diamond, H. J., and Neumann, C. J. (2010). The  
737 International Best Track Archive for Climate Stewardship (IBTrACS): Unifying tropical cyclone best  
738 track data. *Bulletin of the American Meteorological Society*, 91, 363-376.  
739 [doi:10.1175/2009BAMS2755.1](https://doi.org/10.1175/2009BAMS2755.1)

740 Knapp, K. R., Diamond, H. J., Kossin, J. P. , Kruk, M. C., Schreck, C. J. (2018). *International Best Track*  
741 *Archive for Climate Stewardship (IBTrACS) Project, Version 4*. NOAA National Centers for  
742 Environmental Information. [doi:10.25921/82ty-9e16](https://doi.org/10.25921/82ty-9e16) [accessed 23 February 2024].

743 Knutson, T.R., Sirutis, J.J., Zhao, M., Tuleya, R.E., Bender, M., Vecchi, G.A., Villarini, G. and Chavas, D.  
744 (2015). Global projections of intense tropical cyclone activity for the late twenty-first century from  
745 dynamical downscaling of CMIP5/RCP4.5 scenarios. *Journal of Climate*, 28(18), 7203–7224.  
746 <https://doi.org/10.1175/JCLI-D-15-0129.1>.

747 Kpanou, M., Laux, P., Brou, T., Vissin, E., Camberlin, P., & Roucou, P. (2021). Spatial patterns and  
748 trends of extreme rainfall over the southern coastal belt of West Africa. *Theoretical and Applied*  
749 *Climatology*, 143, 473-487.

750 Lavender, S.L., McBride, J.L. (2021). Global climatology of rainfall rates and lifetime accumulated  
751 rainfall in tropical cyclones: Influence of cyclone basin, cyclone intensity and cyclone size. *Int J*  
752 *Climatol.* 41 (Suppl. 1): E1217–E1235.

753 Lvončík, S., Vahalík, P., Bongers, F. et al. (2020). Development of a population of *Boswellia elongata*  
754 Balf. F. in Homhil nature sanctuary, Socotra island (Yemen). *Rend. Fis. Acc. Lincei* 31, 747–759.  
755 <https://doi.org/10.1007/s12210-020-00936-4>

756 Murakami, H., Sugi, M. and Kitoh, A. (2013). Future changes in tropical cyclone activity in the north  
757 Indian Ocean projected by high-resolution MRI-AGCMs. *Climate Dynamics*, 40(7–8), 1949–1968.  
758 <https://doi.org/10.1007/s00382-012-1407-z>.

759 Murakami, H., Vecchi, G. A., and Underwood, S. (2017). Increasing frequency of extremely severe  
760 cyclonic storms over the Arabian Sea. *Nature Climate Change*, 7[12], 885–889.

761 Neumann, C.J. (2017). A Global Tropical Cyclone Climatology. In WMO *Global Guide to Tropical*  
762 *Cyclone Forecasting*, 28-62. [https://cyclone.wmo.int/pdf/Global-Guide-to-Tropical-Cyclone-](https://cyclone.wmo.int/pdf/Global-Guide-to-Tropical-Cyclone-Forecasting.pdf)  
763 [Forecasting.pdf](https://cyclone.wmo.int/pdf/Global-Guide-to-Tropical-Cyclone-Forecasting.pdf)

764 Ng, B., Walsh, K., Lavender, S. (2014). The contribution of tropical cyclones to rainfall in northwest  
765 Australia. *International Journal of Climatology*, 35 (10), 2689-2697. <https://doi.org/10.1002/joc.4148>

766 OCHA Somalia (2020). *Somalia, Tropical Cyclone Gati Update #2. ReliefWeb. UN Office for the*  
767 *Coordination of Humanitarian Affairs. 24 November 2020.* [https://reliefweb.int/report/somalia/ocha-](https://reliefweb.int/report/somalia/ocha-somalia-tropical-cyclone-gati-update-2-24-november-2020)  
768 [somalia-tropical-cyclone-gati-update-2-24-november-2020](https://reliefweb.int/report/somalia/ocha-somalia-tropical-cyclone-gati-update-2-24-november-2020) Accessed 5 December 2023

769 Owuor, A., & David McRae, H. (2022). The Control of the Desert Locusts (*Schistocerca gregaria*) in  
770 Somalia during the Upsurge Between 2019 and 2021. *Outlooks on Pest Management*, 33(6), 221-226.

771 Pedgley, D. E. (1969). Cyclones along the Arabian coast. *Weather*, 24(11), 456-470.

772 Pillay, M. T., & Fitchett, J. M. (2021). On the conditions of formation of Southern Hemisphere tropical  
773 cyclones. *Weather and Climate Extremes*, 34, 100376.

774 Prat, O. P., & Nelson, B. R. (2013). Mapping the world's tropical cyclone rainfall contribution over  
775 land using the TRMM Multi-satellite Precipitation Analysis. *Water Resources Research*, 49(11), 7236-  
776 7254.

777 Priya, P., Pattnaik, S. & Trivedi, D. (2022). Characteristics of the tropical cyclones over the North  
778 Indian Ocean Basins from the long-term datasets. *Meteorol Atmos Phys* 134, 65.  
779 <https://doi.org/10.1007/s00703-022-00904-7>

780 Rajeevan, M., Srinivasan, J., Niranjana Kumar, K., Gnanaseelan, C., & Ali, M. M. (2013). On the epochal  
781 variation of intensity of tropical cyclones in the Arabian Sea. *Atmospheric Science Letters*, *14*(4), 249-  
782 255.

783 Ramsay, H. (2017). The Global Climatology of Tropical Cyclones. *Oxford Research Encyclopedia of*  
784 *Natural Hazard Science*. Retrieved 31 Aug. 2023, from  
785 <https://oxfordre.com/naturalhazardscience/view/10.1093/acrefore/9780199389407.001.0001/acrefore-9780199389407-e-79>.  
786

787 Résumé Mensuel du Temps (1972). *Résumé mensuel du temps en Territoire Français des Afars et des*  
788 *Issas*, Service de la Météorologie, Djibouti, Octobre 1972, 14 p.

789 Ray-Choudhuri, S., Subramanyan, Y. H., & Chellappa, R. (1959). A climatological study of storms and  
790 depressions in the Arabian Sea. *Mausam*, *10*(3), 283-290.

791 Roy Chowdhury, R., Prasanna Kumar, S., Narvekar, J., & Chakraborty, A. (2020). Back-to-back  
792 occurrence of tropical cyclones in the Arabian sea during October–November 2015: causes and  
793 responses. *Journal of Geophysical Research: Oceans*, *125*(6), e2019JC015836.

794 Salih, A. A., Baraibar, M., Mwangi, K. K., & Artan, G. (2020). Climate change and locust outbreak in  
795 East Africa. *Nature Climate Change*, *10*(7), 584-585.

796 Sattar, A. M., & Cheung, K. K. (2019). Comparison between the active tropical cyclone seasons over  
797 the Arabian Sea and Bay of Bengal. *International Journal of Climatology*, *39*(14), 5486-5502.

798 Schreck, C.J., Knapp, K.R., Kossin, J.P. (2014). The impact of best track discrepancies on Global  
799 Tropical Cyclone climatologies using IBTrACS. *Monthly Weather Review*, *142*, 3881-3899.

800 Shanko, D., & Camberlin, P. (1998). The effects of the Southwest Indian Ocean tropical cyclones on  
801 Ethiopian drought. *International Journal of Climatology*, *18*(12), 1373-1388.

802 Singh, K., Panda, J. & Mohapatra, M. (2020). Robustness of best track data and associated cyclone  
803 activity over the North Indian Ocean region during and prior to satellite era. *J Earth Syst Sci* *129*, 84.  
804 <https://doi.org/10.1007/s12040-020-1344-x>

805 Singh, V. K., & Roxy, M. K. (2022). A review of ocean-atmosphere interactions during tropical cyclones  
806 in the north Indian Ocean. *Earth-Science Reviews*, *226*, 103967.

807 Tiwari, G., Kumar, P., Javed, A., Mishra, A. K., & Routray, A. (2022). Assessing tropical cyclones  
808 characteristics over the Arabian Sea and Bay of Bengal in the recent decades. *Meteorology and*  
809 *Atmospheric Physics*, *134*(3), 44.

- 810 Wahiduzzaman, M., Cheung, K., Luo, J. J., Bhaskaran, P. K., Tang, S., & Yuan, C. (2022). Impact  
811 assessment of Indian Ocean Dipole on the North Indian Ocean tropical cyclone prediction using a  
812 Statistical model. *Climate Dynamics*, 58, 1275–1292. <https://doi.org/10.1007/s00382-021-05960-0>
- 813 Wang, B., Xu, S. & Wu, L. (2012). Intensified Arabian Sea tropical storms. *Nature* 489, E1–E2  
814 <https://doi.org/10.1038/nature11470>.
- 815 Wang, S., Murakami, H. & Cooke, W.F. (2023). Anthropogenic forcing changes coastal tropical  
816 cyclone frequency. *npj Clim Atmos Sci* 6, 187. <https://doi.org/10.1038/s41612-023-00516-x>
- 817 Yuan, J., Cao, J. (2013). North Indian Ocean tropical cyclone activities influenced by the Indian Ocean  
818 Dipole mode. *Sci. China Earth Sci.* 56, 855–865. <https://doi.org/10.1007/s11430-012-4559-0>

1 Contribution of Western Arabian Sea Tropical cyclones to rainfall in the Horn of Africa.

2

3

4 P. Camberlin <sup>1</sup>, O. Assowe <sup>2</sup>, B. Pohl <sup>1</sup>, M. Mohamed Waberi <sup>1,2</sup>, K. Hoarau <sup>3</sup>, O. Planchon <sup>1</sup>

5

6

7 <sup>1</sup> Centre de Recherches de Climatologie, UMR 6282 Biogéosciences, CNRS/Université de  
8 Bourgogne, Dijon, France.

9 <sup>2</sup> Observatoire Régional de Recherche sur l'Environnement et le Climat (ORREC), Centre  
10 d'Etudes et de Recherche de Djibouti (CERD), Djibouti-ville, République de Djibouti.

11 <sup>3</sup> PLACES, CY Cergy Paris Université, France

12

13

14

15

16

17

18

19

20

21

22 Submitted to Journal of Geophysical Research : Atmospheres

23

28 February 2024

24

25 Abstract

26 The occurrence of tropical cyclones (TC) in the Horn of Africa and nearby areas is for the first time  
27 examined to document their contribution to local rainfall and their trends over the period 1990-2020.  
28 An average 1.5 TC (of any intensity) per year was observed over the Western Arabian Sea, with two  
29 asymmetrical seasons, namely May-June (30% of cyclonic days) and September-December (70%). Case  
30 studies reveal that in many instances, TC-related rainfall extends beyond 500 km from the TC center,  
31 and that substantial rains occur one to two days after the lifecycle of the TC. Despite their rarity, in the  
32 otherwise arid to semi-arid context characteristic of the region, TCs contribute in both seasons to a  
33 very high percentage of total rainfall (up to 30 to 60%) over the northwestern Arabian Sea, the Gulf of  
34 Aden and their coastlines. Over inland northern Somalia, contributions are much lower. TCs  
35 disproportionately contribute to some of the most intense daily falls, which are often higher than the  
36 mean annual rainfall. A strong increase in the number of TCs is found from 1990 to 2020, hence their  
37 enhanced contribution to local rainfall. This increase is associated with a warmer eastern / southern  
38 Arabian Sea, a decrease in vertical wind shear, and a strong increase in tropospheric moisture content.

39

## 40 1. Introduction

41 Tropical cyclones (TCs) develop over sufficiently warm off-equatorial oceanic regions, which are  
42 generally wet areas receiving well over 1000 mm of precipitation per year. Although the Arabian Sea  
43 is not among the most active cyclonic basins, accounting, together with the Bay of Bengal, for only 4-  
44 6% of the world's TCs (Ramsay, 2017; Neumann, 2017 ; Singh and Roxy, 2022), it stands out by its low  
45 mean annual rainfall, which does not exceed 500 mm in its northwestern half. Very few other arid  
46 regions, like northwestern Mexico (Fors, 1977; Breña-Naranjo et al., 2015) and Western Australia (Ng  
47 et al., 2014), similarly experience TCs. Although considered a very rare occurrence along the coasts of  
48 northern Somalia, Yemen, and to some extent Oman (Pedgley, 1969; Al-Manji, 2021), the recent past  
49 provided evidence of several high intensity systems, e.g. the "very severe cyclonic storms" Gonu in  
50 2007, Chapala and Megh in 2015, Mekunu and Luban in 2018. Their landfall in arid environments  
51 provides unusually high rainfall amounts in a short period of time, which have major short-term  
52 consequences (e.g., flash floods destroying infrastructure, settlements, claiming lives and killing  
53 livestock) as well as longer-term impacts, for instance on groundwater recharge (Abdalla and Al-Abri,  
54 2011) and the dynamics of endangered tree species (Lvonicik et al., 2020). In the late 2010s, the  
55 succession of several unusually wet seasons, in which TCs played a dominant role, induced the worst  
56 locust outbreak of the last decades in Southern Arabia and the Horn of Africa (Salih et al., 2020 ; Owuor  
57 and David-McRae, 2022). In the Republic of Djibouti alone, the desert locust infestation in 2019-2020  
58 caused a loss of 5 million USD over crops and pastures. Even moderately strong tropical systems have  
59 large impacts because of the associated heavy rains. For instance, cyclonic storm Sagar brought 181  
60 mm of rainfall in Djibouti-city on two days in May 2018, extensively flooding huge urban  
61 neighbourhoods and schools, and destroying transportation and sanitation infrastructures (Cherel et  
62 al., 2020). The low income populations of the Horn of Africa, usually confronted to harsh climatic  
63 conditions related to recurrent droughts, are particularly vulnerable to such high intensity rainfall  
64 events, yet to the best of our knowledge there has never been any systematic study of how frequently  
65 TCs affect this part of the continent.

66 Over the Western Arabian Sea (WAS hereafter) and neighbouring coastal areas (Yemen, Somalia,  
67 Djibouti), more generally, the average contribution of TCs to local rainfall is little known. Pedgley (1969)  
68 found that at Salalah (southern Oman), a quarter of the total rainfall from 1943 to 1967 was associated  
69 with cyclones. Jiang and Zipser (2010) and Prat and Nelson (2013) quantified the contribution of  
70 tropical storms to global precipitation from TRMM data. Over the period 1998-2006, it varied from 3  
71 to 11% depending on the basins (Jiang and Zipser, 2010), and 5% for the North Indian Ocean basin  
72 which includes both the Bay of Bengal and the Arabian Sea. Comparable values were obtained by Prat  
73 and Nelson (2013) using 12 years of data from 1998 to 2009. Much higher contributions were found  
74 over localised areas such as the coasts of Baja California in Mexico (Breña-Naranjo et al., 2015) and

75 northwest Australia (Ng et al., 2014), but they decrease significantly within the first 150 km from the  
76 coast (Prat and Nelson, 2013). Khouakhi et al. (2017) examined the contribution of TCs to rain-gauge  
77 precipitation amounts and found that they account for a large portion (35-50%) of mean annual rainfall  
78 in a few regions including northwestern Australia, southeastern China, the northern Philippines, and  
79 northwestern Mexico. However, their study did not document the Arabian Sea area. Prat and Nelson  
80 (2013) published a map covering the North Indian Ocean basin, but due to the small number of years,  
81 the TC-related rainfall contribution is relatively noisy over the WAS. Kabir et al. (2022) studied TC  
82 exposure in the North Indian Ocean. TC-associated rainfall is much higher around the Bay of Bengal  
83 sub-basin than over the Arabian Sea, partly due to the larger number of TCs making landfall around  
84 the Bay of Bengal (155 between 1989 and 2018, as compared to 30 around the Arabian Sea).  
85 Nevertheless, the latter have a high contribution to TRMM total rainfall along the southeastern coasts  
86 of Arabia, reaching 50% in parts of Oman (Kabir et al. 2022).

87 The objectives of the present study are to quantify the mean rainfall amount resulting from TCs in the  
88 WAS, Gulf of Aden and riverine countries (Somalia, Djibouti, Yemen), and their contribution to the total  
89 rainfall amounts, which have never been comprehensively analysed before, since all previous studies  
90 on TC-induced precipitation were actually carried out at a much broader scale. Daily rainfall extremes  
91 associated with TCs will also be examined and compared to local absolute 24-hr maxima. Some case  
92 studies of TCs making landfall over the coasts of Somalia and Djibouti will also be presented in order  
93 to better apprehend the spatial distribution of rainfall during such events and its relationship to the  
94 storms size and track. A better knowledge of TCs in the region and their contribution to the local  
95 climatology is an important issue, because several studies point to a recent (Wang et al. 2012 ;  
96 Murakami et al. 2017 ; Baburaj et al. 2020 ; Deshpande et al. 2021 ; Priya et al., 2022 ; Tiwari et al.  
97 2022) and forthcoming increase (Murakami et al. 2013 ; Knutson et al. 2015 ; Bell et al. 2020) in the  
98 frequency of Arabian Sea TCs. While Murakami et al. (2013) attributed the recent increase to  
99 anthropogenic climate change, more ambiguous results were obtained by Wang et al. (2023). Evan et  
100 al. (2011) found that a recent increase in storm intensity could have been driven by enhanced  
101 anthropogenic black carbon and sulphate emissions, resulting in a reduction of vertical wind shear, but  
102 this was challenged by Wang et al. (2012).

103 Besides documenting the patterns of TC-related rainfall over the north-eastern tip of Africa and  
104 adjacent regions, the present study analyses trends of TC-related and total rainfall over the last 20-30  
105 years. Given the major changes found in TC occurrence in the last decades, a comparison is also made  
106 of the regional oceanic and atmospheric conditions which may have triggered these changes. Section  
107 2 presents the cyclone and precipitation data used in the study. The TC and precipitation climatologies  
108 are depicted in section 3.1, followed by the selected TC case studies (3.2). The statistical analysis of

109 mean rainfall amounts associated with TCs is then presented (3.3), before an appraisal of TC-related  
110 rainfall trends since 1990 (3.4) and the associated oceanic and atmospheric conditions (3.5).

## 111 2. Data and methods

### 112 2.1 Cyclone tracks

113 Data on 3-hourly North Indian Ocean TC locations were extracted from the IBTrACS (International Best  
114 Track Archive for Climate Stewardship, Knapp et al., 2010 & 2018) dataset. All observations west of  
115 75°E were retained. This is slightly further east than the WAS target area (33-65°, 0-22°N) because it is  
116 necessary to extract TC-related rainfall over a wide radius from the TC center. Given that some of the  
117 rainfall data are at daily timescale, the successive locations of each cyclone are averaged over each 24-  
118 hr period. As discussed below, the wide radius which will be retained around the TC center  
119 accommodates the TC propagation within each day.

120 All TC categories were retained in the study, i.e. including weak systems like tropical depressions (wind  
121 speeds between 17 and 34 knots). Substantial rains are sometimes associated with tropical  
122 depressions, which justifies the inclusion of these weaker systems. For instance, Arabian Sea tropical  
123 depression 02A, with weak maximum sustained winds (25 knots), which in 2008 made landfall in  
124 Yemen, caused widespread flooding, 180 deaths and 22 000 displaced people (Evan and Camargo,  
125 2011). Some analyses will be separately carried out on the Very Severe Cyclonic Storms (VSCS  
126 hereafter), the third highest category used by the India Meteorological Department to classify North  
127 Indian Ocean tropical cyclones, and which is equivalent to the Hurricane category (winds of at least 64  
128 knots). Hereafter, TC refers to all categories of disturbances, not just VSCS.

129 The study is restricted to the period from 1990 (2000 for some analyses) to 2020. Data for the pre-  
130 satellite era over the North Indian Ocean are not fully reliable due to a possible undercount of TCs  
131 (Evan and Camargo, 2011 ; Singh et al. 2020 ; Deshpande et al. 2021 ; Wahiduzzaman et al. 2022).  
132 Additionally, Kabir et al. (2022) and Tiwari et al. (2022) warned that TC records over the North Indian  
133 Ocean may not be fully complete prior to 1990 due to missing intensity records. Hoarau et al. (2012)  
134 re-analysed TC data over the Northern Indian Ocean using the Dvorak (1984) method. They warned of  
135 a probable undercount of intense TCs during 1980-1989. From 1990 onwards, the agreement between  
136 North Indian Ocean TC track-data from the Indian Meteorological Department (IMD) and the Joint  
137 Typhoon Warning Center (JTWC) greatly improved (Evan and Camargo, 2011 ; Schreck et al. 2014),  
138 suggesting that working on this period is less uncertain.

139

## 140 2.2 Precipitation data

141 Two daily gridded precipitation datasets based on satellite information calibrated with some ground  
142 data were used and complemented by rain-gauge data for northern Somalia and Djibouti. The gridded  
143 datasets were selected to document both land and oceanic areas, at a relatively high spatial resolution.

144 PERSIANN-CDR (Precipitation Estimation from Remotely Sensed Information using Artificial Neural  
145 Networks–Climate Data Record – Ashouri et al., 2015) uses infrared satellite data as the main input,  
146 from which a neural network model is developed whose parameters are based on radar data. The  
147 resulting rainfall estimates are next calibrated using the monthly Global Precipitation Climatology  
148 Project (GPCP) data. The product is available from 1 January 1983 to the present, at 0.25° spatial  
149 resolution.

150 IMERG (Integrated Multi-satellitE Retrievals for the Global Precipitation Measurement, Huffman et al.  
151 2015) is a gridded rainfall product with global coverage, based on NASA's precipitation algorithm,  
152 applied to data from the TRMM (Tropical Rainfall Measurement Mission) and the GPM (Global  
153 Precipitation Measurement) satellite missions. It covers the period from 2000 to the present day, at a  
154 high spatial (0.1 degree) and temporal (30 minute) resolution. The input data include passive  
155 microwave (PMW) precipitation estimates, considered as more direct retrievals, calibrated to the  
156 combined radar-radiometer product from TRMM and GPM. An interpolation of the PMW estimates is  
157 performed by propagating them forward and backward in time using motion vectors. The resulting  
158 estimates are further combined to infrared (IR) precipitation estimates, and a final bias adjustment to  
159 rain-gauge observations is made over land areas.

160 For both data sets, the region 3°S-22°N, 35-65°E, i.e. the Greater Horn of Africa (GHA) and nearby  
161 regions, was extracted. The period retained is 1990-2020 (2000-2020 for IMERG) to take into account  
162 TC data reliability as exposed above. Note that, unless otherwise stated, the results obtained for  
163 PERSIANN and IMERG are qualitatively similar, hence will not be systematically duplicated. Below,  
164 IMERG is generally preferred to PERSIANN, because it slightly better agrees with rain-gauge data.

165 Daily rain-gauge data for 25 stations in Northern Somalia (mainly Somaliland and Puntland areas) were  
166 obtained from SWALIM (Somalia Water and Land Information Management), a project managed by  
167 FAO. The period covered is 2005-2020, with data availability varying from 10 to 16 years. For the  
168 Republic of Djibouti, data from Djibouti-Airport station, with complete daily rainfall records between  
169 2000 and 2020, were obtained from the National Meteorological Agency of Djibouti.

## 170 2.3 Methods for quantifying TC-associated precipitation

171 Quantifying the contribution of TCs to rainfall requires defining to what distance of the TC center  
172 rainfall is considered as being related to the TC. Most studies consider a 500 km radius (e.g., Jiang and

173 Zipster, 2010 ; Prat and Nelson, 2013; Lavender and McBride, 2021). This threshold is meant to be  
174 within the range of the outer edge of the TC cloud shield (550–600 km) (Englehart et al. 2001, Kabir et  
175 al. 2022). Rather than blindly adopting the same threshold, mean daily rainfall was plotted as a function  
176 of distance to the TC center, for all TCs reported in the period 2000-2020 in the WAS area. Boxplots  
177 were constructed to derive the median rainfall and its variability for 40 km bins (section 3.3). From  
178 these plots an adapted threshold was defined, and all rainfall which fell within this distance from the  
179 TC center was considered as TC-related. Rainfall in the days immediately following the demise of each  
180 TC was also examined in order to find out whether part of it can be ascribed to remnants of the  
181 disturbance. This procedure was used to quantify TC-related rainfall for each disturbance, and to  
182 compute statistics for the period 2000-2020 based on the gridded PERSIANN and IMERG rainfall  
183 estimates, and the stations available in the years 2005-2020 in Northern Somalia and Djibouti.

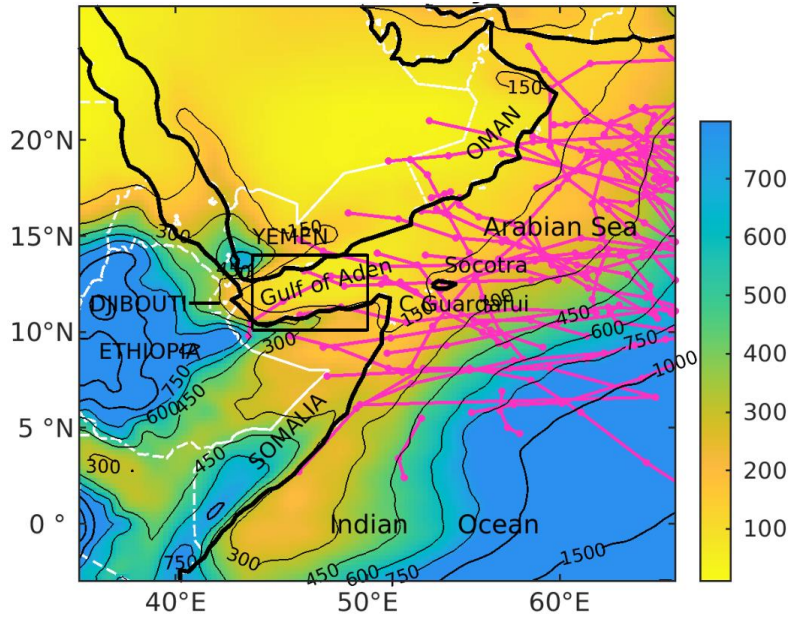
184 The contribution of TC-related rainfall to total rainfall was computed. To document the part played by  
185 TCs on intense rainfall, days recording above 30 mm were extracted and the proportion which are TC-  
186 induced was computed. Maximum 24-hr rainfall at available rain-gauges was also examined to assess  
187 to which extent it relates to TC occurrence. These analyses were carried out separately on the two  
188 cyclonic seasons, i.e. the pre-monsoon (May-June) and the post-monsoon (September-December).

189 Rainfall trends over the period 2000-2020 (extended to 1990-2020 for PERSIANN) were mapped for  
190 total rainfall, TC-related rainfall, non-TC related rainfall and the contribution of TC-related rainfall to  
191 total rainfall amounts. Mann-Kendall Tau statistics were computed to assess the statistical significance  
192 of the trends.

### 193 3. Results

#### 194 3.1 Rainfall and TC climatologies

195 The region around the northeastern tip of Africa is mostly an arid to semi-arid area, with less than 500  
196 mm/yr (fig.1). Mean annual rainfall (MAR) increases to the southeast, in the Central Indian Ocean, in  
197 the west over highland areas (Ethiopia, Kenya, Yemen), and along a narrow subcostal belt stretching  
198 northward from Southern Kenya. The region covering most of South Arabia, the Gulf of Aden and  
199 neighbouring areas is particularly arid (less than 200 mm/yr), with no well-defined rainy season. Much  
200 of Somalia and its surroundings have two brief rainy seasons, in March-May and October-November.  
201 Due to the divergence of large-scale air flows, most of the region experiences dry boreal winters  
202 (December-February) and summers (June-September), the main exception being the Ethiopian  
203 highlands.



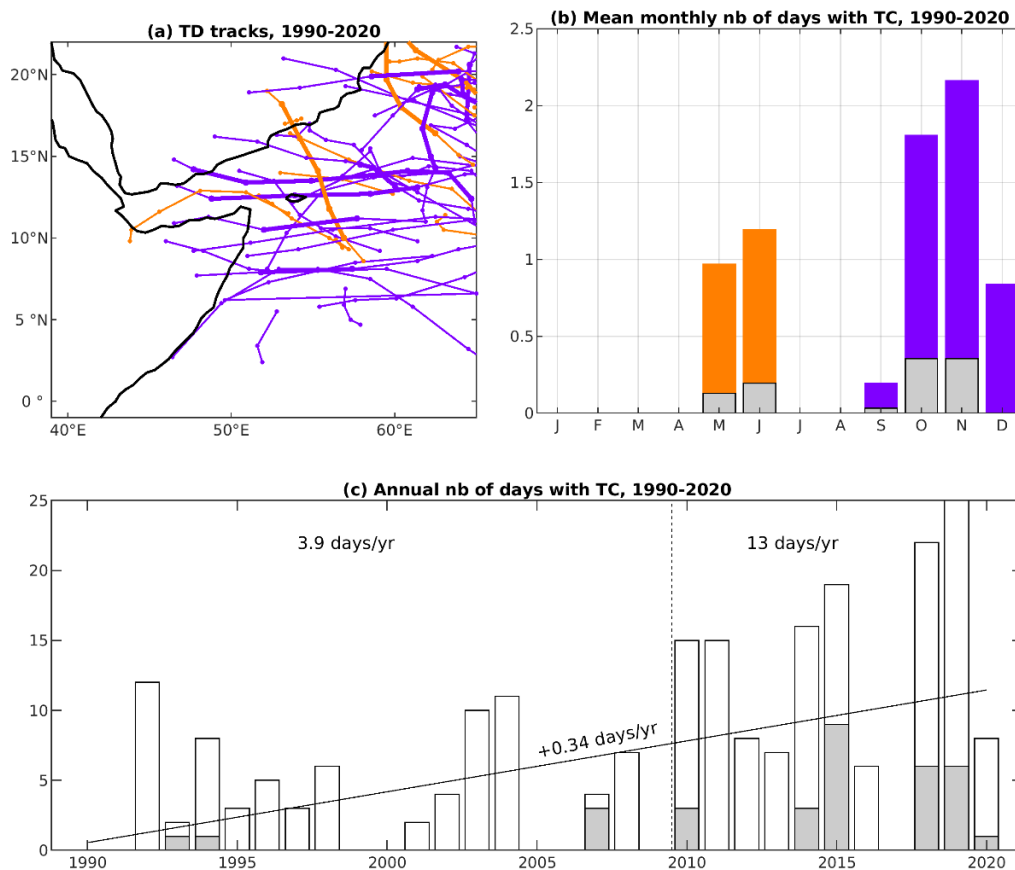
204

205 Figure 1 : Location map, with shadings representing mean annual rainfall (PERSIANN data, 1990-  
 206 2020, in mm) and pink lines TC tracks (same period). The box shows the area over which the Gulf of  
 207 Aden rainfall index is computed (section 3.4).

208 From 1990 to 2020, a total of 47 TCs crossed the WAS, with a mean life-time (within the region) of 4.6  
 209 days. The number of TCs gradually decreases from east to west (fig.2), with tracks generally showing  
 210 E-W or SE-NW directions. A minority of the TCs display more meridional tracks, with southerly  
 211 propagations on rare occasions (e.g. TC Kyarr in 2019). Only about a third of these TCs made landfall  
 212 over the continent, either on the coasts of Southern Arabia or on those of Somalia, with a few  
 213 additional TCs which approached close to the coasts or crossed Socotra island. A small proportion of  
 214 these disturbances belong to the VSCS category. On average, only 1.1 days.year<sup>-1</sup> record a VSCS, as  
 215 compared to 7.1 days.year<sup>-1</sup> for all TC categories.

216 TCs reaching or developing over the WAS are found in two distinct seasons (fig.2), which correspond  
 217 to the pre-monsoon season (May-June) and post-monsoon season (September-December, clearly  
 218 peaking in October-November). During the monsoon season (boreal summer), the strong wind shear  
 219 between the low-level westerlies and the upper-tropospheric Tropical Easterly Jet, as well as lower SST  
 220 over parts of the WAS, disable the development of TCs (Gray, 1968 ; Evan and Camargo, 2011 ; Baburaj  
 221 et al. 2020). TCs are much less frequent in May-June (MJ) than in September-December (SOND). The  
 222 latter season makes up about two thirds of the number of TCs, and 70% of the cyclonic days. This is  
 223 specific to the WAS: for the Arabian Sea as a whole the number of TCs is approximately the same in  
 224 the two seasons (Evan and Camargo, 2011), with some decadal variations (Al-Manji et al. 2021). The  
 225 smaller number of pre-monsoon TCs in the western part of the Arabian Sea compared to post-  
 226 monsoon has rarely been highlighted (Ray-Choudhuri et al. 1959), though it is obvious in Singh and

227 Roxy (2022, their figure 3). There is no current explanation for this difference, but it is not related to  
 228 SST, which are higher in the pre- than in the post-monsoon seasons. Dynamical conditions could be  
 229 more conducive to a westward motion of the TCs initiated over the eastern Arabian Sea. The  
 230 predominantly east-west tracks of many of the post-monsoon TCs is shown on figure 2a. May-June  
 231 tracks are slightly more uneven, and few of them make landfall over northeastern Africa or southern  
 232 Arabia.



233

234 Figure 2 : TC tracks and TC statistics for the Western Arabian Sea, 1990-2020. Orange colours refer to  
 235 the May-June season, purple colours to the September-December season. Grey bars in panels (b) and  
 236 (c) stand for VSCS, which are identified by bold lines in panel (a). In panel (c), white bars show the  
 237 yearly total of TC days (TC center located west of 65°E), with the linear trend computed as Sen's  
 238 slope. The vertical dashed line is the breaking point according to Pettitt's test ( $p < 0.01$ ), with the  
 239 mean number of TC days for the two sub-periods in the top part of the panel.

240 Large interannual variations are found in the number of TC days (fig. 2c). In some years, no TCs are  
 241 recorded in the WAS. There has been a clear and strong positive trend in the number of TC days in the  
 242 period 1990-2020 (+0.34 per year, significant at  $p < 0.01$ ), corroborating Deshpande et al. (2021).  
 243 Pettitt's test for change-point detection indicate a significant upward increase ( $p < 0.01$ ) after 2009. In  
 244 the first sub-period (1990-2009), there was an average of 3.9 TC days/year in the WAS, rising to 13

245 days/year between 2010 and 2020. Statistics for WSCS are less robust, given the rare occurrence of  
246 disturbances in this category. While these storms were exceptional between 1990-2009, they became  
247 much more common from 2010, with each of the last three years (2018, 2019 and 2020) recording  
248 VSCS.

### 249 3.2 Case-studies

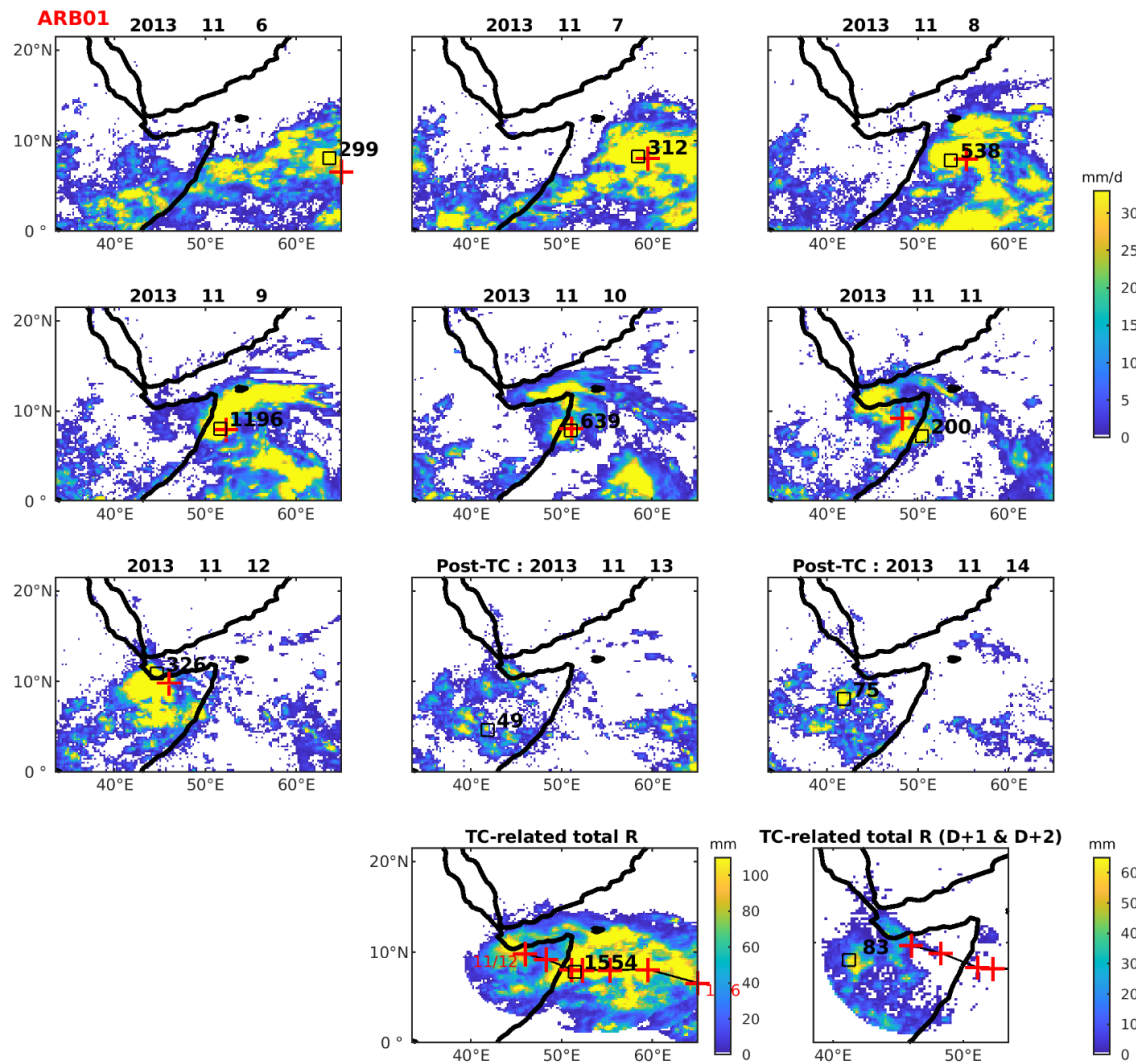
250 Four case studies of TCs which made landfall over the northeastern tip of Africa have been selected,  
251 to document the relationship between the tracks of these systems and the rainfall distribution. They  
252 are ordered here by increasing intensity.

#### 253 - Deep depression ARB01/2013 (November 2013) :

254 This disturbance was first identified as a low pressure centre on 6 November 2013 near 6°N, 65°E  
255 (fig.3), then classified by the IMD as a tropical depression on 8 November 2013, while located 680 km  
256 east of Ras Binnah on the northeastern Somalian coast, moving westward. It slightly intensified on 9  
257 November, with 3-mn sustained winds of 55 km/h, developed an eye feature, and was classified as a  
258 deep depression. It made landfall on 10 November at 8°30'N, north of Eyl in Puntland, northern  
259 Somalia. A large area of active convection was associated with the TC. Very high daily point rainfall  
260 estimates were obtained by IMERG along the track, from 199 mm to an unreliable 1196 mm on 9  
261 November near the coast (fig.3, bottom), in conjunction with very low cloud top temperatures (-70 to  
262 -75°C, not shown). As the TC made landfall, very high rainfall estimates were still shown on 11 and 12  
263 November over a large area covering northern Somalia. On 13-14 November, while the TC is no longer  
264 singularized, scattered but significant convective rains occurred from Djibouti to Central Somalia.

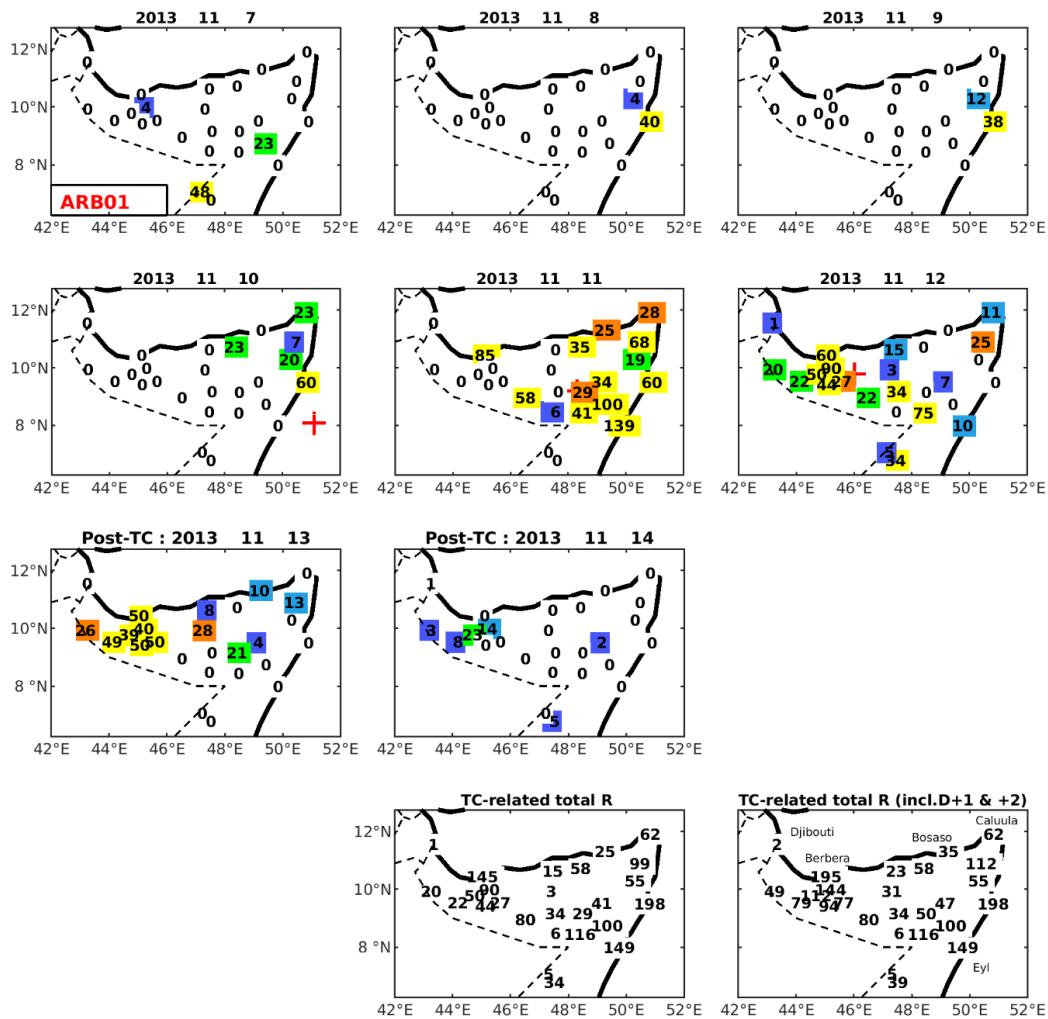
265 Rain-gauge data (fig.4) show that coastal rains associated with the disturbance started on 8 November,  
266 but the bulk of the rains fell on 11 November in arid Puntland (20 to 100 mm, and a peak of 139 mm  
267 at Eyl). The rains shifted westward on 12 November, with substantial rains (40-50 mm) still found on  
268 13 November in western Somaliland. The accumulated rainfall during the TC lifetime (within 750 km  
269 of the TC center, fig.4) generally exceeds 100 mm in the east, and is more contrasted further west.  
270 However, if one adds the precipitation recorded in the following two days (fig.4, bottom right panel),  
271 rainfall amounts ranging from 49 to 144 mm are found in the inland part of western Somaliland. The  
272 coastal town of Berbera (55-yr MAR : 50 mm) even recorded 195 mm during this period. In Somalia,  
273 TC ARB01/2013 caused the death of 162 people, about 100,000 livestock losses and the destruction of  
274 over 1,000 houses according to official statistics (IFRC, 2013).

275



276

277 Figure 3 : IMERG daily rainfall during the lifetime of deep depression ARB01/2013 and in the two  
 278 following days (“post-TC”). Bottom panels : accumulated rainfall amount associated with the TC  
 279 (within 750 km of its center) during its lifetime (left) and in the two following days (right panel). Red  
 280 crosses show the location of the TC center. Black figures : maximum rainfall amount within 750 km.



281

282 Figure 4 : Daily rainfall over Northern Somalia and Djibouti during the lifetime of deep depression  
 283 ARB01/2013 and in the two following days (“post-TC”). Bottom panels show the accumulated rainfall  
 284 amount associated with the TC (within 750 km of its center) during its lifetime (left) and including the  
 285 two following days (right panel).

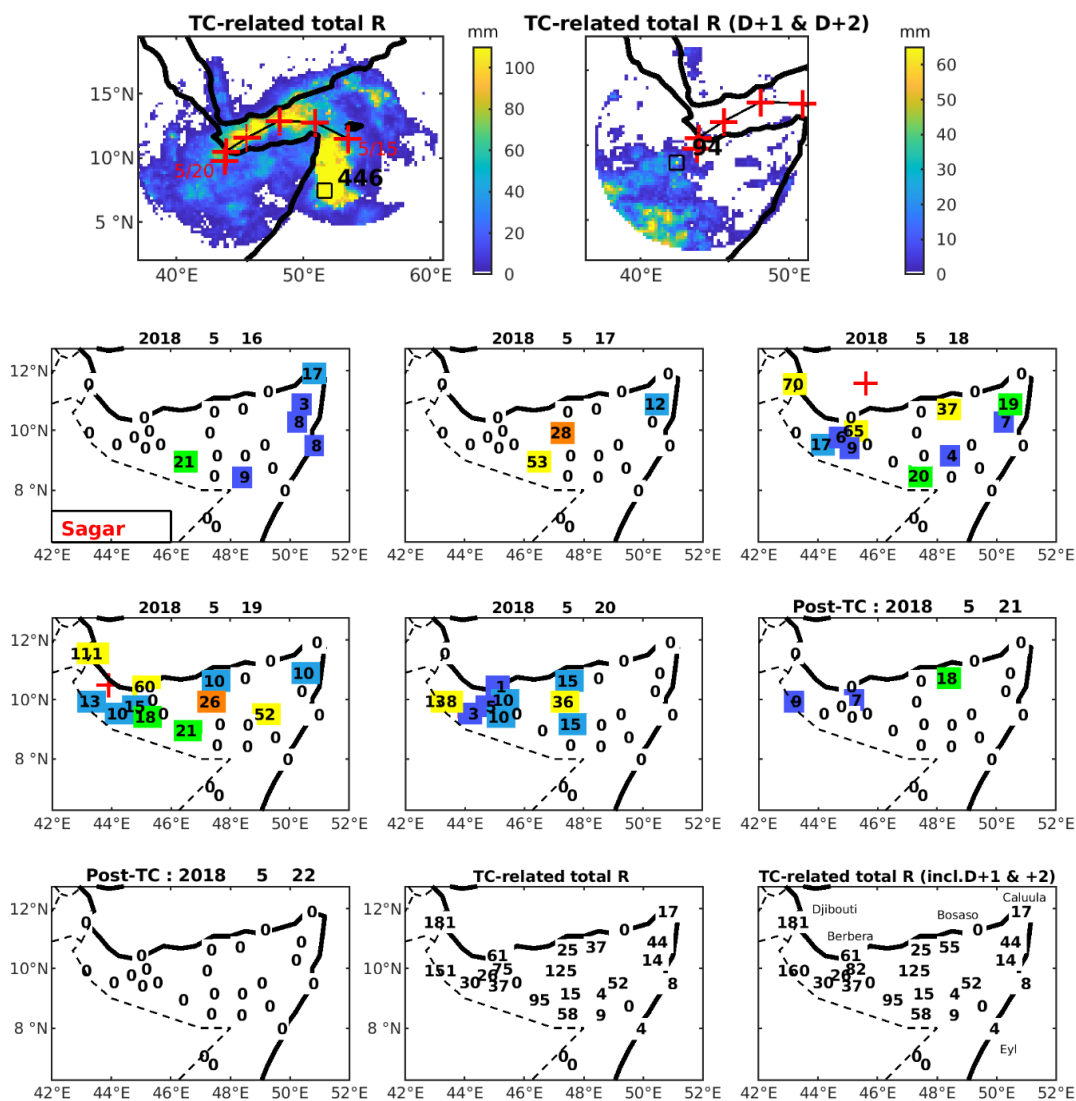
286 - Cyclonic storm Sagar (May 2018)

287 According to the JTWC, this system began as a tropical depression on 15 May south of Socotra. It was  
 288 named Sagar after it reached the tropical storm stage (35 knots) near the entrance to the Gulf of  
 289 Aden on 16 May. The rains recorded off the eastern coast of Somalia on May 16-18 (fig.5, top left  
 290 panel) were mainly due to convective cells developing in the cloud bands at the southern edge of  
 291 Sagar. Proceeding towards the west-southwest, the storm gradually intensified to become a VSCS (65  
 292 knots) on May 18. The VIIRS image from 10:28 UTC in the visible spectrum indicates that Sagar was a  
 293 small diameter cyclone. On 19 May, returning to the severe cyclonic storm category (60 knots), Sagar  
 294 made landfall west of Berbera, Somaliland. The slow movement of the system and very cold cloud  
 295 top (-70°C to -80°C on Meteosat-8 images) largely explain the heavy rains observed in Somalia and

296 Djibouti from 18 to 20 May (fig.5, bottom panels). Substantial rains were also found on the following  
 297 two days in eastern Ethiopia, associated with the overall atmospheric instability and Sagar remnants,  
 298 causing landslides and flash floods destroying villages in the Sitti area.

299 Wadi Ambouli, which crosses Djibouti-city, overflowed and caused heavy damages, particularly on  
 300 the right bank in the Boulaos neighbourhood. Around 20,000 people were affected in the Republic of  
 301 Djibouti. Damage to transport infrastructure amounted to approximately 1.9 billion Djiboutian francs  
 302 (US\$10 million), with a similar figure for the sanitation system (Cherel et al. 2020). At least 53 victims  
 303 were numbered in northern Somalia, particularly in western Somaliland, herds were swept away, and  
 304 many boats were destroyed in the ports of Puntland.

305



306

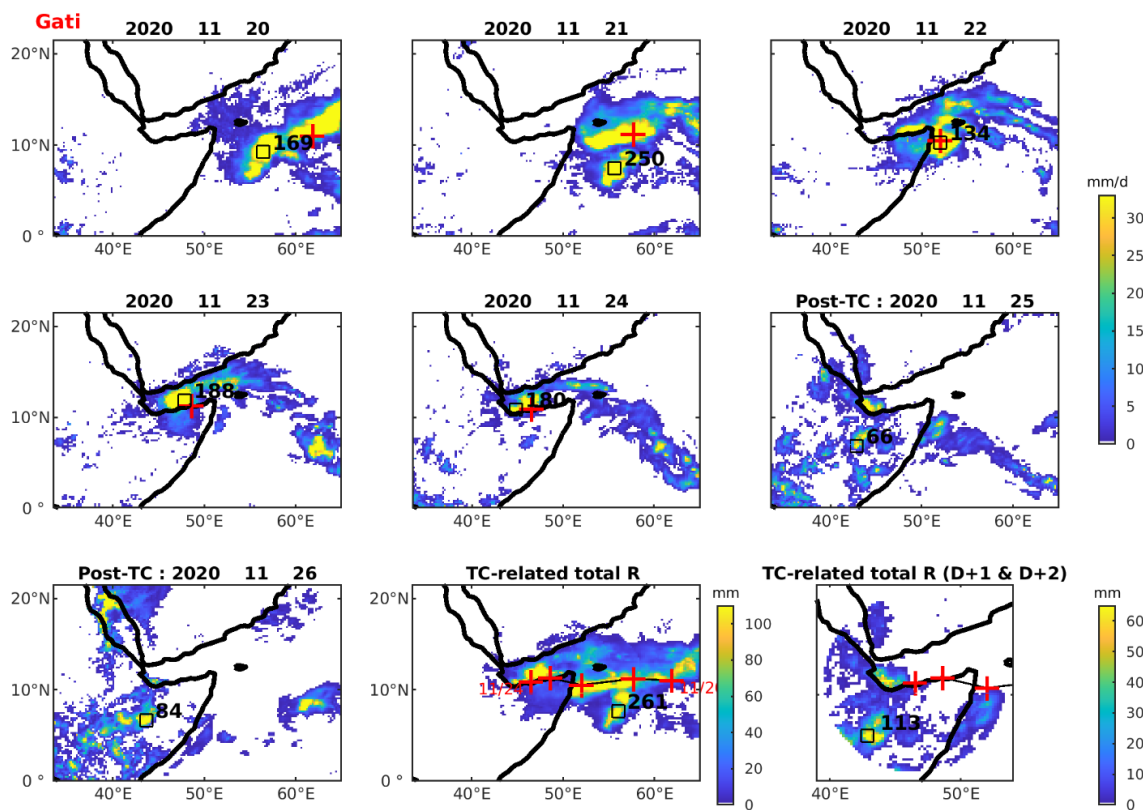
307 Figure 5 : Rainfall associated with TC Sagar. Top panels : accumulated IMERG rainfall during Sagar  
 308 lifetime (15-20 May, top left) and in the two following days (21-22 May, top right). Red crosses show  
 309 the location of the TC center, with indication of the first and last dates of its lifetime. Black squares

310 indicate the maximum accumulated rainfall amount (mm) within the 750 kms of the center. Bottom  
311 panels : daily rainfall over Northern Somalia and Djibouti and in the two following days (“post-TC”).

312 - VSCS Gati (November 2020)

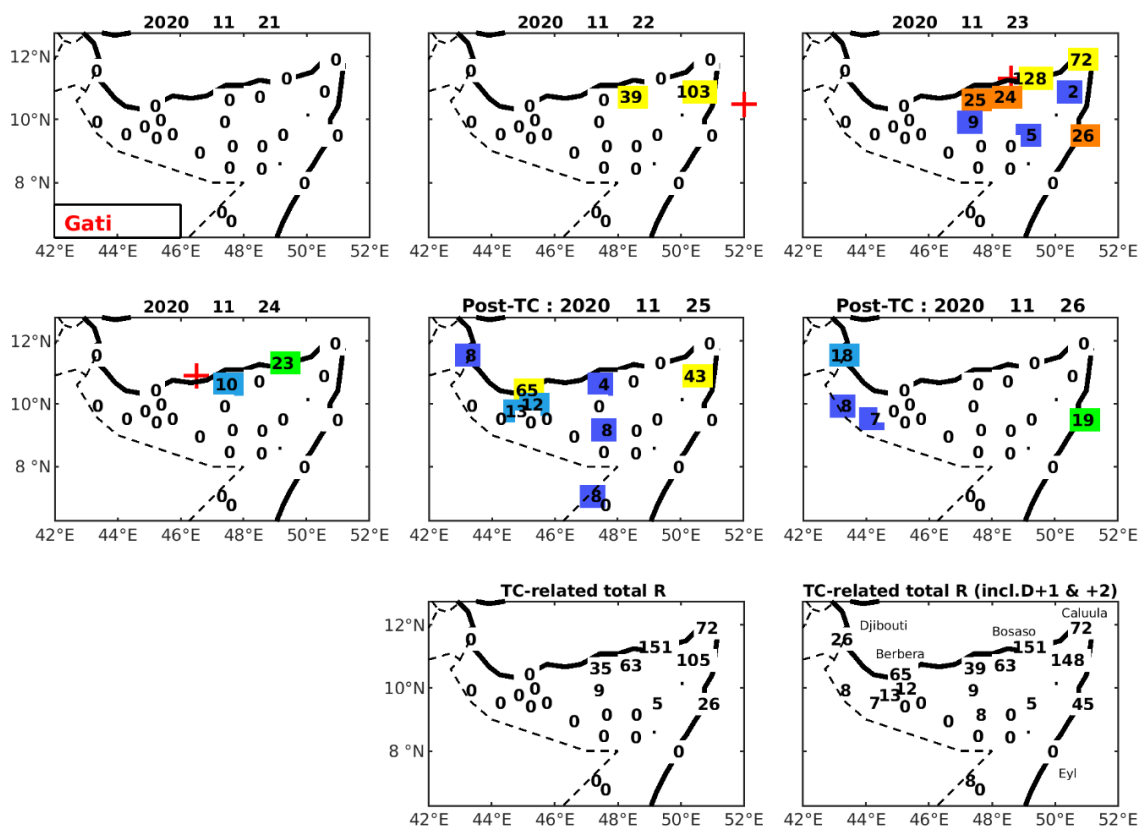
313 Gati is a recent example of a VSCS which showed an explosive intensification from a low pressure area  
314 located in the central Arabian Sea on 20 November 2020. Moving westwards (fig.6), it made landfall  
315 near Hafun in northeastern Somalia on 22 November as a VSCS. Gati quickly weakened as it crossed  
316 land, with a last warning issued on 23 November over the gulf of Aden. It resulted in maximum daily  
317 rainfall exceeding 100-200 mm every day from 20 to 23 November over the WAS, and in northeastern  
318 Somalia (fig.7) several stations recorded daily rains over 70 mm on 22 and 23 November (e.g., at the  
319 hyper-arid station of Bosaso, 128 mm on 23 November, i.e. 780% of the 51-yr MAR). Rainfall was lower  
320 further west, though an IMERG estimate of 180 mm is still noted in the Gulf of Aden on 24 November,  
321 and 65 mm recorded at Berbera on 25 November. Weaker rains were observed in Djibouti, but  
322 remnants of the storm brought heavy local rains on 25-26 November in eastern Ethiopia. 42,000  
323 people were displaced in Bari region, Puntland, Northeastern Somalia, with extensive damages due to  
324 flash floods, coastal submersion and winds (OCHA, 2020).

325 Although Gati had a trajectory roughly similar to that of Sagar, the heavy rains were felt more in the  
326 eastern than in the western part of its track. A detailed meteorological analysis is again out of scope,  
327 but the early landfall of Gati explained its fast weakening, hence the weaker rains in Western  
328 Somaliland and Djibouti. The more curvilinear path of Sagar, over the very warm Gulf of Aden (XBT  
329 soundings indicated that water temperature exceeded 27°C up to a depth of at least 29m, not shown),  
330 provided a considerable heat flux which was sufficient to feed Sagar, despite its relatively slow motion.



331  
332

Figure 6 : same as figure 3 but for VSCS Gati



333  
334

Figure 7 : same as figure 4 but for VSCS Gati.

335

336 - VSCS 12A (October 1972) :

337 Although rainfall maps are not available for this disturbance, since it predates the satellite era, it is an  
338 interesting case typical of the probable underreporting of some TC-related rainfall in the region, in this  
339 case due to incomplete TC tracks before 1982. Storm 12A originated from the southern Arabian Sea,  
340 moving northwestward to cross Socotra Island. It was classified as a VSCS (64-82 knots) just before its  
341 landfall over Socotra, then continued westwards while weakening. According to IBTrACS, this storm  
342 was last located at 12.2°N, 50.8°E, i.e. 20 km north of Caluula, near Cape Guardafui, on 25 October  
343 12:00 (with perfect agreement between the three IBTrACS sources). Yet the October 1972 monthly  
344 weather report in Djibouti (Résumé Mensuel du Temps, 1972) indicated that the storm, after entering  
345 the Gulf of Aden on 25 October at a speed of 5-6 knots, further penetrated westward with increased  
346 velocity (25-30 knots) and reached Djibouti in the morning of 27 October. Wind gusts of 36 knots were  
347 reported at Djibouti-Airport, 45 knots at Arta 40 km westwards. The track of this TC, along the Gulf of  
348 Aden, is therefore closer to Sagar in 2018 than Gati or ARB01. The relatively small size of the tropical  
349 systems which enter the Gulf of Aden, like storm 12A, may, before the satellite era, have resulted in  
350 their underreporting.

351 Exceptionally high rains fell in the Djibouti area (201 mm at Djibouti-Airport on 27 October, 118% of  
352 the MAR), over the Gouda mountains (at Randa, 133 mm on the same day, 94 mm on 28 October) and  
353 at the usually very dry northern coastal station of Obock (105 mm on 27-28 October, compared to a  
354 MAR of only 73 mm). Rainfall quickly decreased further west, with only 2 mm at Dikhil and no rain at  
355 all at As Eyla. There is no daily data available from the northern coast of Somalia, while heavy rains fell  
356 further south in Central Somalia, but unlikely to be directly TC-related. Stations located over the  
357 Northern Somalia Highlands, though close to the Gulf of Aden, reported only little rainfall (Hargeysa 6  
358 mm on 28-29 October 1972), suggesting that the storm was of moderate size at this stage. There is  
359 only scanty information to assess the human losses and damages resulting from the storm. In Djibouti  
360 60 people were reported dead and 5000 homeless. In Somalia, a third of the coastal palm groves in  
361 northeastern Somalia were destroyed by the storm, with long-lasting effects on spring discharges due  
362 to landslides (Chazée, 2017).

363 Overall, several inferences can be made from these four case studies. First, although defining the exact  
364 zone of TC-related rainfall is uneasy, it is clear (e.g., fig.3) that on several days this area extends beyond  
365 500 km from the TC center. Second, in the two days following the reported termination date of the  
366 system, substantial rainfall, especially over land where the disturbance does not meet all the criteria  
367 to qualify as a tropical storm, is associated with remnants of the TC. Land rainfall related to the TC  
368 matches reasonably well between IMERG and rain-gauge data, though a detailed comparison is out of

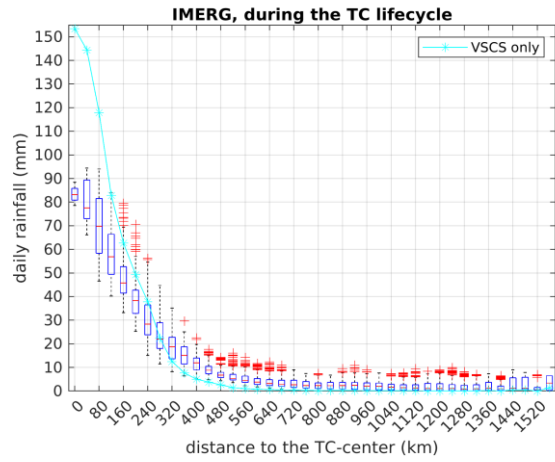
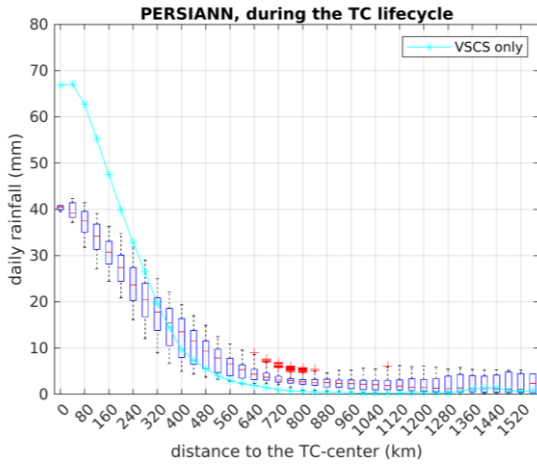
369 scope. Lastly, intense rainfall, with little relationship to the storm category, can be observed at arid  
370 locations. For instance, in northeastern Somalia, rainfall from deep depression ARB01/2013 (35 to 198  
371 mm) often equals or exceeds MAR, which is as little as 15 to 200 mm. Over the ocean, even higher  
372 rainfall amounts are found in IMERG, but they are highly localized.

### 373 3.3 Statistics of rainfall associated with TC occurrence

374 This section aims to produce a statistical analysis of TC-related rainfall, over the period 2000-2020 for  
375 which cyclone data are very reliable and different sources of rainfall data are available. Rainfall on TC-  
376 days is plotted as a function of the distance to the TC center, for PERSIANN and IMERG (figure 8). Both  
377 plots clearly show an exponential decay from the center. However, close to the center, rainfall is more  
378 intense in IMERG (83 mm at 0-20 km) than in PERSIANN (41 mm). This is partly due to the higher spatial  
379 resolution of IMERG, which better resolves very intense but highly localised downpours, and to the  
380 algorithm and input data used to estimating rainfall, which include microwave and radar data in  
381 IMERG. When screening for VSCS only (turquoise lines on fig.9), even higher rainfall is noted close to  
382 the TC center. Gaona et al. (2018) showed the added value of IMERG in depicting rainfall intensities  
383 close to the TC center.

384 After a strong decrease of rainfall amounts with increasing distance, the slope markedly reduces  
385 beyond 400 to 500 km, before gradually flattening out. The distance from which rainfall decreases  
386 becomes negligible and a mere straight line is around 600 km for IMERG and 700 km for PERSIANN.  
387 Given that the boxplot height is smallest around 750 km in PERSIANN, we retain this distance as a  
388 conservative threshold below which rainfall is considered as TC-related (and referred to as such  
389 hereafter). This distance is greater than in most previous studies (500 km), but it is justified by the fact  
390 the daily time-scale used in this study involves some propagation of the TC in a 24-hr period.  
391 Additionally, a cursory look at individual cyclones confirmed that a 500 km radius would exclude, in  
392 some cases, areas of convective activity which are clearly part of the disturbance. Note that for VSCS  
393 only, the drop to very low rainfall occurs at a slightly shorter distance, despite the much higher core  
394 intensities, suggesting more compact disturbances.

395

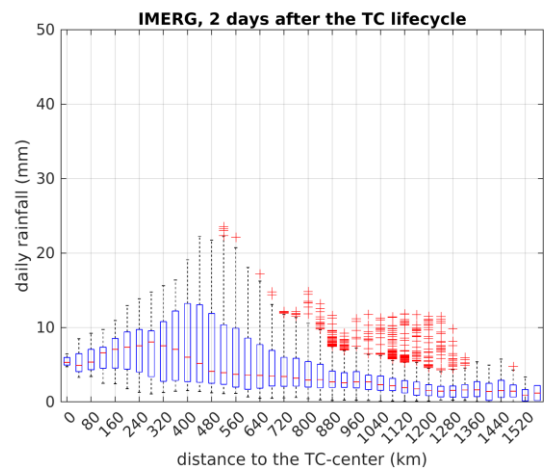
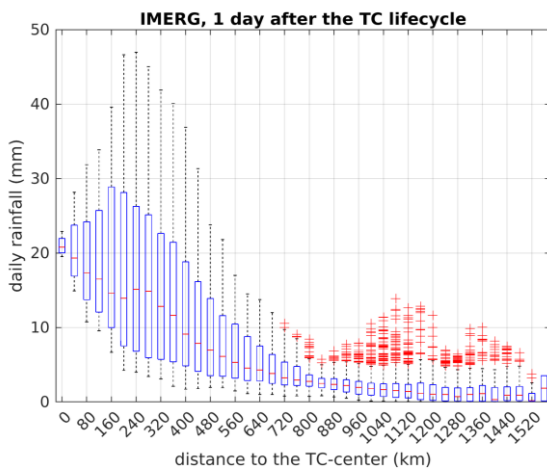


396

397

(a)

(b)



398

399

(c)

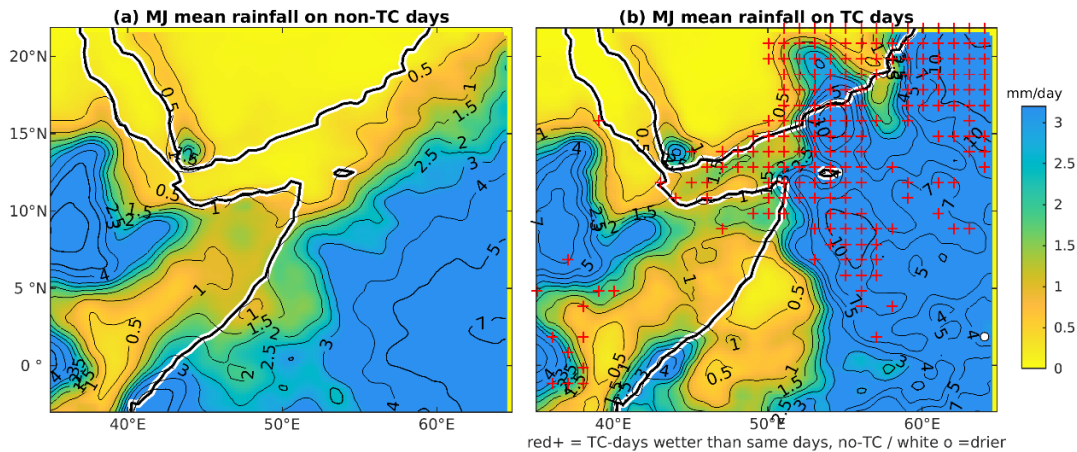
(d)

400 Figure 8 : Boxplots of mean daily rainfall observed on TC-days over the WAS, as a function of the  
 401 distance to the TC center, using PERSIANN (a) and IMERG (b) data for 2000-2020. Bottom row : mean  
 402 IMERG daily rainfall a day (c) and two days (d) after the end of the TC lifecycle (the TC center refers  
 403 to its last known location). The spread of the boxplots refers to spatial variations (i.e., in the mean  
 404 rainfall among the pixels located in each distance bin). On panels (a) and (b), turquoise lines and stars  
 405 show the median rainfall observed on VSCS only. Note the different vertical scales.

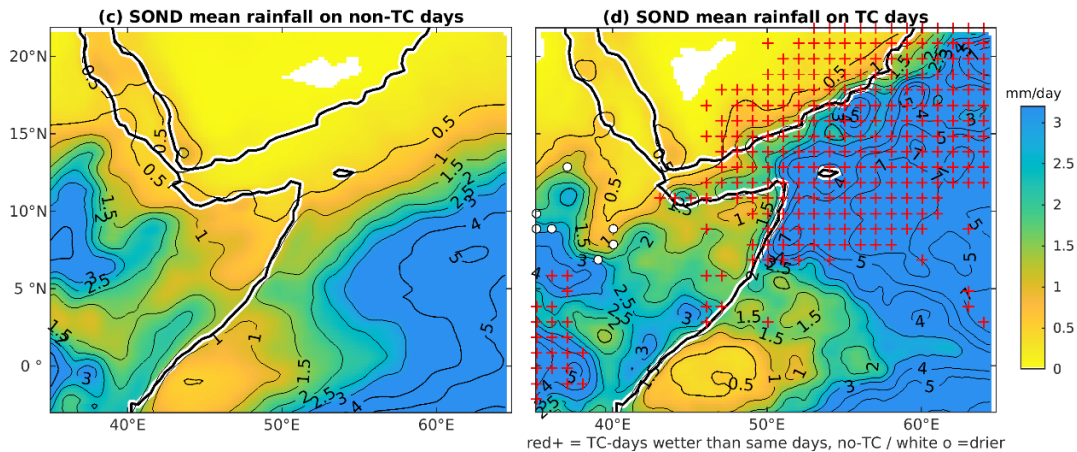
406 As suggested by the above case-studies, TC-related rainfall does not necessarily stop as soon as the TC  
 407 is no longer defined. Figure 8 shows rainfall one (panel c) and two days (panel d) after the TC lifecycle.  
 408 On day+1, heavy rains (median of 21 mm/day) are still found within 20 km of the last known TC  
 409 location. Between 40 and 400 km, although the elongated boxplots denote a diversity of patterns,  
 410 substantial rains (medians from 9 to 19 mm/day) reflect active remnants of the storm. On day+2,  
 411 rainfall markedly decreases, but rains above 5 mm/day (again with a high dispersion) are found up to  
 412 400 km, with a median peaking at 8 mm at 280 km because of the shift of the storm remnants. This

413 suggests that post-TC rainfall cannot be neglected. Hence, in the following, TC-related rainfall will be  
414 considered as the accumulated rainfall during the entire TC lifetime plus the following two days.

415 Mean rainfall on TC days and non-TC days is plotted for MJ and SOND (figure 9). TCs bring substantial  
416 rains in the northwestern Arabian Sea, an otherwise relatively dry area in both seasons. Over the sea  
417 around Socotra and further to the north-east, intensities between 4 and 10 mm/day are recorded on  
418 TC days, while mean rainfall on other days of the same seasons is generally below 1.5 mm/day. The  
419 patterns are quite similar for the two seasons, although more noisy for AMJ because TCs are less  
420 frequent. Near and along the coasts of northern Somalia, southern Yemen, southern Oman and in the  
421 Gulf of Aden, TC-related intensities are lower but in a context of even more arid conditions (<0.5  
422 mm/day on non-TC days). This mostly reflects the smaller number of TCs reaching these areas. Over a  
423 broad area covering the northwestern Arabian Sea and nearby regions, the mean rainfall intensity is  
424 statistically higher (t-test,  $p < 0.05$ ) on TC-days than during the same calendar days for years with no  
425 TCs (i.e., same day climatology: Fig. 9b & d). Interestingly, some significant rainfall anomalies are also  
426 found remotely from the WAS. Over central Ethiopia, localised drier than normal conditions (white  
427 circles) are found in SOND when a TC occurs in the WAS. By contrast, more rains than normal occur  
428 over Western Kenya (36-38°E, 2°S-5°N) in both seasons. This points to the distant effect of TCs, which  
429 will not be addressed here, but was already discussed for Southern Hemisphere cyclones (Shanko and  
430 Camberlin, 1998 ; Finney et al., 2020 ; Kebacho, 2022).



431

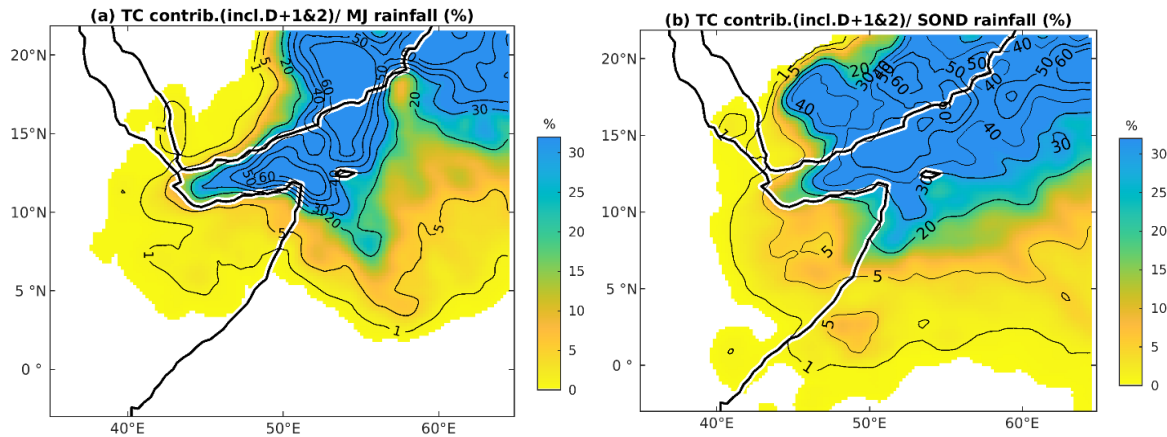


432

433 Figure 9: Rainfall (mm/day) on non-TC days (left panels) and TC days (right panels) for May-June (a,b)  
 434 and September-December (c, d), based on IMERG data (2000-2020). Red plus signs (white circles)  
 435 indicate grid-points where rainfall on TC-days is significantly higher (lower) ( $p < 0.05$ ) than that  
 436 recorded on the same calendar days but with no-TC.

437 TC-related rainfall makes a very high contribution to seasonal rainfall over the Arabian Sea northeast  
 438 of Cape Guardafui (fig.10). Over the northwestern Arabian Sea and Gulf of Aden, contributions reach  
 439 30 to 50% along a belt running from the Gulf of Aden to Socotra island and the Yemen and Oman  
 440 coasts. Contributions are more variable in MJ than SOND due to the small number of disturbances and  
 441 their haphazard tracks. Values locally exceed 60% near the coasts, including inland southern Arabia  
 442 near the border between Oman and Yemen. High contributions are also found at the northeastern tip  
 443 of Somalia (30-50%), quickly decreasing inland. On an annual basis (not shown), contributions exceed  
 444 30%, and even more than 50% over some areas according to PERSIANN. These values are quite  
 445 remarkable given the relatively low occurrence of TCs in this basin. They are higher than those  
 446 published in Prat and Nelson (2013) for the Arabian Sea, for several reasons like the different data set  
 447 they used (TRMM), methodology, and their period of study (1998-2009) which does not include the  
 448 recent very active years. These are among the highest values in the world. Among the cyclonic regions  
 449 examined by Khouakhi et al. (2017), such high contributions are reached over only a few coastal areas

450 in the world, like Northwestern Australia, Baja California, the northern Philippines and Hainan island  
451 in China, although their study did not consider oceanic areas.



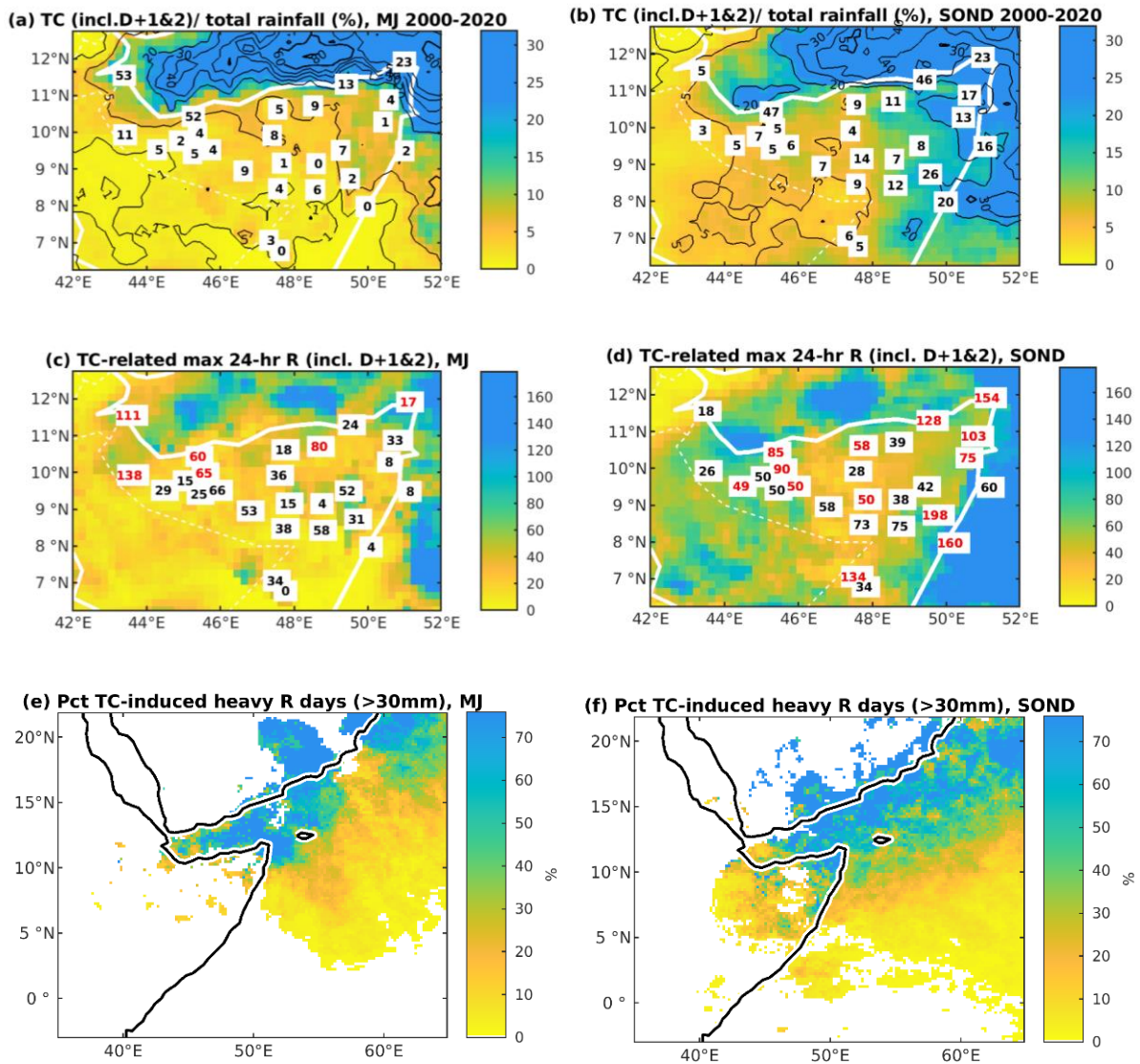
452

453 Figure 10: Percentage contribution of TC-related rainfall to mean seasonal rainfall (IMERG data,  
454 2000-2020), for MJ (a) and SOND (b). TC-related rainfall refers to rainfall within 750 km of the TC  
455 center, during its lifetime or in the next two days

456 Rain-gauge records confirm that over Northern Somalia the contribution of TC-related rainfall is often  
457 moderate, though it strongly increases along the coasts (fig.11). In MJ (fig.11a), it is below 10% inland,  
458 but much higher along the shores of the Gulf of Aden, in agreement with the higher contributions  
459 found over the sea in IMERG. In the western part of the Gulf, a high value (53%) is obtained at Djibouti,  
460 much higher than IMERG (10%). In agreement with IMERG, and with the exception of the Gulf of Aden,  
461 SOND contributions (fig.11b) are generally higher than in MJ, due to a larger number of TCs. A broad  
462 east to west decrease is noted, which highlights the dominant westward tracks (figure 2). However,  
463 arid stations along the Gulf of Aden get SOND contributions as high as 46% (Bosaso) and 47% (Berbera).  
464 Given the small number of TCs making landfall over the GHA, these are exceptionally high  
465 contributions.

466 The importance of TCs on rainfall is further underlined by focusing on intense rainfall events. Rain days  
467 recording more than 30 mm (IMERG data) are examined to find out how much TCs were contributing  
468 to these events. Over most of the Horn of Africa, the northern Arabian Sea, and moreover the southern  
469 Arabian Peninsula, the number of intense rainfall days is small (frequency <1%, i.e. less than 0.6  
470 day.year<sup>-1</sup> in MJ and 1.2 in SOND, not shown). Conspicuously, a large share of these days (>40%, fig.  
471 11e-f) is brought by TCs in the northwestern Arabian Sea and the Gulf of Aden, and in northeastern  
472 Somalia in SOND. This share even exceeds 60% over a belt extending from NE to SW along and offshore  
473 the Arabian Coast.

474



475

476

477 Fig. 11: Rainfall statistics associated with TCs over Northern Somalia, Djibouti and neighbouring  
 478 areas, based on rain-gauge data (figures) and IMERG (shadings), for MJ (left panels) and SOND (right  
 479 panels). Percentage contribution of TC-related rainfall to mean seasonal rainfall (a,b) ; maximum TC-  
 480 related 24-hr rainfall in mm (c,d) ; percent of days above 30 mm which are TC-induced (e,f), 2000-  
 481 2020. In panels c,d, a value in red indicates that it is the highest 24-hr amount recorded at a given  
 482 station in the respective season. TC-related rainfall refers to rainfall within 750 km of the TC center,  
 483 during its lifetime or in the two following days.

484 Rain-gauge data for northern Somalia and Djibouti confirm that in SOND at many stations the highest  
 485 24-hr rainfall is attributed to a TC (figure 11d). In general, the maximum TC-related 24-hr rainfall is  
 486 over 50 mm in this season, reaching values beyond 100 mm in most of the eastern stations. This is  
 487 broadly in line with IMERG values. In MJ (figure 11c), the highest TC-related 24-hr rainfall amounts are  
 488 lower over the continent, and clearly more patchy (over the sea as well) as a result of fewer TCs.

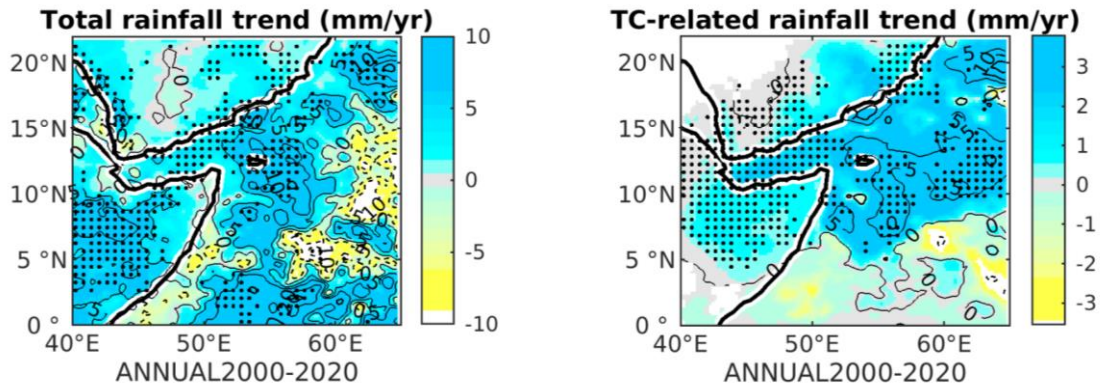
489 Interestingly, high values are nevertheless obtained in the north-west (60 mm at Berbera, 111 mm at  
490 Djibouti and 138 mm at Borama). Very intense rains are also associated with TC landfall over Oman (in  
491 Salalah for example, the absolute maximum rainfall measured during 1990-2020, 238.8 mm, was  
492 associated with the passage of cyclone Mekunu on May 25, 2018), but TC occurrence in this country is  
493 more thoroughly discussed in Pedgley (1969) and Al-Manji et al. (2021). Though IMERG also shows high  
494 values in the Gulf of Aden itself, near the coast satellite estimates are often lower than the observed  
495 contributions, because occasional very heavy precipitation along the coast are not always adequately  
496 resolved by the gridded products. Such an underestimation of coastal intense precipitation in gridded  
497 products is found in other parts of Africa (e.g., the Guinea Coast ; Kpanou et al. 2021).

498 On the whole, despite the high expected variability associated with extreme point rainfall, relatively  
499 consistent patterns emerge in the northeastern Horn of Africa, which confirm the strong role of TCs  
500 on intense rainfall along the northern and eastern coasts in SOND, around the gulf of Aden in MJ, as  
501 well as a substantial contribution inland but in SOND only.

#### 502 3.4 Trends in rainfall and TC-related rainfall

503 Annual rainfall trends are first analysed over the period 2000-2020 (fig.12a). For IMERG data, positive  
504 trends largely dominate, with the largest values (+5 to 10 mm/yr) over inland Somalia and much of the  
505 WAS and Western Indian Ocean, although pockets of negative trends are found further offshore,  
506 notably around 5°N-60°E. There is some uncertainty about these negative trends, as PERSIANN data,  
507 over the same period, display positive trends even far offshore (not shown). Weaker but statistically  
508 significant positive trends ( $p < 0.05$ ) are found over the Gulf of Aden. When focusing on TC-related  
509 rainfall only (fig.12b), there are widespread positive trends for both IMERG and PERSIANN data, though  
510 their magnitude is smaller, except over the Arabian Sea near 10-12°N where trends over +5mm/yr are  
511 noticed. The latter are statistically significant, as well as the (weaker) positive trends which are found  
512 over the Gulf of Aden and neighbouring areas (Djibouti, Yemen, northwestern Somalia). The  
513 contribution of TCs to total rainfall shows significant positive trends over the same regions, with a 21-  
514 yr increase ranging from 20 to 35 points over the areas where the change is the largest, i.e. part of the  
515 WAS, the coasts of Oman and Yemen, and the Gulf of Aden (fig. 12d). When removing TC-related  
516 rainfall from total amounts (fig.12c), trend patterns become close to zero or weakly positive in the  
517 northern part of the region, suggesting that much of the recent increased rainfall is due to the more  
518 frequent (and more intense) TCs. Over the African continent, apart from some coastal areas, there is  
519 little difference between the total and non-TC-related rainfall trends, despite the trend associated with  
520 TCs being significant, because TCs only contribute to a minor fraction of the rains.

521

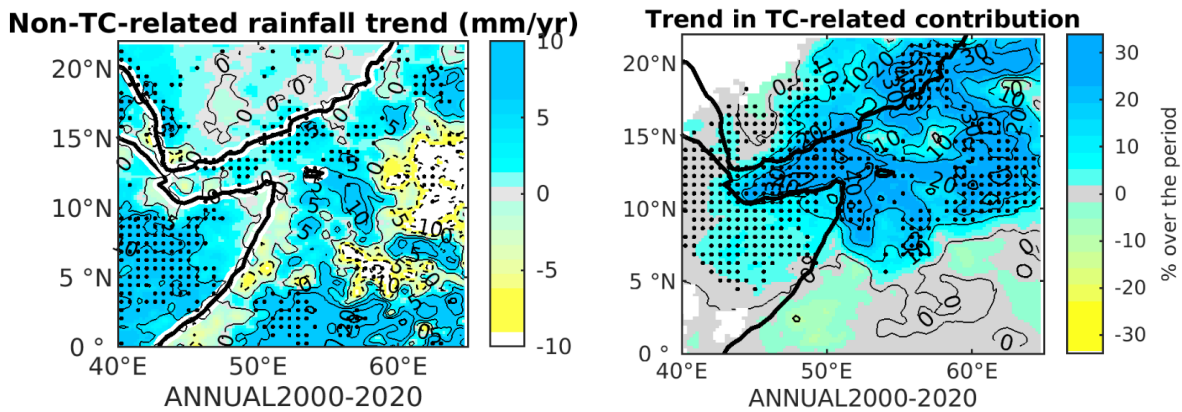


522

523

(a)

(b)



524

525

(c)

(d)

526 Figure 12 : Trends in annual rainfall, IMERG, 2000-2020. Total rainfall (a), TC-related rainfall (b), non-  
 527 TC related rainfall (c) and contribution of TC-related rainfall to the rainfall total (d). Dots indicate  
 528 significant trends ( $p < 0.05$ ) according to the Mann-Kendall test statistic.

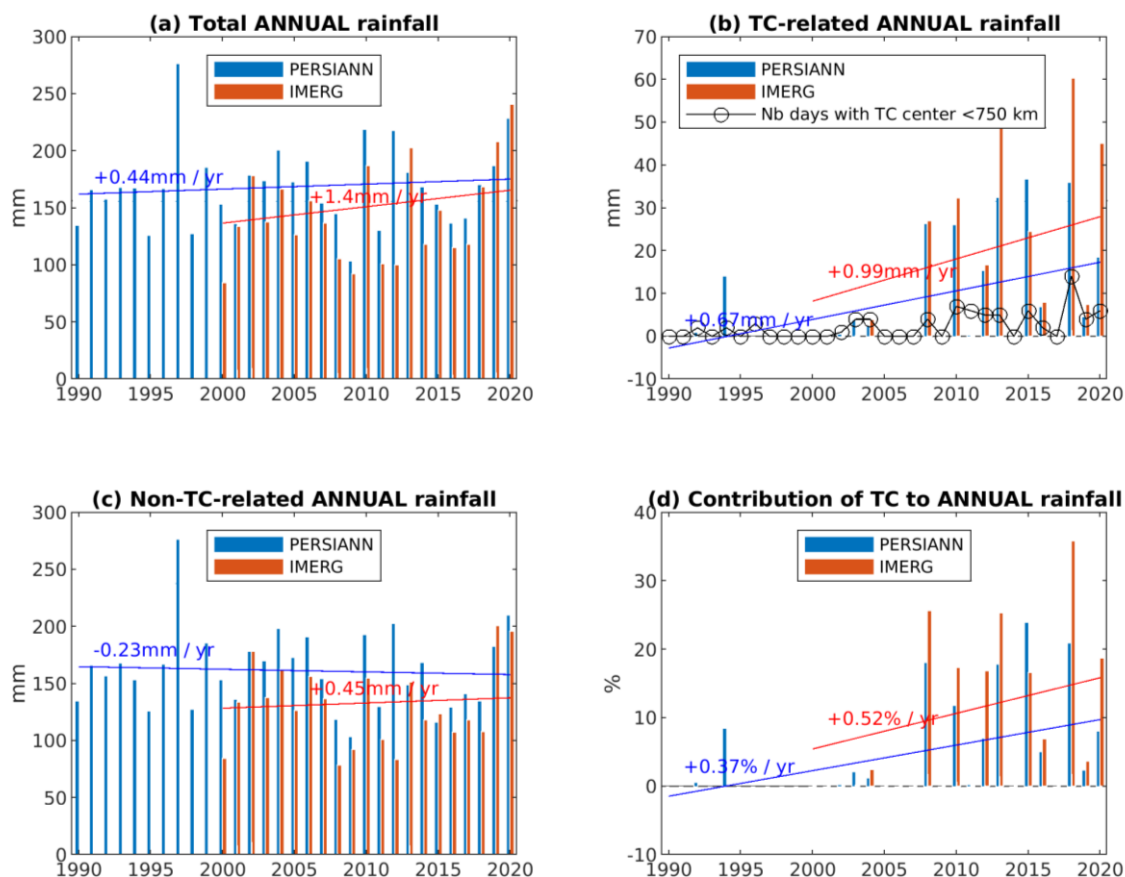
529

530 A seasonal analysis (not shown) indicates that these trends are found during both MJ and SOND,  
 531 although they are stronger and spatially more consistent for SOND. During this season, a very strong  
 532 and significant ( $p < 0.05$ ) increase in the TC contribution is noted between 10 and 17°N. In the 21-yr  
 533 period 2000-2020, the contribution of TCs to SOND rainfall amounts increased by 30 to 50% in the Gulf  
 534 of Aden and the Arabian Sea east of Socotra island. A similar rise is found from the Gulf of Aden to  
 535 southern Oman in MJ, but it is more patchy and seldom significant, due to the rare occurrence of TCs  
 536 in the pre-monsoon season, resulting in many years (even in the more recent period) with nil TC-  
 537 related rainfall.

538 For a better appraisal of trends over the Gulf of Aden and its shores, a regional rainfall index (location  
 539 shown on figure 1) is extracted and plotted in figure 13. For PERSIANN, the time-series were extended

540 to include the full period from 1990 to 2020. Total rainfall shows a weak positive long-term trend  
 541 (+0.44 mm/yr from 1990 to 2020, i.e. +8% in 31 years). TCs strongly contribute to this trend, as shown  
 542 by the conspicuous increase in TC-related rainfall (+0.67 mm/yr fig.13b). If one deducts TC-related  
 543 rainfall from the annual rainfall, the trend becomes slightly negative (-0.23 mm/yr, i.e. about -4% in  
 544 31 years). The contrast between the almost absence of any TC in the sub-period 1990-2007 and the  
 545 relatively frequent TCs in the sub-period 2008-2020 is noteworthy. Besides the higher frequency of  
 546 TCs, rainfall associated with each TC tends to significantly increase between 1990 and 2020 (Mann-  
 547 Kendall tau,  $p < 0.01$ , not shown).

548 Over the period common to the two data sets, IMERG data show a relatively good agreement with  
 549 PERSIANN in the interannual variations of total and TC-related rainfall. Over this period (2000-2020),  
 550 the increase in TC-related rains is strong (+0.99 mm/yr in IMERG, fig.13b). This trend also strongly  
 551 contributes to the overall rainfall trend (+1.40 mm/yr), while the non-TC-related trend is weaker. As  
 552 described above, there is a marked increase in the contribution of TCs to total rainfall, which was close  
 553 to zero before 2007 and reached 9.3% in 2008-2020.



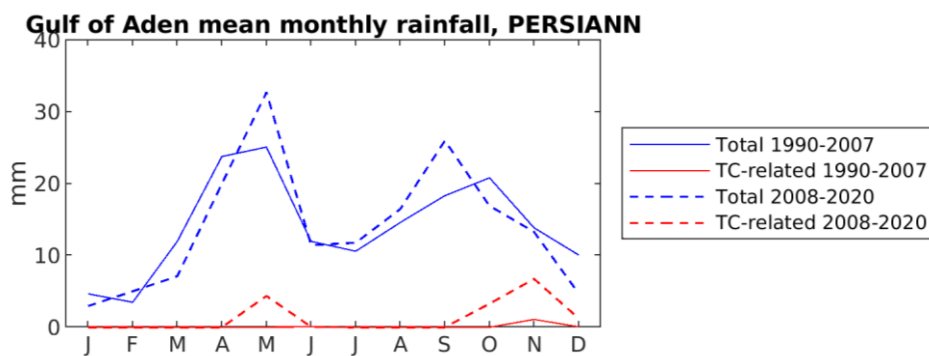
554

555 Figure 13 : Annual rainfall variations and trends over the Gulf of Aden and its shores (44-50°E, 10-  
 556 14°N): total rainfall (a), TC-related rainfall (b), non-TC-related rainfall (c), and contribution of TCs to  
 557 total rainfall (d).

558 The increase concerns both cyclonic seasons, although pre-monsoon TCs are still a rarity in the Gulf of  
 559 Aden (fig.14). The increase in TC-related rainfall boosts the May rainfall peak in the second sub-period,  
 560 and strongly contributes to alleviate the decrease which would have otherwise been found in October-  
 561 December. At that time, TCs have a strong effect on rainfall amounts in the arid environment of the  
 562 Gulf of Aden. In the sub-period 2008-2020, the increase in the frequency of TCs makes the contribution  
 563 of TCs to total October-December rainfall reach 32.4%, from 2.5% in 1990-2007. These statistics are  
 564 based on a sufficient number of events to be meaningful: during this season, from 2008 to 2020, 17  
 565 TCs hit the Gulf of Aden or approached it (within the 750 km radius), as against only 4 in the previous  
 566 sub-period.

567 The on-and-off TC activity in the Gulf of Aden (and the Arabian Sea in general) is a conspicuous feature  
 568 (fig.13). Roy Chowdhury et al. (2020) showed that the positive Indian Ocean Dipole (IOD) event that  
 569 occurred in 2015 stimulated the development of the dual TCs Chapala and Megh in the WAS in  
 570 October-November, through a warmer than normal western Indian Ocean and lower sea-level  
 571 pressure. Similar conclusions were reached by Akhila et al. (2022), who studied cyclones Kyarr and  
 572 Maha in 2019, a positive IOD year. However, Yuan and Cao (2013) and Sattar and Cheung (2019) got  
 573 more ambiguous results on the systematic role of the IOD on Arabian Sea cyclones.

574



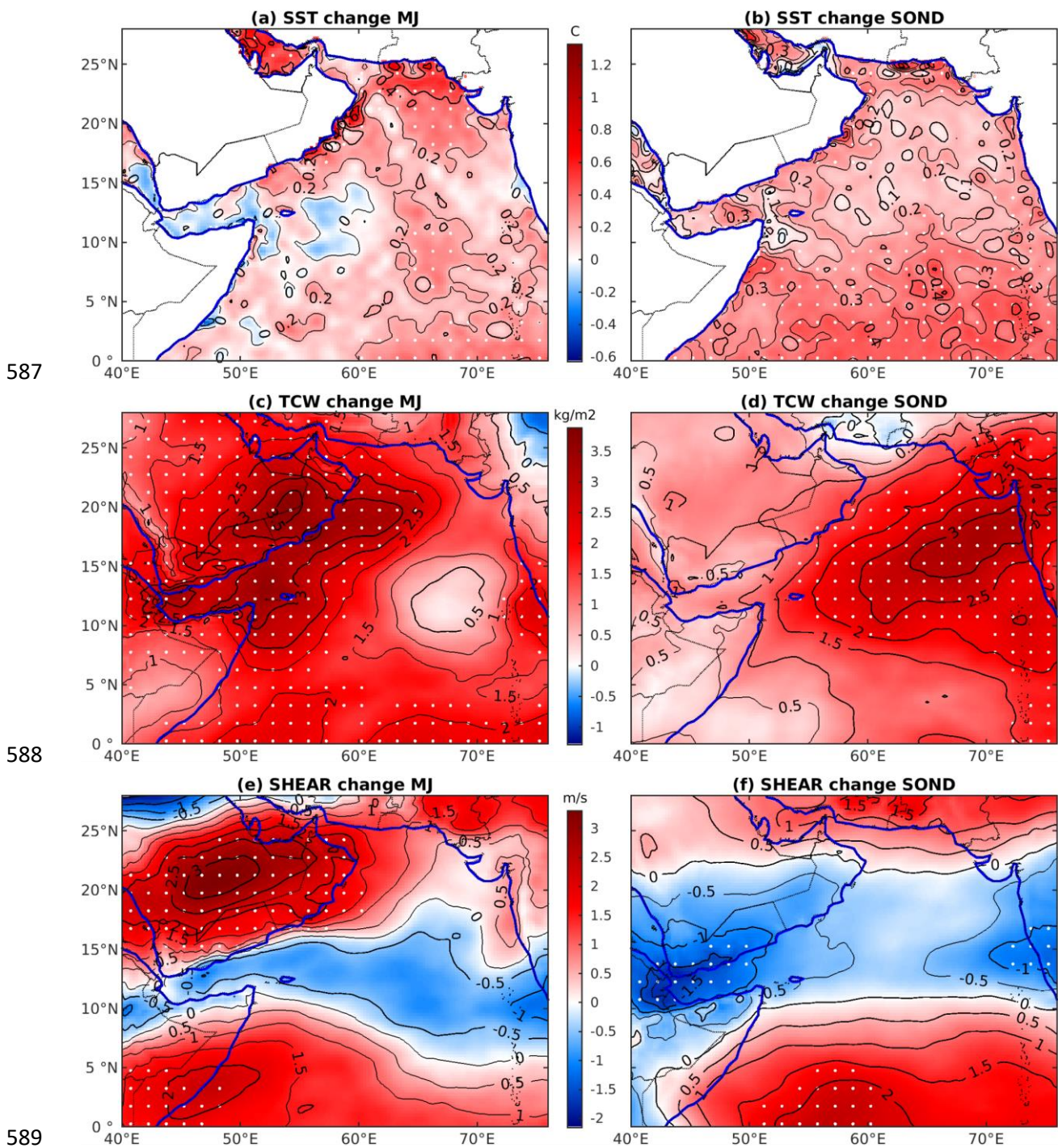
575

576 Figure 14: Mean monthly rainfall over the Gulf of Aden area (PERSIANN data ; IMERG data not shown  
 577 because of the small number of years available in the first sub-period), for 1990-2007 (solid lines) and  
 578 2008-2020 (dashed). Blue lines: total rainfall; red lines: TC-related rainfall.

### 579 3.5 Regional changes contributing to the TC increase

580 The changes in the oceanic and atmospheric conditions which may have accounted for the recent  
 581 increase in the number of TCs or severe storms in the Arabian Sea have been partly documented by  
 582 Deo et al. (2011), Deshpande et al. (2021) and Tiwari et al. (2022). This issue is further documented  
 583 here, separately for the two cyclonic seasons, and by taking into account the detection of a change-  
 584 point (in 2010) in the number of TC days in the WAS (figure 2). Differences between the sub-periods

585 1990-2009 and 2010-2020 are plotted in figure 15 using ERA5 reanalysis data (similar results are  
 586 obtained using the NCEP-NCAR reanalysis).



590 Figure 15: Changes in sea-surface temperature (a-b), total column water (c-d) and vertical wind shear  
 591 (e-f) from 1990-2009 to 2010-2020, for the MJ and SON seasons (ERA5 data). White dots indicate  
 592 statistically significant changes (t-test,  $p < 0.05$ ). The change in wind shear is computed as the  
 593 magnitude change between 200 and 850 hPa wind vectors (Pillay and Fitchett 2021).

594 The tripling of the number of days with TCs between 1990-2009 (4 days per year) and 2010-2020 (13  
 595 days per) in the WAS is found to be associated with three features favourable to TC activity :

596 (1) a decrease in vertical wind shear between 200 hPa and 850 hPa in a belt running from India to the  
597 Gulf of Aden, in both seasons (the decrease is significant in SOND only ; fig.15e-f)

598 (2) a sharp increase in relative humidity in the mid-troposphere (700 to 500 hPa) and of total column  
599 water (fig.15 c-d), mainly in the northwestern part of the region in MJ and in the eastern part in SOND

600 (3) an increase in sea surface temperature (SST, fig. 15a-b), which is more widespread in SOND than in  
601 MJ (for the latter, the Gulf of Aden and neighbouring areas do not show any clear warming)

602 The main source region of TCs, i.e. the southeastern Arabian Sea, displays the strongest sea surface  
603 warming, which may account for more favourable conditions for TC genesis, given that other factors  
604 in the same region (wind shear, atmospheric moisture) also tend to be more favourable. In the WAS,  
605 it is the strong increase in total column water vapour, in MJ, and the reduced wind shear, in SOND,  
606 which seem to constitute the key triggers, likely enabling existing systems to have a longer lifetime or  
607 to intensify. Part of these changes denote the effect of decadal-scale variability, since during the pre-  
608 monsoon vertical wind shear in the WAS for the decade 2000-09 was higher than in 1990-99. This  
609 impacted the lower cyclone activity during part of the first sub-period. Deshpande et al. (2021) also  
610 pointed to an increase of TC genesis at lower latitudes, which due to the dominant easterlies across  
611 the Somalia and Yemen shorelines, contribute to the increased number of WAS cyclones during the  
612 most recent period (examples of 03A in November 2013, Sagar in 2018, Gati in 2020). It is unclear  
613 whether these trends denote changes in TC activity due to anthropogenic climate change, but the  
614 Arabian Sea is one of the ocean basins where models most consistently project a forthcoming increase  
615 in intense TCs (Murakami et al. 2013; Knutson et al., 2015 ; Bell et al. 2020).

#### 616 4. Conclusions

617 The northwestern Arabian Sea and adjacent land areas are among the few regions of the world where  
618 tropical cyclones occur in an arid context. Their contribution to rainfall and associated trends was  
619 analysed using two combined satellite-rain-gauge precipitation products (PERSIANN and IMERG) and  
620 daily rain-gauge data for northern Somalia and Djibouti. Based on case studies and a statistical analysis  
621 of rainfall amounts with respect to the distance to the TC center, it was found that rainfall was  
622 influenced by TCs over a wide area (up to 750 km from the center), and that heavy rains still occurred  
623 one to two days after the TC lifecycle. Despite the rare occurrence of tropical systems (1.5 per year,  
624 whatever the category, with a third making landfall), they strongly contribute (30-50%) to mean annual  
625 rainfall over the northwestern Arabian Sea, Gulf of Aden and their respective coastlines. On a seasonal  
626 basis, this contribution is even higher (40-60 %) in southern Arabia and the adjacent oceanic areas, for  
627 both cyclonic seasons (May-June and September-December). High values were also found at the Gulf  
628 of Aden stations in Somalia in SOND. Over inland northern Somalia, contributions are lower in MJ

629 (generally <5%) and SOND (5 to 20%, increasing eastwards). In a belt running northeastward from the  
630 Gulf of Aden, a large proportion (30-70%) of heavy rain days (>40 mm) are associated with TCs. In  
631 northern Somalia, many 24-hr maximum rainfall amounts are TC-related.

632 From 1990 to 2020, the number of tropical systems showed a marked increase in the region, hence  
633 their enhanced contribution to rainfall totals. Part of the overall upward rainfall trend over the  
634 northwestern Arabian Sea, is actually the outcome of increasing cyclonic activity. Though over the Gulf  
635 of Aden and neighbouring regions of the Horn of Africa (northern Somalia, Djibouti), TCs are very  
636 infrequent, the trend in TC-related rainfall shows a consistent and significant increase, highlighted by  
637 the contrast between the subperiods 1990-2007 and 2008-2020. Both cyclonic seasons are involved in  
638 this increase. The increase in TC frequency is related to a SST increase in the eastern and southern  
639 Arabian Sea, a decrease in vertical wind shear, and a strong increase in tropospheric moisture content.

640 Some caution should be exerted on the interpretation of these trends, which may not necessarily  
641 reflect the effect of anthropogenic climate change. Murakami et al (2013) noted that, under increased  
642 greenhouse gases scenarios, a future westward shift of the mean locations of tropical storms is  
643 projected over the North Indian Ocean during the post-monsoon season (matching the recent increase  
644 in TC days in the WAS). Murakami et al. (2017) found that anthropogenic forcing has likely increased  
645 the probability of post-monsoon severe cyclonic storms over the Arabian Sea. Wang et al. (2023)  
646 likewise found a potentially dominant role of anthropogenic forcing on coastal TC frequency changes  
647 in many basins of the world, including the western coast of the Arabian Sea, but for the latter region  
648 their simulations failed to specifically attribute these changes to the effect of aerosol or greenhouse  
649 gases. Additionally, the low number of TCs in the early part of the period should also be considered in  
650 a broader context, since Rajeevan et al. (2013) showed a decrease in the frequency of intense TCs in  
651 the Arabian Sea from the period 1955-1973 to 1974–1992, suggesting large decadal-scale variability in  
652 the basin. Evan and Camargo (2011) questioned spurious increases in Arabian Sea TC intensity, which  
653 could explain part of the rise in cyclonic storm days they noted between 1979-1991 and 1992-2008  
654 over the Arabian Sea as a whole. Duplicating this study for future periods is now needed, although this  
655 discussion highlights that internal climate variability cannot be neglected to obtain robust projections  
656 of TC activity, and their impacts on rainfall. Large ensembles from the CMIP6 (Eyring et al. 2016) or  
657 MENA-CORDEX (Bucchignani et al. 2015) modelling exercises could be used for that purpose.

658

## 659 Acknowledgements

660 The authors thank the National Meteorological Agency (ANM) of Djibouti for the provision of daily  
661 rainfall data for the Republic of Djibouti and SWALIM for northern Somalia. SWALIM is a project

662 managed by FAO with funding from The European Union, The Swiss Agency for Development and  
663 Cooperation, The Italian Cooperation, DFID, USAID and the Government of France. Calculations were  
664 performed using HPC resources from DNUM CCUB (Centre de Calcul de l'Université de Bourgogne).

665

## 666 References

667 Abdalla, O., & Al-Abri, R. B. Y. (2011). Groundwater recharge in arid areas induced by tropical  
668 cyclones: lessons learned from Gonu 2007 in Sultanate of Oman. *Environmental Earth Sciences*, *63*,  
669 229-239.

670 Akhila, R.S., Kuttippurath, J., Rahul, R. *et al.* (2022). Genesis and simultaneous occurrences of the  
671 super cyclone Kyarr and extremely severe cyclone Maha in the Arabian Sea in October 2019. *Nat*  
672 *Hazards* *113*, 1133–1150. <https://doi.org/10.1007/s11069-022-05340-9>

673 Al-Manji, S., Mitchell, G., and Al Ruheili, A. (2021). Arabian Sea Tropical Cyclones: A Spatio-Temporal  
674 Analysis in Support of Natural Hazard Risk Appraisal in Oman. in R.S. Meena (ed.) : *Agrometeorology*.  
675 IntechOpen. doi:10.5772/intechopen.96961.

676 Ashouri, H., Hsu, K. L., Sorooshian, S., Braithwaite, D. K., Knapp, K. R., Cecil, L. D., ... & Prat, O. P.  
677 (2015). PERSIANN-CDR: Daily precipitation climate data record from multisatellite observations for  
678 hydrological and climate studies. *Bulletin of the American Meteorological Society*, *96(1)*, 69-83.

679 Baburaj, P.P., Abhilash, S., Mohankumar, K., Sahai, A.K. (2020). On the epochal variability in the  
680 frequency of cyclones during the pre-onset and onset phases of the monsoon over the North Indian  
681 Ocean. *Advances in Atmospheric Sciences*, *37*, 634-651.

682 Bell, S.S., Chand, S.S., Tory, K.J., Ye, H. and Turville, C. (2020) North Indian Ocean tropical cyclone  
683 activity in CMIP5 experiments: future projections using a model-independent detection and tracking  
684 scheme. *International Journal of Climatology*, *40(15)*, 6492–6505. <https://doi.org/10.1002/joc.6594>.

685 Breña-Naranjo, J.A., Pedroso-Acuña, A., Pozos-Estrada, O., Jiménez-López, S.A., López-López, M.R.  
686 (2015). The contribution of tropical cyclones to rainfall in Mexico. *Physics and Chemistry of the Earth*,  
687 Parts A/B/C, *83-84*, 111-122.

688 Bucchignani, E., Mercogliano, P., Rianna, G., Panitz, H.J. (2015). Analysis of ERA-Interim-driven  
689 COSMO-CLM simulations over Middle East – North Africa domain at different spatial resolutions –  
690 *International Journal Of Climatology* DOI: 10.1002/joc.4559

691 Chazée, L. (2017). *Patrimoine socio-économique et naturel de la région du Cap Gardafui*.  
692 L'Harmattan, Paris, 330 p.

693 Cherel, J. P., Omar Ali, B., Nour Ayeh, M., & Vinet, F. (2020). Activités cycloniques et nouveaux  
694 risques dans le golfe d'Aden. Exemple des impacts socio-économiques du cyclone Sagar sur Djibouti  
695 en mai 2018. *EchoGéo*, 51. <https://doi.org/10.4000/echogeo.18859>

696 Deo, A.A., Ganer, D.W. & Nair, G. (2011). Tropical cyclone activity in global warming scenario. *Nat*  
697 *Hazards* 59,771–786.

698 Deshpande, M., Singh, V. K., Ganadhi, M. K., Roxy, M. K., Emmanuel, R., & Kumar, U. (2021). Changing  
699 status of tropical cyclones over the north Indian Ocean. *Climate Dynamics*, 57, 3545-3567.

700 Englehart, P. J., & Douglas, A. V. (2001). The role of eastern North Pacific tropical storms in the  
701 rainfall climatology of western Mexico. *International Journal of Climatology*, 21(11), 1357-1370.

702 Evan, A. T., & Camargo, S.J. (2011). A Climatology of Arabian Sea Cyclonic Storms. *J. Climate*, 24, 140–  
703 158.

704 Evan, A. T., Kossin, J. P., Chung, C. E. & Ramanathan, V. (2021). Arabian Sea tropical cyclones  
705 intensified by emissions of black carbon and other aerosols. *Nature* 479, 94–97.

706 Eyring, V., Bony, S., Meehl, G. A., Senior, C. A., Stevens, B., Stouffer, R. J., and Taylor, K. E. (2016).  
707 Overview of the Coupled Model Intercomparison Project Phase 6 (CMIP6) experimental design and  
708 organization. *Geosci. Model Dev.*, 9, 1937–1958, <https://doi.org/10.5194/gmd-9-1937-2016>.

709 Finney, D. L., Marsham, J. H., Walker, D. P., Birch, C. E., Woodhams, B. J., Jackson, L. S., & Hardy, S.  
710 (2020). The effect of westerlies on East African rainfall and the associated role of tropical cyclones  
711 and the Madden–Julian Oscillation. *Quarterly Journal of the Royal Meteorological Society*, 146(727),  
712 647-664.

713 Fors, J.R. (1977). *Tropical cyclone Kathleen*. NOAA Technical Memorandum NWS WR-114, 29 p.

714 Gaona, M. F. R., Villarini, G., Zhang, W., & Vecchi, G. A. (2018). The added value of IMERG in  
715 characterizing rainfall in tropical cyclones. *Atmospheric Research*, 209, 95-102.

716 Gray, W. M. (1968). Global view of the origin of tropical disturbances and storms. *Mon. Wea. Rev.*,  
717 96, 669–700.

718 Hari, V., Pathak, A., & Koppa, A. (2021). Dual response of Arabian Sea cyclones and strength of Indian  
719 monsoon to Southern Atlantic Ocean. *Climate Dynamics*, 56, 2149-2161.

720 Hoarau, K., Bernard, J., & Chalonge, L. (2012). Intense tropical cyclone activities in the northern  
721 Indian Ocean. *International journal of climatology*, 32(13), 1935-1945.

722 Huffman, G. J., Bolvin, D. T., Nelkin, E. J., & Tan, J. (2015). Integrated Multi-satellitE Retrievals for  
723 GPM (IMERG) technical documentation. *Nasa/Gsfc Code*, 612(47), 2019.

724 IFRC (2013). International Federation of Red Cross and Red Crescent Disaster Relief Emergency Fund :  
725 Somalia Tropical Cyclone. [https://reliefweb.int/report/somalia/somalia-tropical-cyclone-dref-](https://reliefweb.int/report/somalia/somalia-tropical-cyclone-dref-operation-n-mdrso002-update-no-1)  
726 [operation-n-mdrso002-update-no-1](https://reliefweb.int/report/somalia/somalia-tropical-cyclone-dref-operation-n-mdrso002-update-no-1) Accessed 25 September 2023.

727 Jiang, H., & Zipser, E. J. (2010). Contribution of tropical cyclones to the global precipitation from eight  
728 seasons of TRMM data: Regional, seasonal, and interannual variations. *Journal of climate*, 23(6),  
729 1526-1543.

730 Kabir, R., Ritchie, E.A., Stark, C. (2022). Tropical Cyclone Exposure in the North Indian Ocean.  
731 *Atmosphere*, 13, 1421. <https://doi.org/10.3390/atmos13091421>

732 Kebacho, L. L. (2022). The role of tropical cyclones Idai and Kenneth in modulating rainfall  
733 performance of 2019 long rains over East Africa. *Pure and Applied Geophysics*, 179(4), 1387-1401.

734 Khouakhi, A., Villarini, G., Vecchi, G.A. (2017). Contribution of Tropical Cyclones to Rainfall at the  
735 Global Scale. *J. Climate*, 30, 359–372.

736 Knapp, K. R., Kruk, M. C. , Levinson, D. H. , Diamond, H. J., and Neumann, C. J. (2010). The  
737 International Best Track Archive for Climate Stewardship (IBTrACS): Unifying tropical cyclone best  
738 track data. *Bulletin of the American Meteorological Society*, 91, 363-376.  
739 [doi:10.1175/2009BAMS2755.1](https://doi.org/10.1175/2009BAMS2755.1)

740 Knapp, K. R., Diamond, H. J., Kossin, J. P. , Kruk, M. C., Schreck, C. J. (2018). *International Best Track*  
741 *Archive for Climate Stewardship (IBTrACS) Project, Version 4*. NOAA National Centers for  
742 Environmental Information. [doi:10.25921/82ty-9e16](https://doi.org/10.25921/82ty-9e16) [accessed 23 February 2024].

743 Knutson, T.R., Sirutis, J.J., Zhao, M., Tuleya, R.E., Bender, M., Vecchi, G.A., Villarini, G. and Chavas, D.  
744 (2015). Global projections of intense tropical cyclone activity for the late twenty-first century from  
745 dynamical downscaling of CMIP5/RCP4.5 scenarios. *Journal of Climate*, 28(18), 7203–7224.  
746 <https://doi.org/10.1175/JCLI-D-15-0129.1>.

747 Kpanou, M., Laux, P., Brou, T., Vissin, E., Camberlin, P., & Roucou, P. (2021). Spatial patterns and  
748 trends of extreme rainfall over the southern coastal belt of West Africa. *Theoretical and Applied*  
749 *Climatology*, 143, 473-487.

750 Lavender, S.L., McBride, J.L. (2021). Global climatology of rainfall rates and lifetime accumulated  
751 rainfall in tropical cyclones: Influence of cyclone basin, cyclone intensity and cyclone size. *Int J*  
752 *Climatol.* 41 (Suppl. 1): E1217–E1235.

753 Lvončík, S., Vahalík, P., Bongers, F. et al. (2020). Development of a population of *Boswellia elongata*  
754 Balf. F. in Homhil nature sanctuary, Socotra island (Yemen). *Rend. Fis. Acc. Lincei* 31, 747–759.  
755 <https://doi.org/10.1007/s12210-020-00936-4>

756 Murakami, H., Sugi, M. and Kitoh, A. (2013). Future changes in tropical cyclone activity in the north  
757 Indian Ocean projected by high-resolution MRI-AGCMs. *Climate Dynamics*, 40(7–8), 1949–1968.  
758 <https://doi.org/10.1007/s00382-012-1407-z>.

759 Murakami, H., Vecchi, G. A., and Underwood, S. (2017). Increasing frequency of extremely severe  
760 cyclonic storms over the Arabian Sea. *Nature Climate Change*, 7[12], 885–889.

761 Neumann, C.J. (2017). A Global Tropical Cyclone Climatology. In WMO *Global Guide to Tropical*  
762 *Cyclone Forecasting*, 28-62. [https://cyclone.wmo.int/pdf/Global-Guide-to-Tropical-Cyclone-](https://cyclone.wmo.int/pdf/Global-Guide-to-Tropical-Cyclone-Forecasting.pdf)  
763 [Forecasting.pdf](https://cyclone.wmo.int/pdf/Global-Guide-to-Tropical-Cyclone-Forecasting.pdf)

764 Ng, B., Walsh, K., Lavender, S. (2014). The contribution of tropical cyclones to rainfall in northwest  
765 Australia. *International Journal of Climatology*, 35 (10), 2689-2697. <https://doi.org/10.1002/joc.4148>

766 OCHA Somalia (2020). *Somalia, Tropical Cyclone Gati Update #2. ReliefWeb. UN Office for the*  
767 *Coordination of Humanitarian Affairs. 24 November 2020.* [https://reliefweb.int/report/somalia/ocha-](https://reliefweb.int/report/somalia/ocha-somalia-tropical-cyclone-gati-update-2-24-november-2020)  
768 [somalia-tropical-cyclone-gati-update-2-24-november-2020](https://reliefweb.int/report/somalia/ocha-somalia-tropical-cyclone-gati-update-2-24-november-2020) Accessed 5 December 2023

769 Owuor, A., & David McRae, H. (2022). The Control of the Desert Locusts (*Schistocerca gregaria*) in  
770 Somalia during the Upsurge Between 2019 and 2021. *Outlooks on Pest Management*, 33(6), 221-226.

771 Pedgley, D. E. (1969). Cyclones along the Arabian coast. *Weather*, 24(11), 456-470.

772 Pillay, M. T., & Fitchett, J. M. (2021). On the conditions of formation of Southern Hemisphere tropical  
773 cyclones. *Weather and Climate Extremes*, 34, 100376.

774 Prat, O. P., & Nelson, B. R. (2013). Mapping the world's tropical cyclone rainfall contribution over  
775 land using the TRMM Multi-satellite Precipitation Analysis. *Water Resources Research*, 49(11), 7236-  
776 7254.

777 Priya, P., Pattnaik, S. & Trivedi, D. (2022). Characteristics of the tropical cyclones over the North  
778 Indian Ocean Basins from the long-term datasets. *Meteorol Atmos Phys* 134, 65.  
779 <https://doi.org/10.1007/s00703-022-00904-7>

780 Rajeevan, M., Srinivasan, J., Niranjan Kumar, K., Gnanaseelan, C., & Ali, M. M. (2013). On the epochal  
781 variation of intensity of tropical cyclones in the Arabian Sea. *Atmospheric Science Letters*, *14*(4), 249-  
782 255.

783 Ramsay, H. (2017). The Global Climatology of Tropical Cyclones. *Oxford Research Encyclopedia of*  
784 *Natural Hazard Science*. Retrieved 31 Aug. 2023, from  
785 <https://oxfordre.com/naturalhazardscience/view/10.1093/acrefore/9780199389407.001.0001/acrefore-9780199389407-e-79>.  
786

787 Résumé Mensuel du Temps (1972). *Résumé mensuel du temps en Territoire Français des Afars et des*  
788 *Issas*, Service de la Météorologie, Djibouti, Octobre 1972, 14 p.

789 Ray-Choudhuri, S., Subramanyan, Y. H., & Chellappa, R. (1959). A climatological study of storms and  
790 depressions in the Arabian Sea. *Mausam*, *10*(3), 283-290.

791 Roy Chowdhury, R., Prasanna Kumar, S., Narvekar, J., & Chakraborty, A. (2020). Back-to-back  
792 occurrence of tropical cyclones in the Arabian sea during October–November 2015: causes and  
793 responses. *Journal of Geophysical Research: Oceans*, *125*(6), e2019JC015836.

794 Salih, A. A., Baraibar, M., Mwangi, K. K., & Artan, G. (2020). Climate change and locust outbreak in  
795 East Africa. *Nature Climate Change*, *10*(7), 584-585.

796 Sattar, A. M., & Cheung, K. K. (2019). Comparison between the active tropical cyclone seasons over  
797 the Arabian Sea and Bay of Bengal. *International Journal of Climatology*, *39*(14), 5486-5502.

798 Schreck, C.J., Knapp, K.R., Kossin, J.P. (2014). The impact of best track discrepancies on Global  
799 Tropical Cyclone climatologies using IBTrACS. *Monthly Weather Review*, *142*, 3881-3899.

800 Shanko, D., & Camberlin, P. (1998). The effects of the Southwest Indian Ocean tropical cyclones on  
801 Ethiopian drought. *International Journal of Climatology*, *18*(12), 1373-1388.

802 Singh, K., Panda, J. & Mohapatra, M. (2020). Robustness of best track data and associated cyclone  
803 activity over the North Indian Ocean region during and prior to satellite era. *J Earth Syst Sci* *129*, 84.  
804 <https://doi.org/10.1007/s12040-020-1344-x>

805 Singh, V. K., & Roxy, M. K. (2022). A review of ocean-atmosphere interactions during tropical cyclones  
806 in the north Indian Ocean. *Earth-Science Reviews*, *226*, 103967.

807 Tiwari, G., Kumar, P., Javed, A., Mishra, A. K., & Routray, A. (2022). Assessing tropical cyclones  
808 characteristics over the Arabian Sea and Bay of Bengal in the recent decades. *Meteorology and*  
809 *Atmospheric Physics*, *134*(3), 44.

- 810 Wahiduzzaman, M., Cheung, K., Luo, J. J., Bhaskaran, P. K., Tang, S., & Yuan, C. (2022). Impact  
811 assessment of Indian Ocean Dipole on the North Indian Ocean tropical cyclone prediction using a  
812 Statistical model. *Climate Dynamics*, 58, 1275–1292. <https://doi.org/10.1007/s00382-021-05960-0>
- 813 Wang, B., Xu, S. & Wu, L. (2012). Intensified Arabian Sea tropical storms. *Nature* 489, E1–E2  
814 <https://doi.org/10.1038/nature11470>.
- 815 Wang, S., Murakami, H. & Cooke, W.F. (2023). Anthropogenic forcing changes coastal tropical  
816 cyclone frequency. *npj Clim Atmos Sci* 6, 187. <https://doi.org/10.1038/s41612-023-00516-x>
- 817 Yuan, J., Cao, J. (2013). North Indian Ocean tropical cyclone activities influenced by the Indian Ocean  
818 Dipole mode. *Sci. China Earth Sci.* 56, 855–865. <https://doi.org/10.1007/s11430-012-4559-0>